Scientific Opportunities at the Oak Ridge Laboratory for Neutrino Detectors (ORLaND)

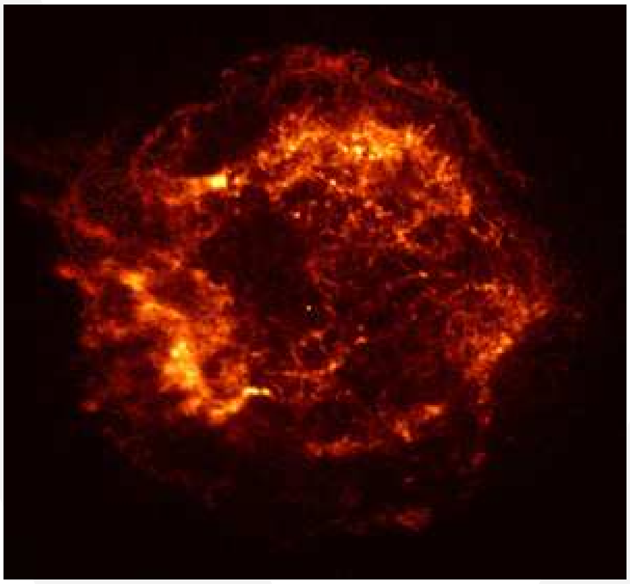

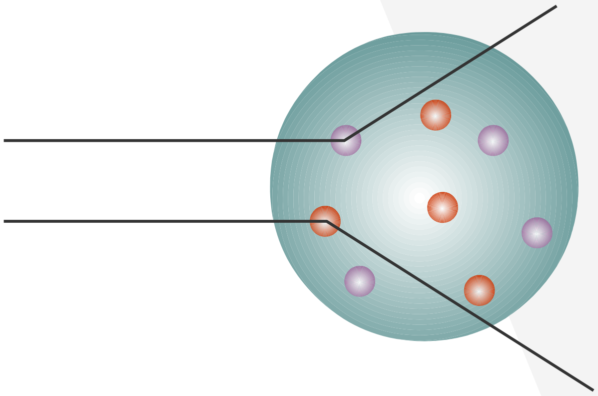

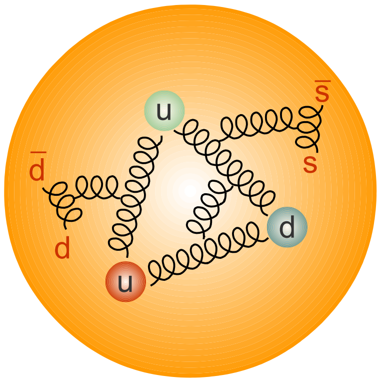

A Report on the Workshop on
Neutrino Nucleus Physics Using a Stopped Pion Neutrino Facility
May 22-26, 2000
Oak Ridge, Tennessee

Scientific Opportunities at the Oak Ridge Laboratory for Neutrino Detectors (ORLaND)

A Report on the Workshop on
Neutrino Nucleus Physics Using A Stopped Pion Neutrino Facility
May 22-26, 2000
Oak Ridge, Tennessee

Foreword

This "white paper" provides a discussion of scientific opportunities for low-energy neutrino physics that may be provided by the constuction of the Spallation Neutron Source, SNS, at the Oak Ridge National Laboratory. The science presented here is based on a workshop held in Oak Ridge in May 2000 that was attended by over 50 scientists from the U.S. and abroad. The construction of the SNS will provide a stopped-pion neutrino source of unprecendented intensity with an extremely favorable pulse structure. The science described in this document would be carried out in an underground detector hall, built near the SNS neutron production target, that is proposed as a national user facility for neutrino science. The detector hall is being designed to accommodate one large ($\sim$ 2000-ton) multi-purpose neutrino detector that could be filled with various liquids. Adequate space will be provided to house as many as eight smaller ($\sim$ 200-ton) detectors. We note that the science made available by this facility encompasses topics generally associated with several fields, including nuclear physics, astrophysics, and elementary particle physics.

We cannot claim to know with any degree of certainty what the highest priority experiments in neutrino science will be in $\sim$ 2006 when the ORLaND facility should be completed. The intention is to build the most versatile stopped-pion facility that is feasible and to incorporate the possible construction of a decay-in-flight neutrino beam as a future development. It is, however, necessary to present as strong a science case as possible to justify construction of this facility. Consequently, we have developed, in this document, a compendium of some of the exciting physics that is feasible with such a facility and identified several experiments that we believe are likely to have a high priority at the time the facility is available. This document is not intended to present a final research plan for the ORLaND facility. The actual research program will be defined by the recommendations of a broadly constituted Program Advisory Committee in response to proposals submitted by independent collaborations, subject to support by an appropriate funding agency.

Finally, we wish to emphasize that our primary motivation is the desire to take advantage of the unique set of circumstances presented to neutrino science by the construction of the SNS. There is a window of opportunity (2004-2005) during which ORLaND's construction that can be coordinated with the construction of the SNS in such a way as to maximize its physics potential and minimize its cost. It would be a great pity to miss this opportunity.

Writing Committee

F. Avignone	University of South Carolina
J. Beene	Oak Ridge National Laboratory
F. Bertrand	Oak Ridge National Laboratory
R. Boyd	Ohio State University
R. L. Burman	Los Alamos National Laboratory
M. Butler	Saint Mary's University, Halifax, NS, Canada
K. Carter	Oak Ridge Associated Universities
L. Chatterjee	Cumberland University
J.-W. Chen	University of Washington
D. Dean	Oak Ridge National Laboratory
Y. Efremenko	Oak Ridge National Laboratory
S. Elliott	University of Washington
J. Engel	University of North Carolina
A. Fazely	Southern University, Baton Rouge, LA
M. Guidry	University of Tennessee
R. Hix	University of Tennessee
B. Holstein	University of Massachusetts
R. Imlay	Louisiana State University
E. Kolbe	University of Basel, Switzerland
K. Lande	University of Pennsylvania
K. Langanke	Aarhus University, Denmark
A. Mezzacappa	Oak Ridge National Laboratory
A. Murphy	Ohio State University
S. Pollock	University of Colorado
M. Savage	University of Washington
M. Smith	Oak Ridge National Laboratory
M. Strayer (Chair)	Oak Ridge National Laboratory
P. Vogel	California Institute of Technology

Contents

List of Figures

List of Tables

1. Executive Summary

Today, at the dawn of the 21st century, the neutrino has established its presence in diverse areas of physics. Neutrino interactions and properties impact our fundamental understanding of the physical universe in many different ways. These encompass the evolution and dynamics of the universe and the life-cycles of its constituent stars, as well as its material content at various levels of structure from atoms and nuclei to valence and sea quarks. From a nuclear physics perspective, the need for a comprehensive program on neutrino science is a timely and important one. Ideally, such a program would study neutrino interactions at energies relevant for nuclear astrophysics and nuclear structure studies. The Spallation Neutron Source (SNS), under construction at the Oak Ridge National Laboratory, will produce neutrinos and antineutrinos at these energies as a natural by-product of spallation.

This document evaluates the scientific prospects for ORLaND, the Oak Ridge Laboratory for Neutrino Detectors, proposed as an underground laboratory located adjacent to the SNS target building, and highlights the compelling advantages of ORLaND as the world's most powerful low-energy pulsed neutrino facility. Unique in its potential to obtain neutrino-nucleus interaction data and enhance our understanding of nuclear structure and stellar astrophysics, ORLaND would be available to users from the international scientific community for dedicated neutrino and neutrino-nucleus science.

A workshop on "Neutrino–Nucleus Physics Using a Stopped Pion Facility (ORLaND)" convened at ORNL, May 23–26, 2000, was attended by 48 national and international scientists. The workshop involved a broad spectrum of the community and addressed ORLaND physics and the formulation of this white paper.

The neutrinos at ORlaND will be obtained from decay of stopped pions produced in the SNS neutron production target during spallation and the decay of the daughter muons. The spectral composition of neutrinos from such stopped pion facilities are well known and their special characteristics will be utilized in planning the ORLaND physics program. Spallation at the SNS will result in the production of about 10^{15} neutrinos of each species ($\nu_\mu, \bar{\nu}_\mu$, and ν_e) per second. The neutrinos will be produced isotropically, and their time structure and flavor components will allow separation of charged and neutral current interactions involving different neutrino families. The pulsed nature of the proton beam and underground location of the facility will provide attractive shielding advantages. The neutrino energy spectrum makes the facility unique for neutrino-nucleus experiments related to solar and supernova physics as well as fundamental nuclear, electroweak, and particle physics.

Charting the importance of neutrino-nuclear-physics might well begin with the ignition of the primal p-p reaction and the p-p chain of stellar burning that involves the emission of electron-neutrinos. Terrestrial detection and study of these neutrnos are critical to our description of solar energy release by the Standard Solar Model. Due to the nature of the weak interaction, the neutrinos provide direct information on the solar core, and the 'solar neutrino deficit' continues to be a key issue. At the other end of a stellar life cycle, the neutrinos produced during core-collapse are the first to signal exploding supernovae. Streaming out from the interior, neutrinos deplete the core of energy and influence the evolution and dynamics of the explosions.

The intense flux of neutrinos emanating from supernovae also affects nucleo-synthesis of heavy elements and forms a valuable tool in our understanding of such cataclysmic stellar events. Studies of supernova and solar physics by their emitted neutrinos and the neutrino-nucleus reactions relevant to these could be carried out at ORLaND and would provide critical advances in our understanding of the nuclear- and astro-physics of such stellar phenomena.

The intrinsic properties of the neutrino, such as mass, impact our fundamental understanding of nuclear and electroweak astrophysics and is a matter of profound importance in our description of nature through the Standard Model. The occurrence of neutrino mass and associated flavor-oscillations infiltrate several aspects of stellar astrophysics including our knowledge of stellar burning, evolution, and explosions. Neutrino oscillations provide an attractive scenario for alleviating the 'solar neutrino

SNS Neutrino Production

The SNS will bombard one GeV protons on a mercury target. The collisions will produce a high flux of positive and negative pions as a by-product. The negative pions will predominantly be captured by the mercury nuclei and the positive pions will be stopped in the target and decay to postive muons and muon neutrinos. The positive muons will in turn decay to positrons, electron neutrinos and anti muon neutrinos.

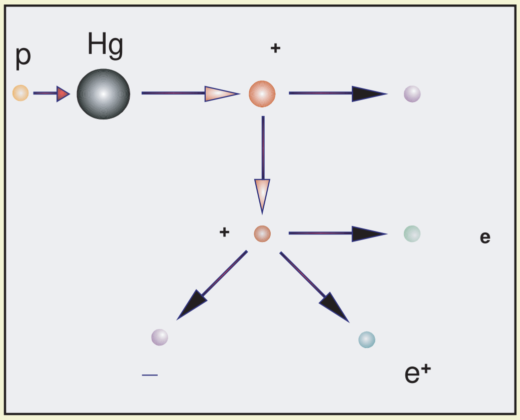

The SNS will thus radiate an intense flux of neutrinos, a colossal 0.94 x 10^{15} neutrinos every second, and their energies make them ideally suitable for experiments designed to study nuclear structure, laboratory simulations of reactions occurring in stellar interiors and cataclysmic stellar explosions as well as calibration of reactions that serve to detect astrophysical neutrinos. The anti-muon neutrinos and the electron neutrinos have the well known muon decay spectra and lag behind the prompt mono-energetic muon neutrinos released by the positive pions decaying from rest.

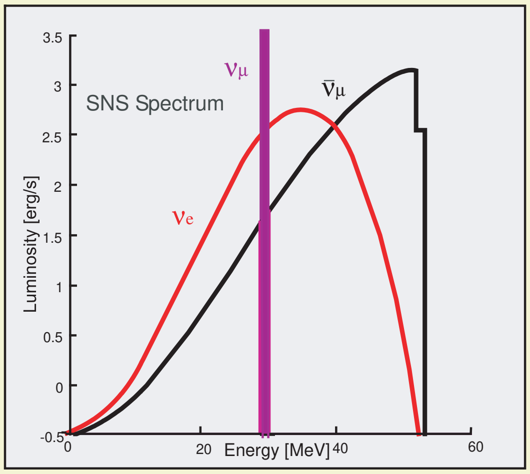

The high intensity and pulsed nature, along with the time structure of the neutrinos, will make the SNS the world's most powerful pulsed neutrino source. Located underground adjacent to the SNS, ORLaND would have adequate shielding from SNS neutrons and the hadronic component of cosmic rays. The pulsed nature of the product neutrinos would minimize hard cosmic ray muon background.

The ORLaND facility would be unique in its potential to obtain neutrino nucleus interaction data and enhance our understanding of nuclear structure and stellar astrophysics, and would be available to users from the international scientific community for dedicated neutrino and neutrino-nucleus science.

deficit' mentioned earlier. In the context of cosmology, a non-zero neutrino mass affects our understanding of galaxy formation and dark matter and influences the eventual fate of the universe.

Apart from its astrophysical and cosmological significance, the neutrino serves as a valuable probe of nuclear and nucleon structure effects. The standard valence quark or nuclear domain model of a nucleon ignores its dressing by sea quarks, predominantly virtual quark-antiquark pairs of 'strange' flavor. Neutrino-nucleus experiments can aid our understanding of the 'strangeness' content of the nucleon by providing information on its weak nucleon form factors. Effects of strangeness on the low-energy properties of the nucleon and nucleus would be exciting physics that could be investigated at ORLaND.

Experimental neutrino physics involves severe difficulties arising from the complexity of large detector systems, small event rates, and long running times. The workshop has identified a class of experiments that could be undertaken with existing technology, as described below. These are given as important examples, most of which are feasible with technologies.

- The importance of a timely experiment serving as a "Calibration of the Sun," suggests neutrino-deuteron scattering as one of the first experiments at ORLaND. The standard solar model tells us that 98.6% of the energy from the sun is generated in a complex series of nuclear reactions starting with $\mathrm{p} + \mathrm{p} \rightarrow \mathrm{d} + \mathrm{e}^+ + \nu_e$. It has been recognized for many years that a direct measurement of this cross section is extremely difficult. At ORLaND, the reaction $\nu_e + \mathrm{d} \rightarrow \mathrm{e}^- + \mathrm{p} + \mathrm{p}$ can be studied and would provide an important result for interpretations of the data from SNO.

- The strangeness content of the nucleus or the nucleon arises from the "sea" of virtual strange quark-antiquark pairs. The effect of such pairs on the low-energy properties of the nucleon is a central question in nuclear physics. A comparison of weak nucleon form factors with the values expected in the nuclear domain approximation (where the sea is ignored), can provide a direct measure of nuclear matrix elements of strange quark operators and thus probe the effects of the sea on static nuclear properties.

  Among the experiments considered is the measurement of neutrino-oxygen cross sections using a 2000 ton water Cerenkov detector. By adding $\mathrm{Gd_2Cl_4}$ to the water, one can attempt to measure the cross section of the reaction $\nu + {}^{16}\mathrm{O} \rightarrow \nu' + \mathrm{n} + \gamma + {}^{15}\mathrm{O}$ by triggering on nuclear gamma-rays, and later on the capture gamma-rays. With the addition of $\mathrm{Gd_2Cl_4}$ it is also possible to observe the gamma rays from the reaction ${}^{16}\mathrm{O} + \nu \rightarrow \nu' + \mathrm{p} + \gamma + {}^{15}\mathrm{N}$, not followed by the capture gamma rays. The ratio of proton to neutron quasielastic cross sections is uniquely sensitive to the desired axial strangeness content.

- The large Cherenkov detector could be filled with mineral oil, together with a dilute sintillator. This configuration would permit a very sensitive search for $\bar{\nu_\mu} \rightarrow \bar{\nu_e}$ oscillations, or a precise measurement of their parameters should they be found. In addition, the accurate measurement of neutron interactions on ${}^{12}\mathrm{C}$ and ${}^{13}\mathrm{C}$ could be carried out at the same time.

- The intrinsic properties of the neutrino could also be studied at any time when data are being acquired with the $\mathrm{Gd_2Cl_4}$-doped $\mathrm{H_2O}$ Cherenkov detector. For example, a very senstive search for $\bar{\nu}_\mu \rightarrow \bar{\nu}_e$ oscillations could be carried out with no added cost. While this would occur after the MiniBooNE result was known, it would serve two purposes. First, if the MiniBooNE result is positive, ORLaND would confirm it and measure the oscillation mixing and mass parameters required to build a "neutrino mass scenario." If the MiniBooNE result is negative, the ORLaND data could search parameter space ten times more sensitively than MiniBooNE using the water detector. Since neutrino electron scattering will be continuously monitored for flux calibration of the beam, one could also use it to measure the electroweak parameters like the weak angle at low momentum transfer.

- ORLaND can also provide a valuable calibration for supernova neutrino detection experiments including those probing supernova temperatures. The reaction ^{16}O + $\nu_e \rightarrow ^{16}$F+e$^-$ is dominated by the electron-neutrino capture channel for thermal sources in the 4-9 MeV range and thus provides a sensitive handle on supernova thermometry. The electron angular distribution is strongly correlated with the ν_e-energy. Measurements of double-differential cross sections, dσ/dΩdE$_e$, of this reaction using a 2000-ton water Cerenkov detector would thus be very valuable for understanding future supernova data from large detectors like SuperKamiokande and the next-generation large Cerenkov detectors. In particular, a strong yield of back-angle electron emission would require ν_e-energies far higher than those expected from standard supernova models and may imply oscillations of tau or muon neutrinos into electron flavor.

- Core collapse supernovae are among the most interesting of known astrophysical phenomena. These enormously energetic stellar explosions occur for stars of mass greater than 8 to 10 solar masses. Neutrino-nucleus interactions play a central role in supernova dynamics and in supernova nucleosynthesis. Many nuclear species participate in these processes, and the corresponding neutrino interaction cross sections are critically important inputs to the large supernova collapse modeling. To undersand this process quantitatively, several neutrino-nucleus cross sections must be measured. One possible experiment is ν_e + ^{56}Fe $\rightarrow$ e$^-$ + ^{56}Co.

  To measure this reaction at ORLaND, a fine-grained detector of iron tubes, each containing a gas proportional tube, has been modeled. This type of detector is similar in concept to the Soudan-2 detector but optimized for this measurement. Our calculations show that a detector 3.5m $\times$ 3.5m $\times$ 3.5m, weighing a total of 37-tons, having a 13.5 ton fiducial volume, could adequately measure this cross section. In addition, the following interesting targets are available in ton quantities that could also be studied using the same technique: ^{9}Be, ^{11}B, ^{27}Al, ^{40}Ca, ^{59}Co, ^{12}C, ^{28}Si, ^{51}V, ^{32}Si, ^{52}Cr, ^{55}Mn, ^{93}Nb, ^{209}Bi, ^{181}Ta, and natural Pb. Several of these detectors could be operated simultaneously.

- To aid in understanding future supernova data, UCLA and OSU have proposed using ORLaND to test and develop lead-neutron counter modules for the OMNIS supernova search detector. Neutrino–lead reactions could be studied at ORLaND as a prelude to lead perchlorate detectors that might separate ν_e and $\bar{\nu_e}$ from supernovae. These data could provide additional gauges of supernova temperatures.

- Identification of neutrinos emanating from the various semi-leptonic electroweak process in the solar interior are needed for use in fully understanding the standard solar model. The ^{8}B electron neutrinos have a distinct energy separation from the approximately one MeV ν_e produced in the ^{7}Be and p-e-p channels. A radiochemical–electronic hybrid detector has been proposed to separately and directly measure the flux of these neutrinos. The detector measures ν_e-induced charge current reactions on ^{37}Cl yielding ^{37}Ar final nuclei. The ^{8}B neutrinos produce electrons with less than or about 14 MeV of energy that generate observable Cerenkov radiation. Similar techniques may be used with ^{127}I and ^{71}Ga target nuclei. The intense low–energy pulsed neutrino beam at ORLaND would allow a much needed calibration of these reactions using small Cerenkov detectors.

Other experiments involving extensive measurements of neutral current reactions and neutrinos from decay-in-flight pions will require research and development and could come at a later stage.

2. Neutrino Physics: Summary and Motivation

2.1. Introduction

The critical importance of neutrino physics to our fundamental understanding of nature makes a compelling case for a high-intensity, pulsed neutrino facility. The rapidly increasing role of neutrinos in nuclear physics makes such a facility particularly attractive for nuclear science and its evolving growth and expansion. Through their impact on solar- and supernovae- nuclear astrophysics, semileptonic electro-weak nuclear physics, and nuclear and nucleon structure physics, neutrino interactions and their studies embrace multi-faceted areas of nuclear physics and their laboratory and cosmic significance.

Using the nucleus as a laboratory, neutrino experiments have the capability to probe the substructure of the proton and the neutron as well as to revise and extend our understanding of the Standard Model. Neutrinos are key players in the ignition of the primal p-p chain of stellar burning and the dynamics of exploding supernovae, and can provide unique information needed to further our understanding of the nuclear–astrophysics of these and other cosmological phenomena. Laboratory measurements of neutrino reactions on various nuclei are in turn equally important for the interpretation of solar neutrino data, anticipated supernova data from the Solar Neutrino Observatory (SNO) and SuperKamiokande and for improved input to the extensive modeling projects that investigate the evolutionary stages of exploding supernovae.

Intrinsic neutrino properties, such as mass, influence the dynamics of the universe through their possible contribution to dark matter. The question of neutrino oscillations between flavor states is intimately related to our understanding of the nuclear astrophysics of supernova evolution and solar neutrino signals as well as the validity of our fundamental description of nature through Standard Model.

From a nuclear physics perspective, the need for a comprehensive program on neutrino science is a timely and high-impact one. The ideal facility for such a program would be one with a generous availability of neutrinos with energies similar to those relevant for nuclear astrophysics and nuclear structure studies. The Spallation Neutron Source (SNS), under construction at the Oak Ridge National Laboratory, will produce neutrinos and antineutrinos satisfying these criteria as a natural by-product of spallation. Proposed as an underground laboratory located adjacent to the SNS target building, the Oak Ridge Laboratory for Neutrino Detectors, ORLaND, would be the world's most powerful pulsed neutrino facility, available to users from the international scientific community interested in a wide range of low-energy neutrino-nucleus physics.

2.2. Solar Neutrino Astrophysics

The mechanism by which stars—especially our sun—generate their prodigious energy has long been of interest to physicists. First proposed at the end of the 1930's by Bethe and Critchfield, the basic process is summarized via

$$4p \rightarrow {}^4He + 2e^+ + 2\nu_e + 25 \text{ MeV} \tag{1}$$

However, despite the fact that this hypothesis has been around now for over six decades, it is only recently, with the advent of large scale neutrino detectors, that direct tests of this picture have become possible.

In 1965 Raymond Davis began operating a neutrino detector that was intended to experimentally demonstrate that the Sun's emitted energy derived from the fusion of hydrogen into helium by observing the neutrino secondaries from these fusion reactions. The neutrinos were observed, but at a flux about 1/3 of that predicted by models of the solar interior. The reduced solar neutrino flux has now been confirmed by four other experiments[1]. A possible explanation for this reduced neutrino flux is that some fraction of the electron neutrinos made in the solar core transform into another neutrino species during their flight from solar core to the Earth.

2.2.1. The proton-proton reaction and its inverse

The standard solar model tells us that 98.6% of the energy from the sun is generated in the complex series of nuclear reactions included in the above

The Standard Solar Model

The Standard Solar Model is based on the following physical assumptions:

1. The Sun was formed from a homogeneous mixture of gases.
2. The Sun is powered by nuclear reactions in its core.
3. The Sun is a body in hydrostatic equilibrium, with the gravitational forces that are attempting to compress it exactly balanced by gas and radiation pressure generated internally.
4. Energy is transported from the core of the Sun, where it is produced, to the surface, where it is radiated into space, by photons (radiative transport) and by large-scale vertical motion of packets of hot gas (convection).

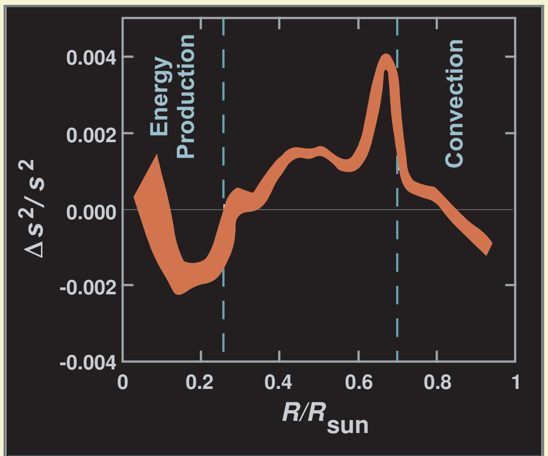

Deviation of Sound Speed in the Sun

The Standard Solar Model can be tested by whether it accounts for the general features that are observed for the Sun. More recently, it has become possible to test the model more directly through helioseismology, which infers the internal structure of the Sun from vibrational waves observed on its surface. The above right figure is based on SOHO helioseismology and illustrates the (squared) deviation of sound speed in the solar interior from that expected theoretically as a function of radius. Note that the deviations are very small and peak in two general regions: the outer part of the energy producing region, and just inside the convective zone.

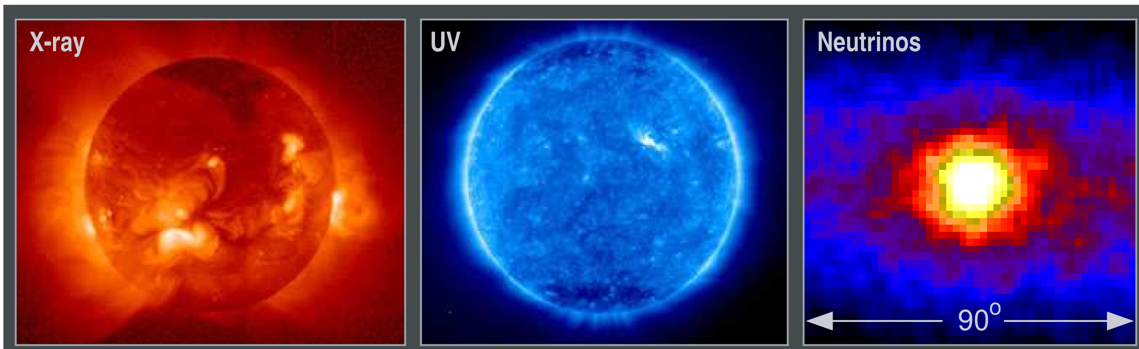

The Sun imaged in X-ray and ultraviolet light, and in secondary electrons from neutrino scattering. X-rays and UV light probe different depths of the solar surface and atmosphere, but neutrinos carry information from the central energy-producing core. The angular resolution of these images is very different. In the left two images the Sun is about 1/2 degree wide, but in the right image from Super-Kamiokande the Sun is at the center of the amorphous blob and the entire field is about about 180 times wider than the Sun.

equation. The chain starts with

$$p + p \to d + e^+ + \nu_e, \tag{2}$$

which combines an electroweak $p \to n$ conversion along with the proton-neutron fusion into the deuteron. It has been recognised for many years that a direct measurement of this cross-section is extremely difficult. However, at ORLaND, the charged current reaction $\nu_e + d \to e^- + p + p$ can be studied. While there are many ways of calculating both pp fusion and neutrino-deuteron breakup, effective field theory provides for a simple connection between the two processes at the few-percent level - a connection through a "counterterm" that is common to both reactions at this precision [2–4]. Thus, a measurement of $\nu_e + d$ at ORLaND can be used to constrain the pp fusion process in the sun. This, in turn, will contribute to our understanding of the sun as a laboratory of nuclear and neutrino astrophysics.

Over the past few decades much effort has gone into calculating the production mechanism $pp \to de^+\nu_e$, both from standard non-relativistic quantum mechanics[5], and from potential model techniques[6]. Over time, there have been a series of progressively more sophisticated calculations of neutrino-deuteron scattering, lately with the goal of providing SNO with high-precision theoretical predictions of the cross-sections in various channels [7–12]. The most sophisticated calculations, by Ying, Haxton, and Henley (YHH) [10], Kubodera and Nozawa (KN) [11], and Nakamura, Sato, Gudkov, and Kubodera (NSGK) [12], including the effects of meson exchange currents, agree with one another to within $5\% - 10\%$ for neutrino energies up to 160 MeV [11,10,12]. However, neither these calculations nor even the crucial weak matrix elements of the deuteron have been tested or constrained by experiment. It is clear that these issues warrant experimental tests.

Recent developments in nuclear theory have led to an effective field theory (EFT) for two-body systems [13–16]. This theory allows for a systematic and model-independent perturbative analysis of interactions involving two-nucleons at low-energy. Neutrino-deuteron breakup in the region relevant for solar neutrino studies is well within the domain of application of EFT [2,3]. Why is this important? The power of EFT is that it uses the known nucleon-nucleon scattering amplitudes and one-body currents directly, along with "counterterms" that represent two-body currents at small distance scales. The same counterterms can appear in many different reaction channels, and thus a high-precision measurement of one reaction can facilitate a high-precision prediction in other channels. Further, at low energies, pions can be integrated out of the theory [17] allowing for precise, analytic calculations (e.g., $np \to d\gamma$ capture in the energy regime relevant to big-bang nucleosynthesis [18,19]).

Recently, the process (2) has been examined with EFT by Kong and Ravndal [20], Park, Kubodera, Min and Rho [21], and by Butler and Chen [4]. Elegant expressions and numerical values for the weak capture cross section that are consistent with previous estimates have been obtained. The cross section depends somewhat on the value of a four-nucleon-one-weak-gauge-boson interaction, with an energy-independent coefficient $L_{1,A}$, as defined in [2]. This interaction does not contribute to nucleon-nucleon scattering (at tree-level) and therefore is not constrained by the very high precision phase shift data that is available. Butler, Chen, and Kong[2,3] have determined the neutrino-deuteron break-up cross sections with EFT and find that knowledge of $L_{1,A}$ is required in order to perform a $\sim 1\%$ calculation. The YHH and NSGK numerical results can be recovered with different choices of $L_{1,A}$, as shown in Figure 1, confirming that the difference between the potential-model calculations is short-distance in origin. Therefore, to predict the break-up cross section with a precision of better than $\sim 5\%$, one has two options. Firstly, compute the β-decay of tritium and use this to determine the EFT counterterm $L_{1,A}$, or equivalently the meson-exchange currents in potential models.[1] Secondly, one can perform an experiment to measure one of the break-up cross sections to high accuracy, and thereby extract $L_{1,A}$, or equivalently the meson-exchange currents.

An important input into determining if neutrinos are changing flavor, as they move through the interior of the sun and then to the earth, is the ratio of

[1]This method of fixing the meson-exchange currents has already been implemented for $pp \to de^+\nu_e$[6].

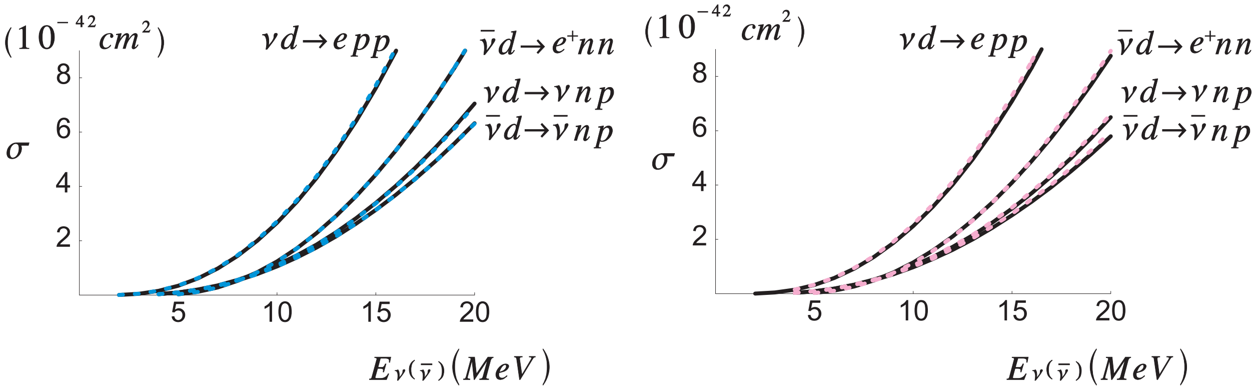

Figure 1. Inelastic $\nu(\bar{\nu})d$ cross-sections versus incident $\nu(\bar{\nu})$ energy from reference [3]. The solid curves in the left graph are NSGK results while the dot-dashed curves, which lie on top of the solid curves, are EFT with $L_{1,A} = 5.6$ fm^3. The solid curves in the right graph are YHH results while the dashed curves, which also lie on top of the solid curves, are EFT with $L_{1,A} = 0.93$ fm^3.

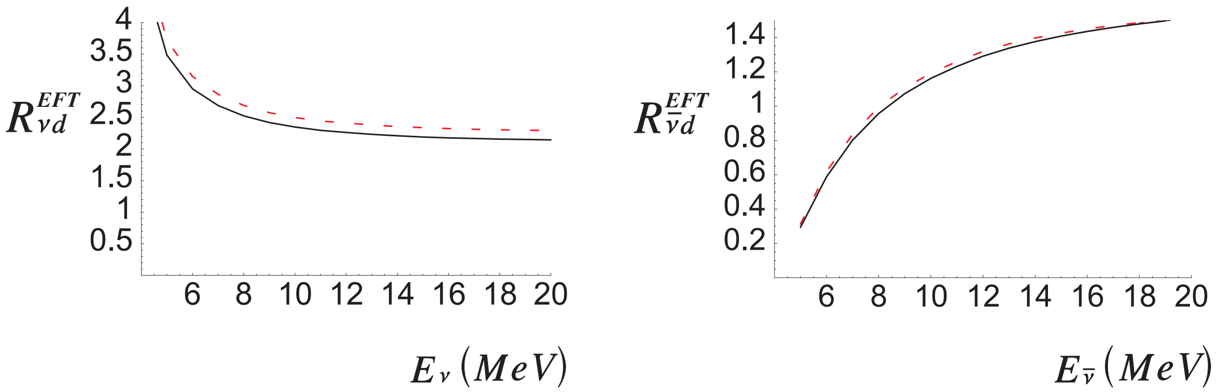

Figure 2. The ratio of charged current to neutral current cross sections in inelastic νd and $\bar{\nu} d$ scattering with $L_{1,A} = -20$ fm^3 (dashed) and 40 fm^3 (solid) from reference [3].

The Solar Neutrino Problem

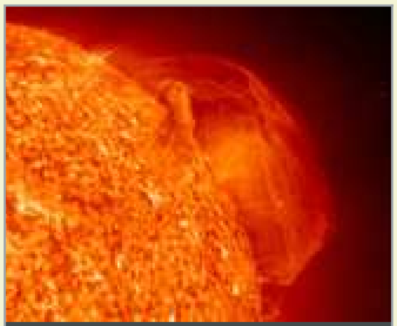

A Solar Prominence

Energy is generated at the core of our Sun through a sequence of nuclear reactions -- the pp-chains. While photons produced in these reactions take millions of years to escape the Sun, the neutrinos have few interactions after they are produced and are a direct probe of the stellar interior. The first verification that nuclear reactions power our Sun, and of the general tenets of stellar evolution, came via the detection in 1968 of high-energy neutrinos from a weak branch of the pp-chain involving the decay of ^{8}B. A few ^{37}Cl nuclei per month, out of a tank of 100,000 gallons of cleaning fluid, were transformed to ^{37}Ar nuclei via neutrino captures and subsequently measured. This capture rate was roughly a factor of 2 - 3 times smaller than predicted by theory, and the disagreement has come to be known as the "Solar Neutrino Problem". A total of five experiments have detected neutrinos from the Sun, including those from the main branch of the pp-chain, and all verify the disagreement. One experiment uses phototubes to detect Cerenkov light emitted in 50,000 tons of water to give real-time, directional information on the neutrinos and demonstrate that the neutrinos came from the Sun. Seven large-scale experiments are currently operating.

The Solar Neutrino Problem has generated intense international attention over the last decade in a wide variety of areas, including solar modeling, neutrino physics, physics beyond the Standard Model, laboratory measurements of the solar nuclear reactions, helioseismology, and plasma physics. A new generation of neutrino detectors is in development, and one -- the Sudbury Neutrino Observatory -- will measure both the charged current interaction $\;_e + d \rightarrow p + p + e$ and the neutral current interaction $\nu + d \rightarrow \nu + p + n$. The counting rate combined with the theoretical cross sections for these reactions will give, respectively, the flux of electron neutrinos and the total neutrino flux independent of flavor. Additionally, they will be able to determine the neutrino energy spectrum. The ratio of the electron neutrino flux to the total flux gives information on oscillations between the different flavors of neutrinos, and would verify the existence of physics beyond the Standard Model. Calibration of these measurements can be accomplished by an independent measurement of the cross section of the $\nu_e + d \rightarrow p + p + e$ and $\nu_e + d \rightarrow p + p + e$ reactions with a controlled neutrino source of known flux.

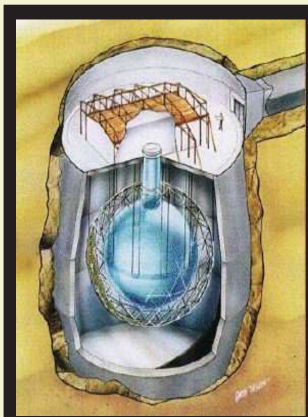

Sudbury Solar Neutrino Observatory (SNO)

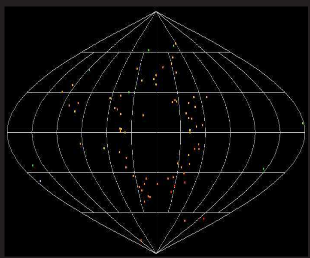

SNO Neutrino Event

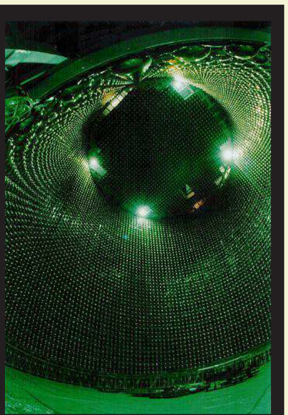

Phototubes in the Super-Kamiokande Detector charged current to neutral current cross sections. Figure 2 shows that this ratio, R_{EFT}, unlike the cross sections themselves, is relatively insensitive to the counterterm $L_{1,A}$.

The cross-sections for two neutral current and two charged current neutrino-deuteron break-up channels are listed in Table 1, parameterized by two energy dependent functions, $a(E)$ and $b(E)$,and the energy independent counterterm $L_{1,A}$, with

$$\sigma(E) = a(E) \; + \; b(E)L_{1,A}. \tag{3}$$

The magnitude of $L_{1,A}$ is estimated to be ~ 5 fm^3 by dimensional analysis and is consistent with the values favored by potential models. The uncertainty introduced by omitting higher order effects is conservatively estimated to be $\sim 3\%$ at threshold and $\sim 2\%$ at 20 MeV (using $L_{1,A} = 5.6$ fm^3 the cross-sections of ref. [12] are reproduced within $\sim 2\%$). It can be seen from Table 1 that if $L_{1,A}$ is constrained by a $\sim 1\%$ measurement of the $\nu_e d \to e^- pp$ cross-section, then the uncertainty in the other channels would also be $\sim 1\%$.

2.2.2. The ^{8}B neutrinos

Intriguing though it may be, the disappearance of electron neutrinos can never demonstrate the existence of neutrino flavor transformations, but only suggest it. What is required is the observation of non-electron neutrinos coming from the Sun. That is the goal of the next generation of solar neutrino observations. Since there is no reaction that can uniquely detect non-electron neutrinos in the solar energy range, the only viable approach is to compare the detection rate in a reaction that is sensitive to all neutrino flavors, for example neutrino-electron elastic scattering or neutral current dissociation of a nucleus such as a deuteron, with that of an electron neutrino specific reaction, namely inverse beta decay. A statistically significant difference between these two classes of measurements would indicate that there is a non-electron neutrino flux from the Sun and thus constitute an appearance observation of neutrino flavor transitions of electron neutrinos.

The flavor independent neutrino flux from ^{8}B decay in the Sun is being determined by neutrino-electron elastic scattering measurements, such as those at Superkamiokande and SNO where the relative cross section of muon neutrino scattering is 1/6 that of electron neutrino scattering. Neutrino-induced inverse beta decay, $\nu_e + n \to p + e^-$, is the unique electron detection reaction. Since free neutron targets do not exist, targets using neutrons in nuclei such as ^{37}Cl, ^{71}Ga, ^{127}I and ^{2}H are employed.

A significant difference between the above two types of measurements requires both good statistics and a precise and reliable knowledge of the relevant neutrino cross sections. It is likely that in the next few years the measurement statistics of these solar neutrino experiments will be in the 2% - 3% range. It is therefore critical that the neutrino cross sections for each of the above channels have a total precision of 2% or better.

The cross sections for energetic electron neutrinos for these targets, such as those from the decay of ^{8}B, are presently obtained from a variety of (p,n) reactions or from considerations of symmetries of nuclei, such as the A=37 system. Although the evaluation of these cross sections has been carried out with great care, it would be most reassuring to directly measure the cross sections with neutrinos in the same energy range as the ^{8}B decay spectrum. In addition to providing precise, neutrino interaction derived cross sections, these measurements will also permit a detailed comparison of interaction strengths in the quark sector with those in the lepton domain.

The precise direct calibration of these detectors with energetic electron neutrinos from the decay of stopped positive muons in the SNS beam target, will be crucial in this potential discovery process. A high neutrino flux experimental room that is reasonably close to the SNS beam target is essential to this endeavor. For example, ^{37}Cl or ^{127}I detectors with about 50 - 100 tons of target material 12 - 15 meters from the beam target should be able to obtain 1% counting statistics in a two-year exposure.

The SNS beam time structure permits separate determination of the neutrino scattering cross sections for ν_μ , and $\bar{\nu_\mu}$ and ν_e. These scattering rates together with the known cross sections can then be used to determine the neutrino flux from the SNS beam target. Another way to view these results is that at ORLaND we can measure the ratio of electron neutrino capture cross section on the

	$\nu_e d \to e^- pp$		$\overline{\nu}_e d \to e^+ nn$		$\nu_x d \to \nu_x np$		$\overline{\nu}_x d \to \overline{\nu}_x np$	
E (MeV)	a	b	a	b	a	b	a	b
2	0.00344	0.000031						
3	0.0439	0.00044			0.00315	0.000035	0.00312	0.000036
4	0.146	0.0016			0.0287	0.00034	0.0282	0.00034
5	0.320	0.0036	0.0264	0.00030	0.0885	0.0011	0.0865	0.0011
6	0.574	0.0067	0.110	0.0014	0.188	0.0024	0.182	0.0024
7	0.914	0.011	0.261	0.0034	0.329	0.0044	0.318	0.0043
8	1.34	0.017	0.482	0.0065	0.514	0.0070	0.49	0.0069
9	1.87	0.024	0.776	0.011	0.744	0.010	0.710	0.010
10	2.48	0.032	1.14	0.016	1.02	0.015	0.968	0.014
11	3.20	0.042	1.58	0.023	1.34	0.019	1.27	0.019
12	4.01	0.054	2.09	0.032	1.72	0.025	1.61	0.025
13	4.93	0.067	2.68	0.041	2.13	0.032	1.99	0.031
14	5.95	0.082	3.33	0.052	2.60	0.039	2.41	0.038
15	7.08	0.098	4.06	0.065	3.12	0.047	2.87	0.046
16	8.31	0.12	4.85	0.079	3.69	0.056	3.37	0.054
17	9.66	0.14	5.71	0.094	4.31	0.066	3.91	0.064
18	11.12	0.16	6.63	0.1	4.97	0.077	4.49	0.074
19	12.70	0.18	7.63	0.13	5.69	0.089	5.11	0.085
20	14.39	0.21	8.68	0.15	6.47	0.102	5.76	0.097

Table 1
Neutrino-deuteron inelastic cross-sections from ref. [3], parameterized by $\sigma(E) = a(E)+b(E)L_{1,A}$,where $a(E)$ and $b(E)$ have units of 10^{-42}cm^2 and $10^{-42}\text{cm}^2/\text{fm}^3$ respectively. ν_x denotes a standard model neutrino, ν_e, $\nu_\mu$or ν_τ.

various inverse beta decay targets to the neutrino electron scattering cross sections. The comparison of these ratios in the controlled SNS beam environment with the same ratio of rates from the Sun is just what is needed to search for the appearance of the neutrino flavor transitions in the solar neutrino flux.

subsectionSUPERNOVA NEUTRINO ASTROPHYSICS

Core collapse supernovae are among the most energetic explosions in the Universe, releasing 10^{53} erg of energy in the form of neutrinos of all flavors at a staggering rate of 10^{57} neutrinos per second and 10^{45} Watts, disrupting almost entirely stars more massive than 8–10 $M_\odot$ and producing and disseminating into the interstellar medium many of the elements in the Periodic Table heavier than hydrogen and helium. They are a key link in our chain of origins from the Big Bang to the formation of life on Earth; a nexus of nuclear physics, particle physics, fluid dynamics, radiation transport, and general relativity; and serve as laboratories for physics beyond the Standard Model and for matter at extremes of density, temperature, and neutronization that cannot be produced in terrestrial laboratories.

Current supernova theory revolves around the idea that the supernova shock wave—formed when the iron core of a massive star collapses gravitationally and rebounds at high (supernuclear) densities after becoming incompressible—stalls as a result of enervating losses to nuclear dissociation and neutrinos. The failure of a "prompt" supernova mechanism sets the stage for a "delayed" mechanism whereby the shock is reenergized by an intense neutrino flux emerging from the proto-neutron star at the center of the explosion. Interactions between this intense neutrino flux and the stellar layers outside the iron core define a "neutrino nucleosynthesis" in which nuclear transmutations resulting from the neutrino-induced spallation of protons, neutrons, and alpha particles produce some of Na-

Core Collapse Supernovae

During its life, a massive star (mass larger than 8-10 times the mass of the sun) undergoes a series of nuclear burning stages, building concentric shells of heavier nuclei, until silicon burning forms an iron core. Because iron and neighboring nuclei are maximally bound, continued heating and compression cannot ignite a new burning stage. Instead, when the iron core grows too large to be supported by electron degeneracy pressure, it collapses under its own gravity. Deleptonization via electron captures speed the collapse until the core reaches supernuclear densities, where it rapidly becomes incompressible and rebounds. A shock wave forms when the infalling layers above the core strike the rebounding "proto-neutron star" and are driven outwards. However, this shock wave stalls as a result of enervating losses to neutrinos and nuclear dissociation.

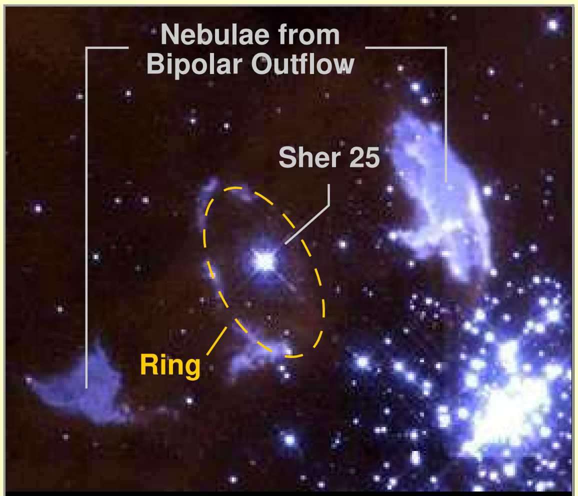

Blue Supergiant Star Sher 25

The failure of this "prompt" or "hydrodynamic" supernova shock sets the stage for the "neutrino reheating" or "delayed" mechanism whereby the shock is re-energized by the intense neutrino flux carrying off the gravitational binding energy of the newly formed proto-neutron star, driving off the stellar envelope. Explosive nucleosynthesis occurs as the shockwave propagates outward through the compositional layers built during the progenitor's life. Interactions between the intense neutrino flux and matter in the innermost of these stellar layers radically changes the local neutronization and therefore determines the isotopic content of this iron-rich ejecta. In more outer layers, nuclear transmutations resulting from the neutrino-induced spallation of protons, neutrons, and alpha particles cause "neutrino nucleosynthesis", thought responsible for some of Nature's rarest isotopes. Moreover, after the explosion is initiated, the neutrino-driven wind emanating from the cooling proto-neutron star is believed to be the key site for the astrophysical "r-process," which produces more than half of the Solar System's abundance of heavy elements and all of its transuranics. As a result, both the mechanism by which supernovae happen and the nucleosynthetic products that result are inextricably linked to the interactions of neutrinos and matter. The images on this page show a star, Sher 25, that is likely to become a supernova soon, and Chandra X-ray observations of the Cas A supernova remnant.

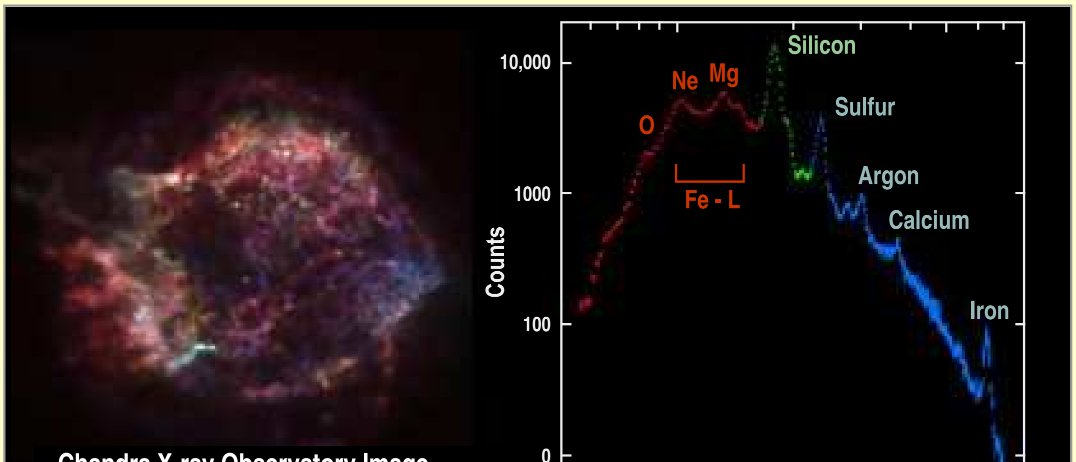

Chandra X-ray Observatory Image and Spectrum of Supernova Remnant Cassiopeia A ture's rarest isotopes. Moreover, after the explosion is initiated, the neutrino-driven wind emanating from the remnant proto-neutron star is believed to be the key site for the astrophysical "r-process," which produces more than half of the Solar System's abundance of heavy elements and all of its transuranics. Thus, core collapse supernova dynamics and core collapse supernova nucleosynthesis are neutrino-driven.

A new facility to measure judiciously chosen neutrino–nucleus cross sections would provide an experimental foundation for the many theoretically predicted cross sections needed in supernova models. We are presented with a unique opportunity, given the intensity of the SNS as a neutrino source (producing them at the rate of 10^{15} neutrinos per second) and given the overlap (shown in the figure below) between the spectra of SNS and supernova neutrinos, to make such measurements.

2.2.3. Neutrino–nucleus cross sections

Neutrino–nucleus cross sections of relevance to supernova astrophysics fall into three categories: cross sections for (1) supernova dynamics, (2) supernova nucleosynthesis, and (3) terrestrial supernova neutrino detection.

Whether or not a supernova occurs is set at the time the shock forms and the entire post–stellar-core-bounce evolution is set in motion. Where the shock forms in the stellar core at bounce and how much energy it has initially are set by the "deleptonization" of the core during collapse. The deleptonization occurs as electrons are captured on the free protons and iron-group nuclei in the core, producing electron neutrinos that initially escape. Deleptonization would be complete if electron capture continued without competition, but at densities of order 10^{11-12} g/cm^3, the electron neutrinos become "trapped" in the core, and the inverse reactions—charged-current electron neutrino capture on neutrons and iron-group nuclei—begin to compete with electron capture until the reactions are in weak equilibrium and the net deleptonization of the core ceases on a core collapse time scale. The equilibration of electron neutrinos with the stellar core occurs at densities between 10^{12-13} g/cm^3. Additionally, as the stellar core densities increase, the characteristic nuclei in the core increase in mass, owing to a competition between Coulomb contributions to the nuclear free energy and nuclear surface tension. For densities of order 10^{13} g/cm^3, the nuclear mass is of order 140. Thus, cross sections for charged-current electron neutrino capture on iron-group nuclei through mass 100 are needed to accurately simulate core deleptonization and to accurately determine the postbounce initial conditions.

Table 2.2.3 summarizes the thermodynamic conditions in the core at the three densities discussed above and gives the representative nuclear mass and charge and mean electron neutrino energy. The data were taken from a core collapse simulation carried out by Mezzacappa and Bruenn[23,24]. Electron neutrino capture would remain important until the neutrinos equilibrate with the matter, which in our simulation would occur when the representative nucleus in the core is between mass 88 and 138.

The size of the inner, unshocked core is proportional to $\langle Y_{\rm e}\rangle^2$, where $\langle Y_{\rm e}\rangle$ is the *mean* electron fraction in the inner core. Moreover, the shock loses $\sim 10^{51}$ erg of energy (an explosion energy) for every 0.1 $M_\odot$ it dissociates, which is ∼10%–20% of the total inner core mass. Thus, an ∼5%–10% change in the mean electron fraction would have a significant impact on the postbounce evolution. The mean electron fraction at bounce results from many capture reactions during infall, and it is clear that accurate electron and electron neutrino capture rates are needed and that theory must be checked against experiment even if only in a few strategic cases.

One goal of the proposed ORLaND facility will be to accurately measure the cross section for electron neutrino charged-current capture on ^{56}Fe,

$$\nu_e +^{56} \mathrm{Fe} \rightarrow e^- +^{56} Co. \tag{4}$$

Later in this document we discuss in detail a possible experiment to do this. It is among the first proposed experiments at ORLaND. Moreover, the same proposed technique to measure the cross section for electron neutrino capture on iron can be used to measure the electron neutrino capture cross section on any of the following nuclei: ^{7}Li, ^{9}Be, ^{11}B, ^{27}Al, ^{40}Ca, ^{51}V, ^{52}Cr, ^{55}Mn, ^{59}Co, ^{93}Nb, ^{115}In, ^{181}Ta, and ^{209}Bi.

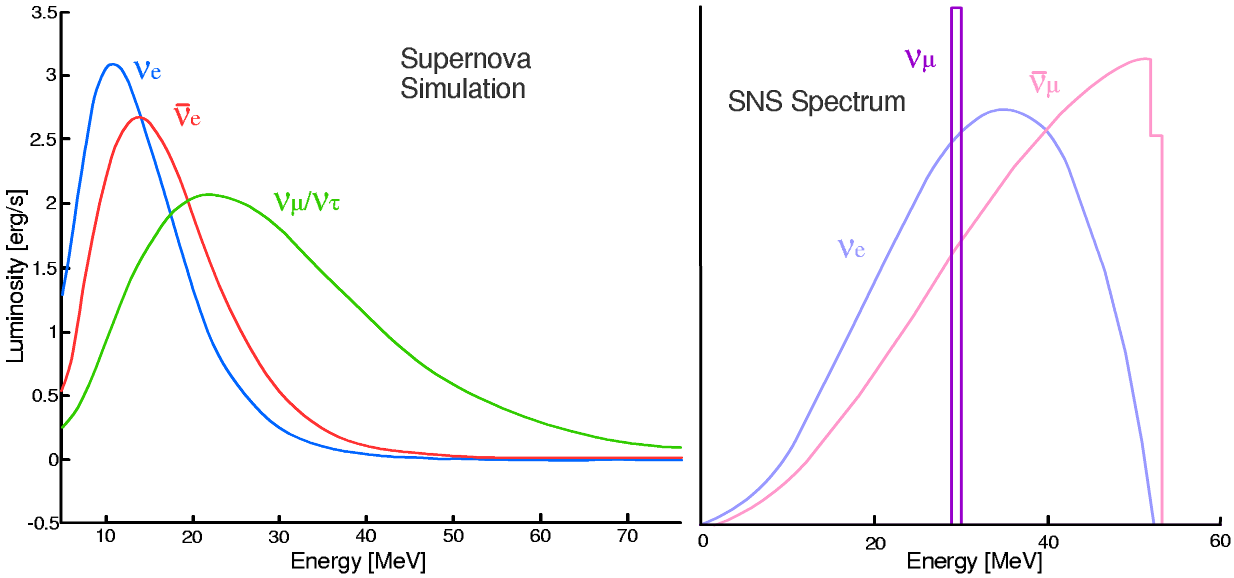

Figure 3. Supernova neutrino spectra at 100 ms after core bounce from the simulation of Liebendörfer et al.[22] (left), and the Michel spectra from the SNS (right)

Table 2
The thermodynamic conditions in the star at three densities.

ρ (g/cm^3)	$\mathrm{Y_e}$	T (MeV)	A	Z	$<\epsilon_{\nu_e}>$ (MeV)
10^{11}	0.4	1	70	30	12
10^{12}	0.35	2	88	36	19
10^{13}	0.3	4	138	52	43

2.2.4. ν–process nucleosynthesis

Neutrino nucleosynthesis is driven by the spallation of protons, neutrons, and alpha particles from nuclei in the stellar layers by the intense neutrino flux that is emanating from the central protoneutron star powering the supernova[25]. Moreover, neutrino nucleosynthesis continues after the initial inelastic scattering reactions and the formation of their spallation products. The neutrons, protons, and alpha particles released continue the nucleosynthesis through further reactions with other abundant nuclei in the high-temperature supernova environment, generating new rare species. Neutrino nucleosynthesis occurs in two stages: (1) through the neutrino irradiation and nuclear reactions prior to shock arrival and (2) through the continuation of nuclear reactions induced by neutrinos as the stellar layers expand and cool. Neutrino nucleosynthesis is thought to be responsible for the production of, for example, ^{11}B, ^{19}F, and two of Nature's rarest isotopes: ^{138}La and ^{180}Ta.

The production of the two isotopes, ^{11}B and ^{10}B, appears observationally to be linear with metalicity, i.e., primary mechanisms that operate early in the history of our galaxy produce as much of these isotopes as secondary (quadratic) mechanisms that operate after the galaxy has been enriched with metals. On the other hand, neutrino nucleosynthesis in supernovae, which is a primary process, is not expected to have produced much ^{10}B, unlike the secondary process, cosmic ray spallation. Thus, a laboratory calibration of the spallation channels producing these two isotopes can be used in conjunction with future HST observations. Discriminating between ^{10}B and ^{11}B would be invaluable in resolving this controversy and in supporting the theory that neutrino nucleosynthesis in supernovae is an important source of ^{11}B in the galaxy[26]. ^{11}B and ^{10}B are produced through the following spallation channels:

$$
\begin{aligned}
&\nu +^{12}\mathrm{C} \to \nu^{'} +^{11}\mathrm{B} + \mathrm{p},\\
&\nu +^{12}\mathrm{C} \to \nu^{'} +^{11}\mathrm{C} + \mathrm{n},\\
&e^{+} +^{11}\mathrm{C} \to \nu +^{11}\mathrm{B},\\
&\nu +^{12}\mathrm{C} \to \nu^{'} +^{10}\mathrm{B} + \mathrm{d},\\
&\nu +^{12}\mathrm{C} \to \nu^{'} +^{10}\mathrm{B} + \mathrm{pn}.
\end{aligned} \tag{5}
$$

The final abundance of ^{19}F produced in a supernova can serve as a "supernova thermometer." If the abundance of ^{19}F produced in the supernova is attributed to neutrino nucleosynthesis, the ratio of $[^{19}\mathrm{F}/^{20}\mathrm{Ne}]/[^{19}\mathrm{F}/^{20}\mathrm{Ne}]_{\odot}$ (the denominator is the measured ratio in the Sun) is a measure of the muon and tau neutrinosphere temperatures[26]. ^{19}F is produced through the following spallation channels[26]:

$$
\begin{aligned}
&\nu +^{20}\mathrm{Ne} \to \nu' +^{19}\mathrm{Ne} + \mathrm{n}\\
&^{19}\mathrm{Ne} \to^{19}\mathrm{F} + \mathrm{e}^{+} + \nu_{\mathrm{e}},\\
&\text{and,}\\
&\nu +^{20}\mathrm{Ne} \to \nu' +^{19}\mathrm{F} + \mathrm{p}.
\end{aligned} \tag{6}
$$

No obvious site for the production of the rare isotopes, ^{138}La and ^{180}Ta, has been proposed. That they can be produced via neutrino nucleosynthesis in supernovae is compelling, and may be very important in that their existence, however rare, may be a fingerprint of the neutrino process. ^{138}La and ^{180}Ta are produced through the following spallation channels: $^{139}\mathrm{La}(\nu,\nu^{'}\mathrm{n})^{138}\mathrm{La}$, and $^{181}\mathrm{Ta}(\nu,\nu^{'}\mathrm{n})^{180}\mathrm{Ta}$.

2.2.5. r-process nucleosynthesis

As the neutrino-driven wind expands rapidly and cools, charged particle reactions "freeze out" while neutron capture reactions continue on the "seed" nuclei present at freeze-out. Neutron capture (n,γ) reactions come into equilibrium with neutron disintegration (γ,n) reactions as an equilibrium is established between the free neutrons and the nuclei in the wind. The establishment of this equilibrium is then followed by beta decays, which then allow further neutron capture on the nuclei present (neutron capture on any given nucleus is limited by neutron drip, i.e., further capture on the nucleus is not possible unless it is preceded by a beta decay). The simultaneous operation of these three types of reactions in the wind and the accompanying nucleosynthesis constitutes the r-process [27].

Qian et al. [28] in both the $(n,\gamma) \leftrightarrow (\gamma,n)$ equilibrium and the "postprocessing phase" after these reactions fall out of equilibrium have demonstrated that neutrino-induced reactions can significantly alter the r-process path and its yields. In the presence of a strong neutrino flux, ν_{e}-induced charged-current reactions on the waiting point nuclei at the magic neutron numbers $N = 50, 82, 126$ might compete with beta decays and speed up passage through the bottlenecks there. Also, neutrinos can inelastically scatter on r-process nuclei via ν_e-induced charged-current reactions and ν_x-induced neutral-current reactions, leaving the nuclei in excited states that subsequently decay via the emission of one or more neutrons. This postprocessing may for example shift the abundance peak at $A = 195$ to smaller mass. Taking things one step further, Haxton et al. [29] pointed out that neutrino postprocessing effects would provide a fingerprint of a supernova r-process. Eight abundances are particularly sensitive to the neutrino postprocessing: ^{124}Sn, ^{125}Te, ^{126}Te, ^{183}W, ^{184}W, ^{185}Re, ^{186}W, and ^{187}Re. *Observed abundances of these elements are consistent with the postprocessing of an r-process abundance pattern in a neutrino fluence consistent with current supernova models.*

On a more pessimistic note, Meyer, McLaughlin, and Fuller[30] have investigated the impact of neutrino–nucleus interactions on the r-process yields and have discovered that electron neutrino capture on free neutrons and heavy nuclei (in the presence of a strong enough neutrino flux) can actually hinder the r-process by driving the neutrino-driven wind proton-rich, posing a severe challenge to theoretical models. However, the same authors point out an exciting scenario where electron neutrinos are converted to other neutrino flavors by matter-enhanced processes in the region about the neutron star surface, the large flux of antineutrinos would drive protons into neutrons ensuring a large initial neutron richness.

During the r-process and subsequent postprocessing in the supernova neutrino fluence, neutrinos interact with radioactive, neutron-rich nuclei. Thus, relevant direct neutrino–nucleus measurements cannot be made. However, indirect measurements of charged- and neutral-current neutrino–nucleus interactions on stable nuclei that serve to gauge theoretical predictions would be invaluable.

2.2.6. Supernova neutrino detection

The nineteen neutrino events detected by IMB and Kamiokande for SN1987A confirmed the basic supernova paradigm—that core collapse supernovae are neutrino-driven events—and marked the birth of extra-Solar-System neutrino astronomy. For a Galactic supernova, thousands of events will be seen by Super-K and SNO, which, for the first time, will give us detailed neutrino "lightcurves" and bring us volumes of information about the deepest regions in the explosion. In turn, these lightcurves can be used to test and improve supernova models and their offshoot predictions. Moreover, comparing these detailed neutrino lightcurves with sophisticated supernova models could provide new evidence for neutrino oscillations.

Among the neutrino–nucleus interactions of relevance for supernova neutrino detection are neutrino interactions on deuterium in SNO, ^{16}O in Super-K, and ^{56}Fe and ^{208}Pb in the proposed neutrino detector, OMNIS.

Measurement of the reaction, $\nu_e + \mathrm{d} \rightarrow \mathrm{p} + \mathrm{p} + \mathrm{e}^-$ at ORLaND, which is being considered to calibrate the reaction $\mathrm{p} + \mathrm{p} \rightarrow d + e^+ + \nu_e$ (part of the chain of reactions powering the Sun), would also provide a calibration of the SNO as a future supernova neutrino detector.

The charged-current reaction $^{16}O(\nu_e, e^-)^{16}F$ is the principal-channel for electron neutrino interactions for thermal sources in the range $T_{\nu_e} \geq 4 - 5$ MeV in water detectors, and its rate exceeds that of neutrino–electron scattering by an order of magnitude for $T_{\nu_e} \geq 7 - 9$ MeV[31]. Moreover, the electron angular distribution is strongly correlated with the electron neutrino energy, providing a way to measure the incident neutrino energy and, consequently, the electron neutrino spectra. By inference, one would then be able to measure, for example, the electron neutrinosphere temperature in a core collapse supernova, i.e., we would have a supernova thermometer. In addition, the appearance of back-angle electron emission from this reaction in, for example, Super-K would result from very energetic electron neutrinos, more energetic than predicted by supernova models. This would be evidence for flavor oscillations. Muon and tau neutrinos in the stellar core couple to the core material only via neutral currents, whereas electron neutrinos and antineutrinos couple via both neutral and charged currents. As a result, the former decouple at higher density and, therefore, temperature, and have harder spectra. *In fact, terrestrial detection of electron neutrinos at energies predicted for tau* *and mu neutrinos from a Galactic or near–extra-Galactic core collapse supernova may be our only hope of ever observing oscillations between these two neutrino flavors.*

Utilizing reactions on ^{16}O, Langanke, Vogel, and Kolbe[32] have suggested a novel way of also unambiguously identifying muon and tau neutrino signatures in Super-K. The large average energies for these neutrino flavors are sufficient to excite giant resonances via the neutral-current reactions $^{16}\mathrm{O}(\nu_{\mu,\tau},\nu^{'}_{\mu,\tau})^{16}\mathrm{O}^*$. These resonances are above particle threshold and subsequently decay via the emission of protons, neutrons, and gamma rays. The gamma rays would provide the muon and tau neutrino signatures. The decay channels are: $^{16}\mathrm{O}^* \rightarrow^{15}\mathrm{O} + \mathrm{n} + \gamma$ and $^{16}\mathrm{O}^* \rightarrow^{15}\mathrm{N} + \mathrm{p} + \gamma$.

Thus, accurate measurements of both charged- and neutral-current neutrino cross sections on ^{16}O would be foundational to interpreting the neutrino data from the next Galactic core collapse supernova and to using that data to potentially observe, for the first time, flavor oscillations involving the tau and electron neutrinos.

The use of iron and lead in OMNIS will provide yet another way of measuring neutrino oscillations in core collapse supernovae[33]. Iron has a sufficiently high threshold for neutron production via charged-current neutrino interactions that such production is negligible, whereas, in lead, neutrons are produced by both charged- and neutral-current interactions. Oscillations between the more energetic muon and tau neutrinos and the electron neutrinos would boost the charged-current event rate while leaving the neutral-current rate roughly unchanged. Thus, the ratio of the event rate in lead to that in iron would serve as an indicator that oscillations had occurred.

To develop OMNIS, experiments to measure the neutrino–iron and neutrino–lead cross sections could take place at ORLaND. For iron, the charged-current reaction,

$$^{56}\mathrm{Fe}(\nu_e,e)^{56}\mathrm{Co}^* \rightarrow^{55}\mathrm{Co} + \mathrm{n}$$

dominates. For lead, a total cross section would be measured resulting from the following neutral- and charged-current channels:

$$^{208}\mathrm{Pb}(\nu,\nu')^{208}\mathrm{Pb}^* \rightarrow^{207}\mathrm{Pb} + \mathrm{n},$$

$$^{208}\mathrm{Pb}(\nu,\nu')^{208}\mathrm{Pb}^* \rightarrow^{206}\mathrm{Pb} + \mathrm{n} + \mathrm{n},$$

and

$$^{208}\mathrm{Pb}(\nu_\mathrm{e},e^-)^{208}\mathrm{Bi}^* \rightarrow^{207}\mathrm{Bi} + \mathrm{n}$$

including the channels for the isotopes ^{206}Pb and ^{207}Pb. The iron and lead cross section measurements are described in detail later in this document.

2.3. Neutrino Oscillations and Non-Standard Model Physics

We have discussed the role of neutrinos in the various stages of stellar life-cycles and our understanding of such stellar astrophysics, as well as the efficacy of the neutrino as a probe of nuclear structure and electroweak responses of nuclei. Neutrino interactions with charged leptons open additional windows for studying the weak mixing angle and other parameters of the Standard Model. Measurements of neutrino electron cross sections at ORLaND could yield low-energy measurements of the weak angle that involve less radiative corrections than those from DIS or charged lepton experiments. Since ν - e reactions will be monitored while experiments are running for calibration of the neutrino flux, the data could be used to extract information on the weak angle. The flavor composition and time structure of the ORLaND Decay at Rest (DAR) neutrinos allow a clean determination of this parameter by using the ratios of the cross sections for the various neutrino species.

The intrinsic properties of the neutrino feature yet another facet of neutrino physics that imprints not only nuclear and electroweak astrophysics and our fundamental understanding of nature, but "literally" comprises a matter of cosmic significance. The fact or otherwise of finite neutrino mass, signaling departures from its chirality and allowing flavor-mixing in the lepton sector, is a matter of profound importance in our fundamental description of nature through the Standard Model. Extrapolating to the cosmic context, a non-zero neutrino mass affects our understanding of galaxy formation and makes the cosmic neutrino population a serious contender to hot dark matter and consequently an influential player in the evolution of the universe.

The Neutrino

Neutrinos are fermions and neutral leptons that come in three flavors and interact via exchange of weak gauge bosons and possibly gravity. Neutrinos are traditionally believed to be of zero mass. Today this has become an open question. The best evidence for non-zero neutrino mass comes from the SuperKamiokande oscillation results. The consequences of finite neutrino mass are several fold. Neutrinos can be a constituent of dark matter and can explain subtle effects associated with galaxy formation in the infant universe. It allows for the possibility of non-zero magnetic moments for the neutrino. A non-zero neutrino mass allows the possibility of a violation of Standard Model flavor conservation and flavor oscillations between the different generations of neutrinos. Flavor oscillations in turn provide the best evidence for the possible existence of neutrino mass. The consequences of oscillations are multifold and include explanations of the solar neutrino deficit and the atmospheric neutrino discrepancies. Oscillating neutrinos might also influence supernova evolution and explosion.

If neutrinos have masses, one could describe the states of observed neutrinos (see adjacent table) that interact by the electroweak gauge bosons as combinations of the mass eigenstates. A given flavor of neutrino, composed of a combination of the mass eigenstates, could then evolve over time to a different flavor. The effect can be characterized by a parameter, the oscillation length *L* which depends on the quantity generally described as δm^2, which is the difference between the squared masses of the neutrino mass eigenstates. The oscillation can be further enhanced by the MSW mechanism, which refers to matter-enhanced oscillations.

Leptons Spin = 1/2		
Flavor	Mass (GeV)	Charge
e	0.000511	-1
ν_e	$< 10^{-8}$	0
μ	0.106	-1
ν_μ	< 0.0002	0
τ	1.7771	-1
ν_τ	< 0.02	0

Weak bosons Spin = 1		
	Mass (GeV)	Charge
W^-	80.4	-1
W^+	80.4	+1
Z^0	91.187	0

Pictorally one might for instance depict the oscillations between muon neutrinos and tau neutrinos as:

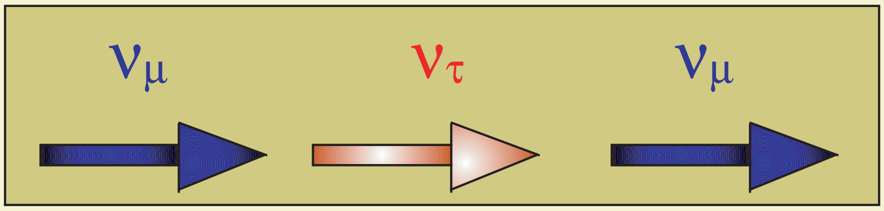

The SuperKamiokande detector experiments measured just this brand of oscillations and predict values of 3 x 10^{-3} eV^2 for δm^2 and a maximal mixing of the masses. These results are generally perceived as a dramatic development favoring the existence of oscillations. Currently several experiments are in planning or developemental stage to test this property of neutrinos and their wide-ranging consequences.

Diluting the absolute rigidity of flavor conservation in lepton hierarchy, the occurrence of neutrino mass and associated flavor-oscillations infiltrate several aspects of stellar astrophysics including our knowledge of stellar burning, evolution and explosions. The problem with the solar neutrino flux in connection with the Standard Solar Model has been a long-standing one that could be alleviated by invoking neutrino oscillations. The recent impressive evidence for oscillations according to $\nu_\mu, \bar{\nu}_\mu \rightarrow \nu_\tau, \bar{\nu}_\tau$, (or to a yet unseen sterile species), reported by the SuperKamiokande collaboration [34] is generally perceived as a dramatic development favoring the existence of oscillations. The atmospheric neutrino deficit demarcates parameter space where it would be useful to search for oscillation. The results of the approved oscillation experiments, including Miniboone, Kamland and Minos, partially motivated by the Liquid Scintillator Neutrino Detector ($LSND$) reports of $\bar{\nu}_\mu \rightarrow \bar{\nu}_e$ flavor oscillations at Los Alamos [35], will not close the issue of oscillations but restrict further the currently open options for the various models and their effective parameter space.

The strong suppression of $\bar{\nu}_e$ in the blend of neutrino species produced at the SNS makes ORLaND an attractive contender for any '$\bar{\nu}_e$ appearance' oscillation experiments. This low contamination from $\bar{\nu}_e$ arises from the high Z nature of the spallation target, mercury that rapidly absorbs negative pions by strong capture and negative muons by electroweak capture as discussed in Section III. As all other ongoing oscillation experiments focus on high-energy neutrinos, a measurement of '$\bar{\nu}_e$ appearance' at ORLaND in an intense low-energy pulsed neutrino flux has a unique appeal.

If vacuum and MSW neutrino oscillations are indeed fact, then their effects influence supernova evolution and dynamics via the explosion mechanism and nucleosynthesis channels. These effects must then be included in the codes that simulate supernova and incorporated in the interpretation of terrestrial neutrino signatures that provide information on such cosmic explosions. Muon and tau neutrinos in the stellar core couple to the core material only via neutral currents, whereas electron neutrinos and antineutrinos couple via both neutral and charged currents. The former therefore, decouple at higher density and temperature and with harder spectra. If neutrino oscillations moving higher flavor neutrinos to the electron type were to occur, muon and tau neutrinos could be converted to electron flavor and add to the heating behind the shock via charged-current absorption of electron neutrinos and antineutrinos on the protons and neutrons. The interpretation of terrestrial neutrino signatures of supernova diagnostics and thermometry are also dependent on flavor oscillations. OMNIS, the Observatory for Multiflavor NeutrInos from Supernovae, proposes to investigate such oscillations by measuring neutrino reactions in iron and lead, while backward scattering in charged current ν_e- ^{16}O scattering provides a mode of supernova thermometry. Such reactions could be measured at ORLaND, and the general compatibility in energy of the ORLaND neutrinos with those relevant for stellar astrophysics makes it a good laboratory for understanding supernova and solar neutrino physics.

Signatures other than oscillations of physics beyond the Standard Model could be probed by searching for rare decay modes of the neutral pion and η mesons at ORLaND if a Decay in Flight (DIF) beam is constructed. Additional studies of oscillation physics could also be undertaken at a future DIF facility.

2.3.1. Status of neutrino oscillation experiments

Presently there are three experimental indications of possible neutrino oscillations: the atmospheric neutrino anomaly, solar neutrino deficit, and LSND effect.

At present due to the very impressive results from the SuperKamiokande detector, neutrino oscillations is a leading hypothesis to explain the atmospheric neutrino anomaly. The best fit of SuperK data for muon and electron neutrinos is for ν_μ to ν_τ oscillations with mixing parameters of $\delta m^2 = 3 \times 10^{-3}\ eV^2$ and $\sin^2 2\theta = 1$. The same region of parameter space, however, with a much larger uncertainty, is favored for the Soudan2 neutrino events, as well as the angular distribution of up-going muons for the MACRO and SupeKamiokande detectors. SuperKamiokande data disfavors at a 99% confidence level the hypothesis of the oscillation of muon neutrinos to sterile ones. Running at present, the K2K long baseline experiment has so far 27 muon neutrino events with 40.3 expected, which implies the same region of oscillation parameters as that of atmospheric neutrinos. MINOS - another long baseline experiment, presently under construction, will cover this region in more detail in the future.

The solar neutrino deficit, or the disappearance of ν_e neutrinos on their way from the sun's core, is seen by many experiments with different detection techniques, namely Chlorine, Gallium, and water Cherenkov detectors. The distinguishing feature of those experiments is that they have different neutrino detection thresholds. A global fit of three sets of experiments produced three different solutions for ν_e oscillations: one set of parameters for vacuum oscillations and two sets of parameters for matter-enhanced oscillations, large mixing (LMA) and small mixing (SMA) MSW solutions. Recent results from the SuperKamiokande detector on the day/night assymetry of the solar neutrino flux gives strong evidence against the vacuum and SMA solutions. The present best fit of the solar neutrino data implies LMA oscillations of ν_e to ν_μ or ν_e to ν_τ neutrinos with parameters of δm^2 between 2×10^{-5} and 1×10^{-4} eV^2, and $\sin^2 2\theta = 0.9$. The SuperKamiokande data at the 95% confidence level disfavors oscillation of solar ν_e to sterile neutrinos. The long baseline reactor neutrino experiment, KamLAND, should be on line in 2001 and will have a sensitivity to cover the LMA solution of solar neutrinos. The novel SNO heavy water detector is sensitive to the all neutrino flavors. It will be able to give a definite unswer to the question, is the solar neutrino deficit due to oscillations or to some yet unknown process?

The third indication for neutrino oscillations is the positive result of the LSND collaboration on the appearance of $\bar{\nu}_e$ neutrinos. The region of parameters has a central value around $\sin^2 2\theta = 10^{-2}$ and δm^2 between 1 and 0.2 eV^2. The latest result from the KARMEN experiment at ISIS excludes about half of the LSND region. The experiment is still running, however will not have enough sensitivity to eliminate the allowed region completely. The MiniBooNE experiment, which is now under construction at FNAL, is designed to test the LSND region of neutrino oscillation parameters. ORLaND at the SNS, because of the low intrinsic contamination of the beams by $\bar{\nu}_e$ from μ^- decay, will have an order of magnitude better sensitivity than MiniBooNE.

2.4. Nuclear Strangeness

Elastic form factors of the nucleon provide information on matrix elements of current quark operators, which in turn describe the underlying electric, magnetic, and axial spatial distributions of quarks. The Standard Model *exactly* relates weak and electromagnetic vector form factors, at all momentum transfers, in the so-called "nuclear domain" approximation, where only up and down quarks contribute to nucleon structure, and isospin symmetry is assumed. However, there has been considerable recent discussion of the possibility that strange quark content of the nucleon may not be entirely negligible[36]. This strangeness content arises from the "sea" of virtual $q - \bar{q}$'s, the effect of which on low-energy properties of the nucleon is a central question of QCD (or effective models of the nucleon inspired by, or derived from, QCD.) Thus, a precise comparison of weak nucleon form factors with the values expected in the nuclear domain approximation can provide a direct measure of matrix elements of strange quark operators in the nucleon, and thus a direct measure of the effects of the sea on static properties of the nucleon.

At ORLaND, the most promising such measurement would be the elastic axial form factor, $G_A^Z(Q^2)$, at low momentum transfer. In the Standard Model, the axial current operator at tree level is pure isovector, and is thus related by a simple isospin rotation to the (known) charge changing axial current. The difference between $G_A^Z(Q^2)$ and $G_A^W(Q^2)$ (i.e. the corresponding charge changing matrix element, obtained at low Q^2 directly from β-decay or from charge changing neutrino cross sections) measures the strange axial form factor, $G_A^s(Q^2)$ assuming only strong SU(2) isospin symmetry at the nucleon level. Earlier attempts to measure G_A^s include polarized deep inelastic scattering of electrons, and moderate energy $\nu - p$ elastic cross sections at BNL. Unfortunately, both results require theoretical inputs (including SU(3) and Q^2 evolution in the case of DIS, and Q^2 extrapolation for BNL) which result in significant uncertainty in the extracted value of $G_A^s(0)$, the axial strange charge of a nucleon at rest.

A ν-p elastic cross section at low Q^2 at ORLaND would provide a clean and significant measure of $G_A^s(0)$. Experimentally, the detection of low-energy recoil protons from a decay at rest neutrino spectrum is extremely challenging; such a measurement would be considerably easier with the slightly higher energies available from a decay in flight (DIF) neutrino spectrum. The issues of integration over energy spectrum, and the theoretical uncertainties arising from final state interactions involved if the proton originates from quasielastic scattering off target nuclei, are both significant. The possibility of measuring the ratio R=$\sigma(\nu,\nu'p)/\sigma(\nu,\nu'n)$ of proton to neutron quasielastic cross sections would be extremely valuable for providing a more accurate measure of $G_A^s(0)$. In the ratio, FLUX normalization, final state interactions, and Q^2 dependence of the axial form factor all cancel to leading order. The ratio is thus uniquely sensitive to the desired axial strangeness content, and would be of considerable interest for this study of low energy QCD and nucleon structure.

2.4.1. Strangeness of the nucleon

The subject of the strangeness content of the nucleon is one of intense current theoretical and experimental interest [36]. A naive "valence-quark" picture of hadrons states that the nucleon consists solely of u and d quarks. Such a constituent quark picture provides qualitative understanding of the spectrum of baryons and mesons, including masses, magnetic moments and radii, couplings, decays, etc. However, there exist various hints that some low-energy properties of the nucleon cannot be understood within such a simple valence picture - the "sea" of heavier quarks may play an essential role in some observables. Since the net strangeness of the nucleon is zero, strange quarks can *only* manifest themselves in the sea, so any measurement of an operator involving purely strange quarks in the nucleon provides invaluable insight into the role of the sea in the static structure of hadrons.

One of the original motivations for work in this area was that analysis of the pion-nucleon sigma term[37] coupled with experimental study of inclusive spin-dependent structure functions of the nucleon in the DIS region.[38] This suggested the possibility that a significant fraction of the nucleon mass may be generated by $\bar{s}s$ sea effect, and that a sizable fraction of the momentum and spin of the nucleon are carried by the sea[39]. One expects, in the limit of vanishing quark masses, that the nucleon mass should approach some nonzero value M_0. In the real world, with nonzero quark mass, the nucleon mass is modified to become

$$M_N = M_0 + \sigma_s + \sigma \tag{7}$$

where, defining $\hat{m} = (m_u + m_d)/2$,

$$\sigma_s = \frac{1}{2M_N}\langle N|m_s\bar{s}s|N\rangle \tag{8}$$

$$\sigma = \frac{1}{2M_N}\langle N|\hat{m}(\bar{u}u + \bar{d}d)|N\rangle \tag{9}$$

are the contributions to the nucleon mass from strange, non-strange quarks respectively. One constraint in this regard comes from study of the hyperon masses, which yields

$$\begin{aligned}\delta &= \frac{\hat{m}}{2M_N}\langle N|\bar{u}u + \bar{d}d - 2\bar{s}s|N\rangle \\ &= \frac{3}{2}\frac{m_\pi^2}{m_K^2 - m_\pi^2}(M_\Xi - M_\Lambda) \simeq 25MeV \end{aligned}\tag{10}$$

and increases to about 35 MeV when higher order chiral corrections are included. A second constraint comes from analysis of πN scattering, which says that σ can be extracted directly if an isospin even combination of amplitudes could be extrapolated via dispersion relations to the (unphysical) Cheng-Dashen point

$$F_\pi^2 D^{(+)}(s = M_N^2, t = m_\pi^2) = \sigma \tag{11}$$

When this is done the result comes out to be ~60 MeV, which is lowered to about 45 MeV by higher order chiral corrections. If $\langle N|\bar{s}s|N\rangle = 0$, as might be expected from a naive valence quark picture, then we would expect the value coming from the hyperon mass limit and that extracted from πN scattering to agree. The fact that they do not can be explained by postulating the existence of a moderate strange quark matrix element

$$f = \frac{\langle N|\bar{s}s|N\rangle}{\langle N|\bar{u}u + \bar{d}d + \bar{s}s|N\rangle} \simeq 0.1 \tag{12}$$

implying $M_0 \simeq 765$ Mev and $\sigma_s \simeq 130$ MeV, which already indicates a modest contribution of strange quarks to the structure of the proton. Some recent analyses have suggested a rather larger value of the sigma term, leading to $f \simeq 0.2$, $M_0 \simeq 500$ MeV and $\sigma_s \simeq 375$ MeV, which appear surprisingly large. This problem is ongoing, and much theoretical work has been done in the subject of strangeness content of the nucleon[40].

In any case it is of interest to study the possibility of a significant strange quark matrix element in other contexts. One quantity which has been extensively studied is the nucleon electromagnetic matrix element, which has the form,

$$\begin{aligned}
&\langle N|V_\mu^{em}|N\rangle \\
&= \langle N|\frac{2}{3}\bar{u}\gamma_\mu u - \frac{1}{3}\bar{d}\gamma_\mu d - \frac{1}{3}\bar{s}\gamma_\mu s|N\rangle \\
&= \bar{u}(p')\{\gamma_\mu(F_1^{ns}(q^2) + F_1^s(q^2)) \\
&\quad -\frac{i}{2M_N}\sigma_{\mu\nu}q^\nu(F_2^{ns}(q^2) + F_2^s(q^2))\}u(p). \quad (13)
\end{aligned}$$

One can look for the existence of strange quark pieces $F_1^s(q^2), F_2^s(q^2)$ in parity-violating electron scattering. This has been done in the forward direction by the HAPPEX experiment at JLab[41] and in the backward direction by the SAMPLE experiment at MIT-Bates[42]. The HAPPEX result is consistent with $\langle r_E^2\rangle^s = 0$, although the measurement is at sufficiently high momentum transfer ($Q^2 = 0.48\text{GeV}^2$) that some (uncertain) extrapolation to $Q^2 = 0$ is required. Meanwhile the Bates result presently indicates a positive value for $F_2^s(0) = \mu_s$, the vector magnetic strangeness matrix element. [43] This result is somewhat sensitive to radiative corrections in the additional *axial* contributions to the asymmetry, which are rather uncertain[44]. Indeed, a preliminary experimental estimate of the axial corrections from quasielastic parity violation on deuterons may result in a significantly less positive value for μ_s.

Another independent probe for nucleon strangeness comes from the realm of deep inelastic electron scattering wherein, defining the quark helicity content Δq via

$$\Delta q\sigma_\mu = \langle p,\sigma|\bar{q}\gamma_\mu\gamma_5 q|p,\sigma\rangle \quad (14)$$

one has the constraint

$$\begin{aligned}
\int_0^1 dx g_1(x) &= \frac{1}{2}\left[\frac{4}{9}\Delta u + \frac{1}{9}\Delta d + \frac{1}{9}\Delta s\right] \\
&\times \; (1 - \frac{\alpha_s(q^2)}{\pi}). \quad (15)
\end{aligned}$$

When combined with the Bjorken sum rule and its SU(3) generalization

$$\begin{aligned}
\Delta u - \Delta d &= g_A(0) = F + D \\
\Delta u + \Delta d - 2\Delta s &= 3F - D \quad (16)
\end{aligned}$$

one finds the solution,

$$\begin{aligned}
\Delta u &= 0.81, \\
\Delta d &= -0.42, \\
\Delta s &= -0.11, \quad (17)
\end{aligned}$$

indicating a small negative value for the axial strange matrix element.

The axial strangeness matrix element extracted (above) indirectly by polarized DIS at high Q^2 can be measured more directly at low Q^2 via neutral current neutrino scattering. The form of the elastic matrix element of the standard model axial current is

$$\begin{aligned}
&\langle N|\bar{u}\gamma_\mu\gamma_5 u - \bar{d}\gamma_\mu\gamma_5 d - \bar{s}\gamma_\mu\gamma_5 s + \ldots|N\rangle \\
&= \bar{u}(p')\left[G_A^Z(Q^2)\gamma_\mu\gamma_5\right]u(p) \quad (18)
\end{aligned}$$

where we neglect the contributions of quark flavors heavier than s. The axial neutral current is purely isovector in the case that the strange matrix element vanishes and can therefore be exactly predicted from the known charged current axial matrix element, assuming only good SU(2) symmetry for the nucleon. A conventional (phenomenological) dipole fit for the axial charge changing form factor gives

$$G_A^Z(Q^2) \approx 1.262/(1 + Q^2/M_A^2) + G_A^s(Q^2) \quad (19)$$

A moderate energy elastic ν-p experiment was performed at BNL over a decade ago and yielded a result[45] $G_A^s(Q^2 = 0) = .15 \pm .09$. The data was extrapolated from $Q^2 = 0.5 - 1.0$ GeV^2 to $Q^2 = 0$, and the resulting value for $G_A^s(0)$ is highly correlated with the assumed value of the axial dipole mass (obtained from charge changing neutrino-nucleon form factors) $M_A = 1.032 \pm .036$

GeV. The result for $G_A^s(0)$ is consistent with that for Δs found from the deep inelastic sector, but a more precise value is clearly needed.

Most of the experiments mentioned above have yielded surprisingly large strangeness matrix elements in the nucleon, but none of the results is unambiguous. From the point of view of theory, there are a wide variety of models of single-nucleon structure, ranging from attempts to solve QCD numerically (on a lattice) to dispersion, loop, chiral models, Skyrme approaches, and more. There is not a clear consensus among the models with regard to strangeness form factors. E.g, the model predictions for the vector magnetic strangeness matrix element μ_s range from -0.8 to +0.5 nuclear magnetons (with the majority of models predicting negative values, in disagreement with the published SAMPLE result). Clearly, there is strong motivation for improved experimental measurement of all the strangeness matrix elements.

At ORLaND, there are several possibilities for extracting a strangeness matrix element of the nucleon. The semileptonic $\nu - p$ reaction provides a direct measure of the axial nucleon form factor at low Q^2, G_A^Z, so the axial strangeness contribution G_A^s is the most likely candidate for measurement. This is in contrast to parity violating electron scattering experiments at low Q^2, where the axial nucleon form factor is always associated with the vector electron coupling constant, $1 - 4\sin^2\theta_W \approx 0.1$. Neutrino cross sections thus provide a much cleaner means to learn about G_A^s. There is another important advantage to ν cross sections in this regard: next to leading order radiative corrections in parity violation experiments are significantly larger (arising from photon-couplings), and less under theoretical control than the corresponding one-loop radiative corrections in ν scattering.

The neutrino cross section at low energy, expanded to leading order in energy, is [46]

$$d\sigma(\epsilon)/dQ^2 = (G_\mu^2/8\pi)\{(1+\rho^2)(G_A^Z)^2 - 4\rho\sqrt{\tau}[\frac{1}{2}((G_A^Z)^2 + (G_E^Z)^2) \mp (G_A^Z)(G_M^Z)] + (1-\rho^2)(G_E^Z)^2\} \tag{20}$$

where $\rho \equiv \sqrt{\tau}(m_N/\epsilon)$, or equivalently, $\rho = \sqrt{Q^2/4\epsilon^2} = \sqrt{1+\tau}\cos\theta_N - \sqrt{\tau}$. Here, ϵ=incident neutrino beam energy, $\tau = Q^2/(4m_N^2)$, and θ_N is the scattered (recoil) nucleon angle. Unfortunately, this inclusive elastic cross section is not directly measurable, since the recoil neutrino is unobservable. Instead, one must measure the recoil nucleon and average over the incident neutrino spectrum. With a nuclear target, if one is looking at the (closely related) quasielastic emission of nucleons, the measurement is not a conventional inclusive cross section, but is more analogous to a coincidence (semi-inclusive) electron scattering experiment where the scattered electron is not detected. Furthermore, the effects of final state interactions for quasielastic scattering will significantly modify this cross section, and must be taken into account.

For low-incident energy neutrinos, this cross section is insensitive to the electric strangeness radius of the nucleon, is moderately insensitive to the vector magnetic strangeness moment, is only slightly sensitive to the axial dipole mass, M_A, and is comparatively strongly sensitive to the strangeness axial form factor. E.g, at $\epsilon = 150$ MeV, and $Q^2 = .05$ GeV^2, a variation in M_A of $\pm 3\%$ only changes the neutrino cross section by approximately 1%, whereas a variation in $G_A^s(0)$ of $\pm .09$ changes the neutrino cross section by 10% (the antineutrino cross section by 15%).

This example assumes an energy appropriate to a DIF neutrino source. At the significantly lower energies of a stopped pion neutrino source, the uncertainty due to M_A is completely negligible, and one is almost completely sensitive to the desired $G_A^s(0)$. Unfortunately, at such low energies, the recoil proton will have less than 5 MeV of kinetic energy, making this more challenging experimentally. This low-energy channel should probably be investigated further. The fast beam-spill structure of the SNS will suppress cosmic rays and may allow a "looser" trigger requirement. This unique property of the SNS together with a fine segmented detector could provide the necessary tools for a DAR ν-p elastic scattering cross section measurement.

Given a DIF neutrino source, an extremely interesting possibility would be to measure the *ratio* of quasielastic proton knockout to neutrons[46]. In such a ratio, the beam flux normalization effectively cancels, and more importantly, theoretical calculations indicate that the final state interaction corrections in numerator and denominator *also* cancel to a large extent. The sensitivity to M_A also largely cancels. Formally, the ratio determines

$$\sigma(\nu,\nu' p)/\sigma(\nu,\nu' n) \approx 1-(16/5)G_A^s, \quad (21)$$

and thus provides a clean, sensitive measure of G_A^s.

It is noteworthy that the recoil energy of protons from ^{12}C nucleus can be higher than that of the $\nu-p$ elastic. This is because of the Fermi momentum of the nucleus, typically about 220 MeV/c for light nuclei. Experimentally one has to trigger on high energy protons, for example, those with energy above 60 MeV. In a fine segmented detector neutrons and protons can be identified by two heavily ionizing tracks with and without associated energy, respectively. Here again a detector with good energy resolution will be required in order to minimize the uncertainties with the energy cuts affecting the cross section ratio just described.

2.4.2. Strangeness allowed transitions

An alternative, if slightly less direct, method to search for evidence of nonzero hadronic matrix elements of the strange axial current operator is to look for isoscalar transitions from a nuclear ground state to specific excited states[47]. In general, one expects the axial matrix element to dominate for an allowed M1 transition, but since the axial current operator at tree level is pure isovector, the exclusive transition cross section for a T=0 ground state to T=0 excited state will then be allowed by the presence of the strangeness (isoscalar) axial current. There are several difficulties associated with this method which must be taken into account. First, most T=0 excited states for light nuclei lie at fairly small excitation energy. One must resolve the resulting state experimentally from, e.g., nearby T=1 states which are more strongly coupled to the ground state. For single photon decays, this would require energy resolution of order a few MeV. Second, one needs to consider the possibility of admixtures of T=1 into the nominally T=0 excited state. If there are nearby levels, a careful calculation of these more conventional isospin breaking admixtures will be essential to then extract the remaining contribution from the strangeness current.

Large A nuclei tend to have a high density of excited states, which makes both of the above problems increasingly serious. Thus, one should use light nuclei with the desired properties. E.g, ^7Li has a T=0 ground state, with a T=0 (Δ J=1) excited state at 4.31 MeV. The primary decay, unfortunately, is via deuteron or alpha emission, which would be difficult to detect. The nearby 5.37-MeV T=1 state is close enough to provide a possible small isospin admixture in the excited state. The decay photon energy difference between these two T=1 excited states would need to be resolved experimentally to reliably yield the strangeness contribution. Another possibility is ^{10}B, which has a T=0 ground state, with a T=0 excited state at 3.6 MeV. Here, the 5.2 MeV T=1 state admixtures must still be calculated. Similarly, ^{12}C has a 12.7 MeV T=0 state with a measurable photon decay (2% b.r.). The primary concern would be calculating the admixture from the T=1 level at 15.11 MeV. Considerable additional study, both of the theoretical interpretability, and the experimental feasability, is clearly still required for such a measure of strangeness in nuclei. As mentioned earlier, a fine segmented detector may allow resolving the 15.11 and the 12.7 MeV states in ^{12}C.

2.4.3. Elastic (coherent) nuclear scattering

A final, more exotic possibility to search for strangeness in the nucleus, this time in the vector sector, would involve elastic neutrino scattering off nuclei. Experimentally, this is extremely challenging, but from a theory point of view, the observable is interesting. Consider, e.g., elastic scattering from ^4He. This spin-0 target has only one (electric) form factor. The peak cross section for a ν beam energy of 150 MeV is about $d\sigma/d\Omega = 4.6{\cdot}10^{-41}$ cm^2 sr^{-1}. This cross section is proportional to the (well-known) elastic electromagnetic nuclear form factor, times the (well-known) weak isoscalar-vector coupling (-2$\sin^2\theta_W$), times a correction factor involving isospin-breaking, which can be written as $1+\gamma(q)$[36,48]. Due to gauge-invariance, and zero net strangeness of the He nucleus, $\gamma(q)$ vanishes as $\gamma_0\tau$. γ_0 has two primary components - a piece from electromagnetic isospin admixtures in the ground state, and a strange electric form factor contribution. Donnelly's estimate of the isospin admixtures [48] gives a contribution of 0.04 to γ_0, while Jaffe's estimate of strange electric radius of the nucleon [49] contributes 100 times as much. Jaffe's prediction is admittedly on the extreme high end of theoretical estimates for the strangeness electric radius. On the other hand, there is a possibility of enhancements of strangeness content in the nuclear medium. For $Q^2 = 0.045$, this correction is only a few percent on the absolute cross section. For heavier nuclei, the relative correction from electromagnetic isospin admixtures becomes correspondingly larger[48]. Thus, coherent neutrino scattering cross sections would need to be measured with absolute normalization at the few percent level to allow any hope of extracting information on the strangeness radius in this way.

A precise measurement of the cross section for $\nu_e d \to ppe^-$ at low energies will do more than provide an absolute normalization of the rate for $pp \to de^+\nu_e$ and the cross sections for other neutrino-deuteron break-up processes. The SAMPLE experiment at MIT-Bates has measured electron-deuteron parity violating breakup at energies higher than currently accessible to EFT. One of their goals is to study strangeness in nucleons, with the deuteron serving as a "neutron target" for lower energy measurements. However, two-body currents complicate the interpretation of data directly in terms of neutron properties. Given that these two-body currents are again described by $L_{1,A}$ at low-energies, a determination of $L_{1,A}$ will improve understanding of more complicated electroweak processes and shed light on the role of the strange quark in nuclear systems.

From the astrophysical point of view, a measurement of coherent neutrino scattering in nuclei would be quite welcome as this is the dominating neutrino trapping mechanism in a core collapse supernova.

2.5. Nuclear Structure Issues

Neutrino-nucleus reactions at ORLaND will require nuclear theory input in order to interpret experimental data. Both neutral- and charged-current reactions will excite nuclei to states that decay by particle and/or gamma emission depending on whether the neutrino excites the nucleus above the nucleon emission thresholds. Since ORLaND will, in its DAR mode, be primarily a low-energy neutrino laboratory, several nuclear physics inputs will be needed in order to understand the experimental results: 1) neutrino-nucleus cross sections are determined by the correlations in the nuclear ground- and excited-states. Since the neutrinos from ORLaND will excite nuclear levels (particularly in the charged-current reactions), an accurate description of the nuclear structure in the target nuclei will be important to precisely calibrate the cross sections. 2) The neutrino reactions will in many cases excite nuclei beyond the particle-emission thresholds. Understanding the particle decay modes and predicting the decay widths by using statistical decay models will be crucial in order to determine the experimental signatures one should expect to see. This second step requires the implementation of a statistical model (such as SMOKER [50]) that considers proton, neutron, α, and γ emission from each final state that has well defined angular momentum, energy, and parity. As possible final states in the residual nucleus, the SMOKER code considers the experimentally known levels supplemented at higher energies by an appropriate level density formula [50].

We now turn to the more difficult problem of calculating the neutrino-nucleus cross sections.

2.5.1. Cross sections

The neutrino reactions at ORLaND energies and below proceed largely through a few multipoles with $J \leq 3$. Thus a limited number of nuclear operators determine the cross sections, and information about their matrix elements can be extracted from the other kinds of experiments, in which kinematics are better controlled. Finally, the strength in the few important multipoles is often concentrated in collective nuclear resonances, which usually have relatively simple structure, are subject to sum rules, and can be modeled effectively through, e.g., the random phase approximation or the shell model. The important resonances in (ν, e^-) reactions are the allowed $J^\pi = 1^+$ Gamow-Teller (GT) mode, and the forbidden 1^- dipole and 0^- – 1^- – 2^- spin-dipole (SD) modes. In neutral current reactions, the analogs of these resonances are the most important. Just knowing where such states are centered takes us a long way towards accurate calculations of reactions with supernova neutrinos.

The formalism necessary to calculate total and differential neutrino cross sections on nuclei has been known for many years [51]. As an example, the charged-current cross section at a given incident neutrino energy E_ν is

$$\begin{aligned}\sigma_{CC}(E_\nu) &= \frac{G}{2\pi}\int_{-1}^{+1} d\cos\theta \\ \times\ \delta(E_i - E_f + E_\nu - E_l)p_l E_l \mid M \mid^2 ,\end{aligned} \quad (22)$$

where E_i and E_f are initial and final energies of the nuclear states involved, E_l and p_l are the energy and momentum of the emitted lepton, p_ν is the neutrino momentum, and $\cos\theta = \frac{p_l \cdot p_\nu}{|p_l||p_\nu|}$. The reduced matrix elements of the transition matrix element M, connects states i and f

$$M_{fi} = \sum_{ab} \psi_{fi}(ab)\langle a \mid \Omega(q) \mid b\rangle, \quad (23)$$

where a and b are single-particle labels of the individual nucleons in the nucleus. We represent the expansion of the weak interaction in terms of multipoles Ω^{JT} of a given spin and isospin (JT) multipolarity. We note that Ω carries a momentum transfer dependence q. The one-body matrix elements $\langle f \mid\mid \Omega^{JT} \mid\mid i\rangle$ were tabulated [52], and are readily calculable. The more difficult computation involves the one-body density matrix elements which are calculated between the final and initial nuclear *many-body* states.

2.5.2. Methods of solution to the nuclear many-body problem

Various approaches to solutions of the nuclear many-body problem exist. For light nuclei ($A \leq 8$) Greens Function Monte Carlo methods have been employed to solve for ground-state properties using realistic two- and three-nucleon interactions [53,54]; however, these methods are limited to light systems and have not been developed for calculating scattering cross sections to highly excited states.

The shell model provides a tractable solution to the nuclear many-body problem in a truncated model space. Thus one divides the complete Hilbert space into an active and inactive space. The active space is usually referred to as the valence space. One natural form of truncation is to work in a major oscillator shell. For example, if we choose ^{40}Ca as a core of inactive nucleons, we can work in the region of $21 \leq N, Z \leq 39$. Thus, by solving the resulting eigenvalue problem for a given nucleus, we obtain detailed information concerning its spectroscopy and one-body density matrix.

One must necessarily use many-body perturbation theory to project the realistic nucleon-nucleon interaction into the model space [55]. This approach, while theoretically correct, encounters problems for nuclei towards the mid-shell. In light nuclear systems such as ^{12}C, it is possible to obtain directly from experimental data enough information to fit nuclear matrix elements [56]. This is also possible in the *sd*-shell (nuclei from ^{16}O to ^{40}Ca) [57]. Over the years, good effective interactions have also been developed for the *fp*-shell (iron group nuclei) [58].

Even in cases where reasonable effective interactions are available, one always faces the explosion in the dimension of the many-body basis in which one must diagonalize the effective Hamiltonian. Increasing computer power allows one to incrementally solve for larger problems by diagonalization. Alternate methods of solution based on quantum Monte Carlo techniques have been developed and used in regions where standard diagonalization could not at the time be successfully applied [59]. Another complication comes when one extends calculations beyond one major oscillator shell. In such cases, contamination from spurious center-of-mass effects must be corrected.

Thus, calculations of the neutrino-nucleus cross sections within a shell model approach will always have a systematic uncertainty arising from a) the effective interaction used; b) the size of the active model space; and c) center-of-mass contaminations.

For dipole or higher multipoles of the weak interaction matrix elements, defining a sufficient shell-model space in which to calculate the necessary structure information becomes difficult except for the lightest systems. One then turns to RPA-based approaches [60]. These methods typically begin with Skyrme Hartree-Fock generated basis states, thus determining the mean-field and single-particle occupied levels of the nucleus. When available, experimental single-particle energies are employed. The unoccupied levels are obtained by diagonalizing the Hartree-Fock mean field using a harmonic oscillator basis. Thus, the continuum part of the single-particle spectrum is discretized, and discrete particle-hole configurations coupled to the appropriate spin and parity are used as a basis in order to cast the RPA equations into a matrix form. Hartree-Fock is sometimes augmented by BCS pairing correlations. In this case, uncertainties arise from the effective interactions used and the allowed correlations available for the ground state. The lack of correlations beyond RPA typically causes an increased total cross section and a narrower distribution of strength within the various interaction channels. While this may not be a serious defect for high multipole parts of the weak interaction, it does affect the Gamow-Teller strength distributions.

Recent applications of continuum RPA and the shell model to ^{12}C scattering at LSND give ($17 - 19 \times 10^{-40}$ cm^2 (CRPA[61]), $13.4 - 14.5 \times 10^{-40}$ cm^2 (shell model[62]) for the total cross sections. The experimental value is 12.3×10^{-40} cm^2 [35].

2.5.3. A guide from electron capture

Nuclear structure studies have shown that inclusion of the full space is necessary if one wishes to describe the Gamow-Teller and Fermi strength distributions. These allowed transitions will be responsible for a substantial part of the scattering cross section at ORLaND. Gamow-Teller resonances in nuclei were studied using (p, n) transfer reactions. In order to theoretically study the Gamow-Teller transitions, $0\hbar\omega$ calculations have been carried out in the p-, sd-, fp-, and gds-shells. Total Gamow-Teller strengths are well reproduced for a variety of fp-shell nuclei using a modified version of the Kuo-Brown interaction for this region [63]. These calculations were carried out using shell-model Monte Carlo techniques [59], and more recently, standard diagonalization techniques in a truncated but still sufficient model space [64]. These shell-model results should be compared with the more naive non-interacting shell-model results of Fuller, Fowler, and Newmann.[65,66] The total strengths of FFN are usually a factor of 2-10 larger than the full calculation. FFN places that strength into one transition peak. However, experimentally the strength is fragmented across many states, and the centroid is usually displaced from the FFN value. The lesson learned from these studies of the Gamow-Teller strength in nuclei is that inclusion of nuclear correlations in calculations is important to properly understand the experimental data. At ORLaND, low lying excitations that contribute to the cross sections must be correctly modeled in order to accurately understand the experimental cross sections.

3. The SNS as a Neutrino Source

3.1. Advantages of ORLaND as a Neutrino Facility

ORLaND is a proposed underground laboratory for neutrino research in nuclear physics, astrophysics, and particle physics. Located adjacent to the SNS, ORLaND will be a high-intensity pulsed neutrino (antineutrino) facility, with neutrino energies in the range conducive to low- and medium-energy nuclear physics and nuclear astrophysics research. The neutrinos will be obtained from decay of stopped pions produced in the SNS neutron production target during spallation and the decay of the daughter muons. The spectra, composition, and fluxes of neutrinos from such stopped pion facilities are well known, and their special characteristics will be utilized in planning the ORLaND physics program.

Spallation at the SNS will result in the production of 0.94×10^{15} neutrinos of each species ($\nu_\mu, \bar{\nu}_\mu$, and ν_e) per second, originating from 'Decay at Rest' (DAR) positive pions for 9.6×10^{15} protons sec^{-1} on target. The neutrinos will be produced isotropically and their time structure and flavor components will allow separation of charged and neutral current interactions involving different neutrino families. The pulsed nature and underground location will provide attractive shielding advantages. The energy spectrum of the beam makes the facility unique for neutrino-nucleus experiments related to solar and supernova physics as well as fundamental nuclear, electroweak, and particle physics. In particular, the remarkable similarity of the energies of the neutrinos in the proposed facility with those from supernovae make an ideal laboratory for supernova physics. There are no other existing or approved facilities that could provide the neutrino-nucleus data that can be obtained at ORLaND.

It may be noted that none of the three other global spallation sources, LANCE operating with the Pulsed Storage Ring (PSR), KEK, or ISIS, could serve as a neutrino laboratory due to low currents, lower neutrino intensities, and lack of detector space. The SNS is therefore unique and the only site for a comprehensive neutrino laboratory accessing the most powerful pulsed source of low-energy neutrinos in the world. Studies investigating a possible neutrino factory to be derived from muon storage rings strengthen the need for intensive neutrino science, but focus on oscillation research and the high-energy regime, beyond 20 GeV.

3.2. The Accelerator and the Target Station

The Spallation Neutron Source (SNS), under construction at the Oak Ridge National Laboratory, will produce the most intense 2 MW pulsed-proton beam in the world. It consists of a 493-m-long linac, an accumulator ring with a radius of just over 35 meters, and a target station. A second target station is planned in the future. The SNS will be used primarily for material science research, however, it also will be the world's most powerful neutrino factory. The high intensity and the pulsed nature of the SNS provide an ideal laboratory for neutrino physics research at medium energies. The short-pulsed beam ($\leq 0.6\mu$sec, 60 Hz) provides a virtually cosmic-ray-free measurement of various neutrino interactions. It also provides the ability to distinguish between neutrinos from pion decay and muon decay. The only neutrino detector with this capability is the much smaller KARMEN experiment at the Rutherford Laboratory with significantly lower beam intensity (200μA).

A plan view of the completed SNS facility is shown in Fig. 4. Note that in this figure the future second target station is shown. It will have an intensity of 0.6 mA and repetition rate of 10 Hz. The two target stations will receive beams at different time slots.

Table 3 shows the design parameters of the SNS.

Figure 5 shows a cross section of the target station. A beam of protons enters from the lower left and strikes the target. The beam has a 7-cm by 21-cm spot size in order to reduce the local heat load in the target. The target, shown in Fig. 6, has dimensions of 40 cm by 10 cm by 65 cm. The mercury is contained within a multiple wall structure made of 316-type stainless steel. To remove heat, the mercury of the target is constantly circulated at the rate of 140 kg/sec. The room temperature moderators, filled with water, are placed under the target. The cryogenic liquid hydrogen moderators are located at the top. Target and moderators

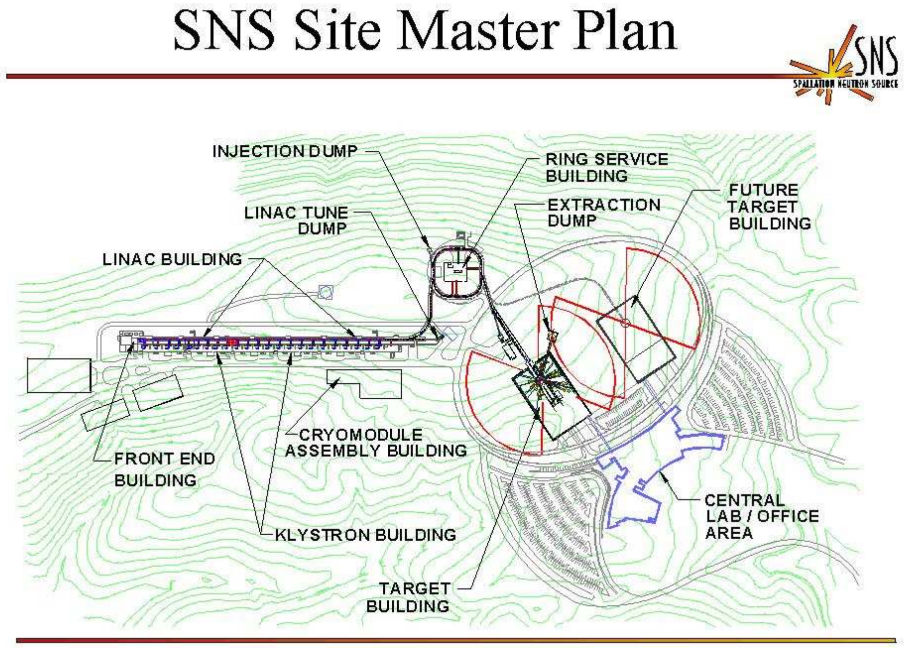

Figure 4. Plan view of the SNS facility.

Table 3
SNS design parameters.

	baseline
linac length	493 m
accumulator ring circumference	221 m
beam power on the target	2 MW
beam energy on the target	1.3 GeV
average beam current	1.54 mA
repetition rate	60 Hz
ion type, source-linac	H^-
linac-beam duty factor	6.2%
number of injected turns	1225
particles stored in ring (ppp)	1.5×10^{14}
extracted pulse length	600 nsec
peak current on target	45 A
target	mercury
beam spot on target	7×21 cm
moderators ambient	2 (water)
moderators cryogenic	2 (LH_2)
neutron beam ports	18

are surrounded by a lead reflector which extends at least to a radius of 1 meter around the target. All of this structure is encapsulated inside a thick steel vessel, to prevent neutrons from escaping into the experimental hall. There will be 18 neutron channels looking at the moderators, rather than at the target. Shutters are provided on each channel.

3.3. Neutrino Production at the SNS

Monte Carlo simulations have been performed of neutrino production by a proton beam striking the SNS target composed of liquid mercury. Production rates were calculated for the ν_e, ν_μ, and $\overline{\nu}_\mu$ from π^+ and μ^+ decay at rest. Also, the $\overline{\nu}_e$ background was calculated.

At 1.3 GeV, about 20% of the incident protons produce a pion in interactions within a spallation target. The charged pions produced in a mercury target stop very quickly ($<$ 3 ns) because of their relatively low energies ($\sim$200 MeV), and because of the high stopping power of the target material, so that most of the π^+ decay at rest. Because the pion has spin 0, both the μ^+ and the associated 30 MeV ν_μ are emitted isotropically. The π^+ decay at rest is followed by the μ^+ decay within 0.2 g/cm^2 of the point at which the π^+ stopped. The muon kinetic energy is 4.1 MeV. Again, the 0-53 MeV $\overline{\nu}_\mu$ and ν_e fluxes are isotropic. Spectra for the three neutrino species ν_e, ν_μ, and $\overline{\nu}_\mu$ from π^+ and μ^+ decay at rest are displayed in Fig. 7. The majority of the pions and muons decay in the immediate vicinity of their production point, and thus a neutron spallation facility represents an extremely intense, approximately point-like, source of neutrinos for nuclear and particle physics studies.

The Monte Carlo code for the present study was initially designed [67] for a slightly lower-energy proton beam. Measured cross sections for proton reactions, and for proton production of pions at proton energies of 585 and 730 MeV, were first parameterized and then incorporated into a Monte Carlo simulation of pion production in a thick target, followed by Monte Carlo tracking of pions and decay muons. A measurement of the stopped π^+ rate as a function of position within a thick target, for pions produced by protons of 700-800 MeV, was used as an absolute calibration [68] of the output from the computer code. This computer code has been used to calculate neutrino production at an 800-MeV proton accelerator; for experiments E225, E645, E764, E1173 (LSND), and E1213 at Los Alamos, and for the KARMEN experiment at Rutherford.

The measured pion production cross sections at 730 and 585 MeV cover a reasonable range of nuclei and a reasonable part of the pion energy-angle phase space. Above 730 MeV, however, there is a paucity of published data. Therefore we resorted to a calculation of pion production cross sections and then normalized the calculated cross sections to the 730 and 585 MeV data. These calculations were based on the intra-nuclear cascade model of Bertini, which uses the extensive store of nucleon-nucleon data to produce energetic outgoing particles from complex nuclei by initial cascade reactions. The cascade model includes single and double pion production, e.g., $pp \to \pi^+ pn$ and $pp \to \pi^+\pi^+ nn$, both of which should be important for proton energies of 1300 MeV. A particularly convenient package of codes for nucleon-induced reactions, the LAHET system [69] from the Los Alamos National Laboratory, which incorporates the Bertini [70] model, was used for the calculations. Doubly-differential (in pion energy and angle) and total cross sections were computed for hydrogen, carbon, copper, and lead at incident proton energies of 800, 1000, 1500, and 2000 MeV. The resulting total cross sections for positive pion production from carbon, copper, and lead are shown in Fig. 8. The points at 585 and 730 MeV are the measured data; the points at 1000, 1500 and 2000 MeV are the (normalized) LAHET calculations.

At a proton beam energy of 1300 MeV, the design energy for the SNS facility, the predicted neutrino fluxes for three neutrino species: ν_μ, ν_e, $\overline{\nu}_\mu$ are 0.098 ($\nu\ p^{-1}$). Production of $\overline{\nu}_e$ is 10^{-3} - 10^{-4} orders of magnitude lower. A large reduction in the $\overline{\nu}_e$ flux is due to the strong absorbtion of π^- and μ^- in the SNS mercury target. Decay of μ^- is the only source of $\overline{\nu}_e$. Even larger reduction in the $\overline{\nu}_e$ background will result from the use of the time structure in the SNS proton beam. The time spectrum of $\overline{\nu}_e$ from the decay at rest of μ^- in the mercury spallation source consists of two basic components: (1) an exponential decay in low-Z materi-

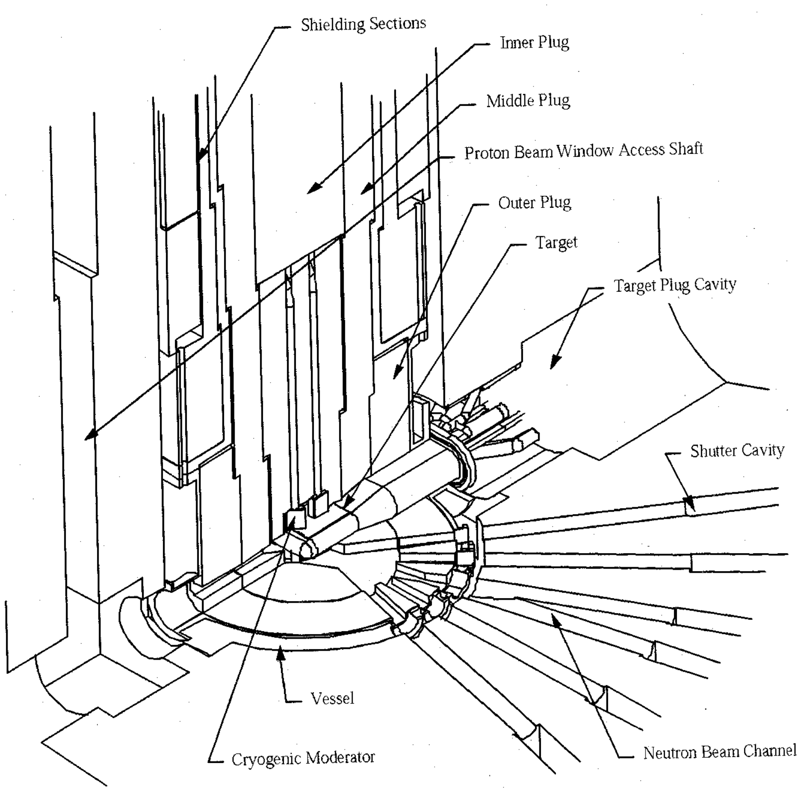

Figure 5. Perspective view of the target station.

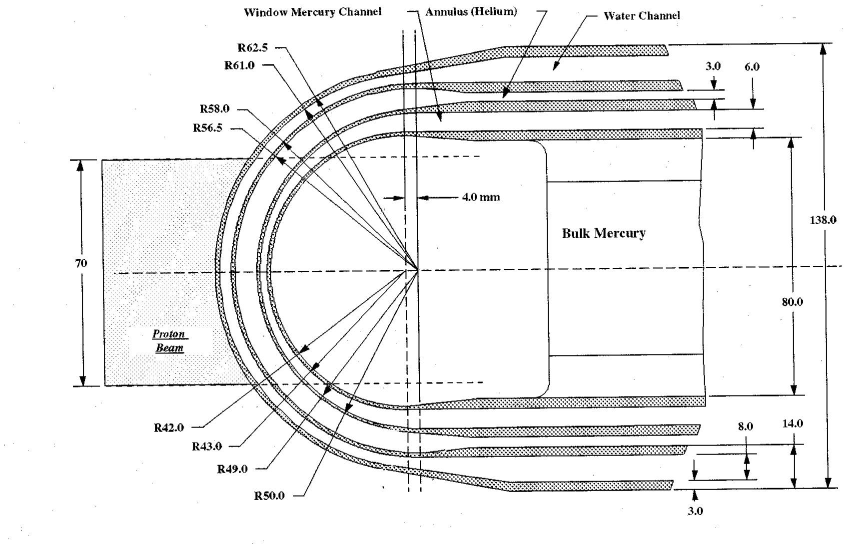

Figure 6. An enlargement of the mercury target.

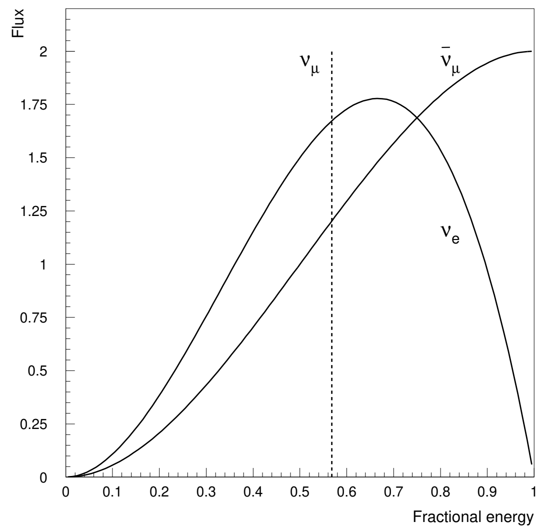

Figure 7. The energy spectra for the three neutrino species ν_e, ν_μ, and $\overline{\nu}_\mu$ from π^+ and μ^+ decay at rest. The maximum energy is 52.8 MeV.

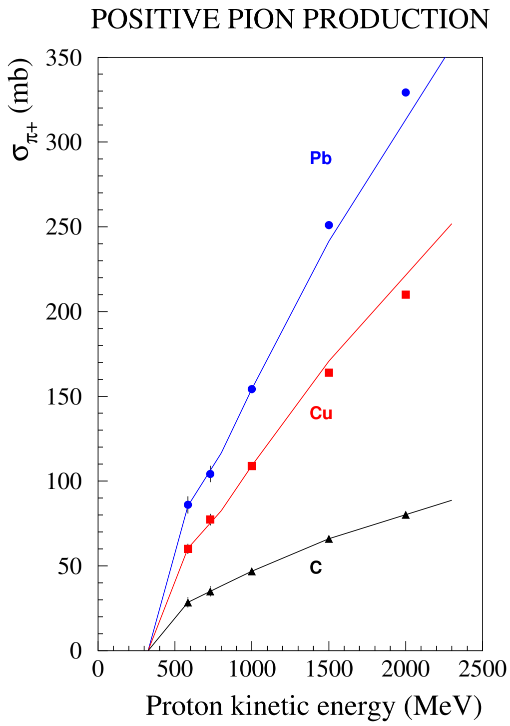

Figure 8. The total π^+ production cross sections, σ_{π^+}, for carbon, copper, and lead as functions of the proton energy. A simple piece-wise linear energy dependence is assumed, with σ_{π^+} decreasing to zero at 325 MeV.

als, such as D_2O and Al, dominated by the 2.2 μs muon mean life, and (2) the much faster exponential decay in high-Z materials mercury, lead, and iron characterized by a fast absorption rate. For the neutrino oscillation search; which relies upon the $\overline{\nu}_\mu$ flux (from the 2.2 μs μ^+ decay at rest), events are separated into two time groups, above and below 1000 ns from the start of the proton pulse. A time-cut at 1000 ns would eliminate the $\overline{\nu}_e$ background from μ^- decay in mercury and iron, thereby reducing the background by factor of two. More importantly, comparing the rates of appearance of $\bar{\nu}_e$ before and after the 1,000 ns cut provides for the first time an opportunity to experimentally evaluate the ν_e background.

It is difficult to estimate the uncertainties in these calculations because the accuracy of the pion production cross sections from the LAHET code are not well known. There are certainly additional nuclear effects that are important, beyond those incorporated into the Bertini intra-nuclear cascade model. However, the extrapolation from 800 MeV to 1300 MeV is not large. The error estimate at 800 MeV, mostly due to the uncertainty in the absolute calibration experiment, was $\pm 7\%$; for the SNS we would estimate the uncertainty in the neutrino production rate to be $\pm 10\%$. Future data on π^+ and π^- production can reduce the uncertainty significantly.

Calculated energy and time distribution for the four types of neutrinos to be produced at SNS are shown in Fig. 9, and Fig. 10.

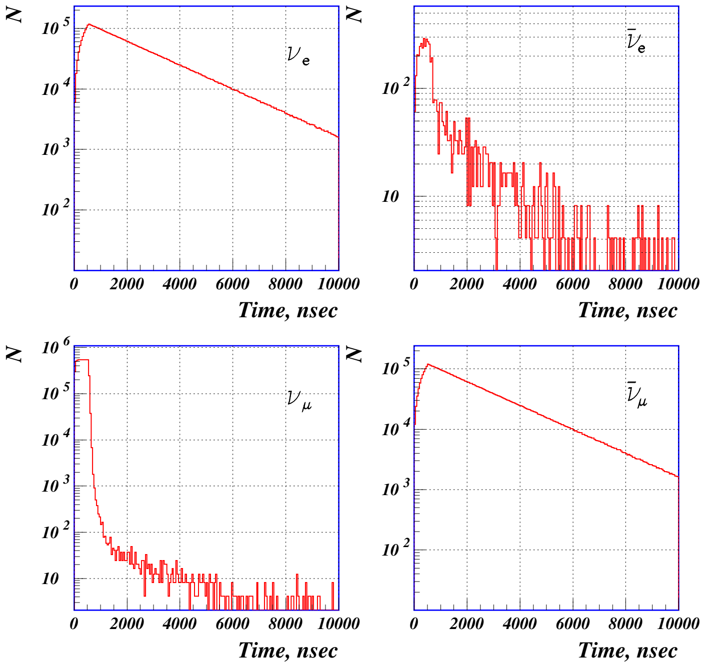

Figure 9. Time distributions for four neutrino types produced at SNS.

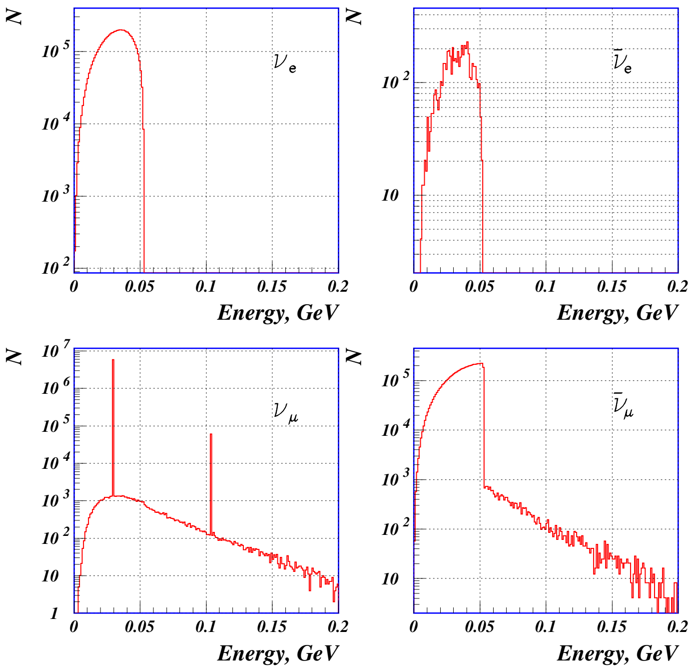

Figure 10. Energy distributions for four neutrino types produced at SNS. The monoenergetic line for the muon neutrino near 100 MeV does not include broadening due to nuclear effects.

4. Possible Experiments

4.1. Calibrating the Sun

Weak interaction processes involving the deuteron are central to current research efforts in nuclear physics. In addition to the accelerator based programs that will elucidate the flavor structure of the nucleon, such as the SAMPLE experiments[43] at Bates, the interactions between neutrinos and the deuteron form the core of our efforts to learn about the neutrino and look beyond the standard model of electroweak interactions. Neutrino-deuteron interactions also play a pivotal role in our understanding of the mechanism of energy generation in the sun and other Main Sequence stars. Both in the production process, e.g. $pp \to de^+\nu_e$, and in detection at the Sudbury Neutrino Observatory [71,72], e.g. $\nu d \to \nu np$, charged and neutral current weak interaction matrix elements between the deuteron and continuum states are required. Thus measurements of νd processes can provide valuable information on the stellar ignition reaction

$$p + p \to d + e^+ + \nu_e \tag{24}$$

which begins the p-p chain of stellar burning. A theoretical evaluation of the above reaction is required here since the only experimental measurement—

$$\begin{aligned}&\sigma(\nu_e + d \to p + p + e^-)_{exp} = \\ &(53 \pm 18) \times 10^{-42}\ \mathrm{cm}^2\end{aligned} \tag{25}$$

by LAMPF E31[73]—while in agreement with the corresponding theoretically calculated value[11]

$$\sigma(\nu_e + d \to p + p + e^-)_{th} = 52 \times 10^{-42}\ \mathrm{cm}^2, \tag{26}$$

has only $\sim 35\%$ precision.

On the theoretical side, calculation of the reaction Eq. 24 consists of two components:

i) convolution of the one-body operator, obtained from neutron beta decay, with the deuteron and pp wavefunctions;

ii) evaluation of the two-body piece, which is generally described via a meson-exchange approach.

The first part is reasonably secure, which cannot be said for the two-body part of the calculation. This is evidenced by the fact that two such calculations of total cross sections for the related reaction

$$\nu_x + d \to n + p + \nu_x \tag{27}$$

by Ying, Haxton, and Henley (YHH)[10] and by Kubodera and Nozawa 2(KN) [11] differ by $\sim 5\%$.

These are both fairly traditional nuclear physics calculations and their disagreement offers a picture of the state of the art at the present time. While such discrepancies are perhaps not important for some applications, in the case of the reaction Eq. 24, which initiates the solar burning chain, and Eq. 27, which is used as a signal for neutrino-initiated neutral current reactions at the SNO detector, such a considerable uncertainty is unacceptable. Recently, however, a new approach to such low energy reactions—that of effective field theory (EFT)—has been proposed[74]. In this procedure, one foregoes the traditional detailed picture involving an assumed potential which is then solved to yield predictions at various kinematics, in favor of an "effective" picture *involving only experimentally measured quantities*, but which is valid only at relatively low momenta—say $p << m_\pi$. The latter limitation does not represent a problem for the solar and SNO applications which we desire and offers an attractive and rigorous framework, within which the neutrino reactions in question can be described.

The inputs required for such calculations are simply the neutron decay axial decay constant g_A and the experimental value of the deuteron binding energy, together with the experimental np, pp scattering lengths and effective ranges. Since this is a low energy reaction the rescattering corrections which renormalize the basic decay process can be reliably included, and such calculations for the charged and neutral current neutrino reactions have recently been done by Butler and Chen[75]. A parallel and related calculation for the reaction Eq. 24 has been performed by Kong and Ravndal[76].

In both evaluations, however, there exists the same unknown quantity—a four-nucleon axial current counterterm of the form

$$\vec{A}^{(2)} = \frac{1}{8}L_{1A}(N^T\sigma_2\vec{\sigma}\tau_2 N)^\dagger(N^T\sigma_2\tau_2\tau_- N) \tag{28}$$

where L_{1A} has units of fm^3 and is expected by is by EFT scaling arguments to be in the range $-6\ \mathrm{fm}^3 \leq L_{1A} \leq +6\ \mathrm{fm}^3$, corresponding to a cross section difference of $\sim 10\%$. In fact, Butler and Chen have shown that the calculations of YNN and KN can be completely characterized via the values

$$L_{1A} = \begin{cases} 6.3\ \mathrm{fm}^3 & YHH[10] \\ 1.0\ \mathrm{fm}^3 & KN[11] \end{cases} \tag{29}$$

This large difference for values of L_{1A} simply corresponds to differing assumptions about the short-range properties of the nucleon-nucleon interaction associated with the meson-exchange calculations.

Obviously, one can generate alternative values of L_{1A} via other descriptions of short-range structure, but it is clear that the best approach would be to measure this counterterm experimentally. For example, a determination $\Delta L_{1A} \sim \pm 2$, corresponds roughly to a $\sim 2\%$ uncertainty in the total cross section. At ORLaND one could envision, *e.g*, a 61 ton heavy water target with a ~ 30 ton fiducial volume, which would generate $\sim 10^4$ events per year via the charged current reaction

$$\nu_e + d \rightarrow p + p + e^- \tag{30}$$

where the electron is detected via its Cerenkov radiation, providing energy and momentum measurement of the outgoing lepton. The low Q-value of the above reaction makes it possible to subtract the ^{16}O charged-current reaction via a simple energy cut. Note too that the experimental value of the counterterm can also be used to yield a theoretically rigorous $\sim 2\%$ prediction for the reaction rate for the pp neutrino process which initiates the solar burning cycle *and* for the neutral current deuteron disintegration reaction Eq. 27 which is used in the SNO detector in order to indicate that a neutral current neutrino reaction has occurred. Finally, it is clear that careful measurement to pin down the size of the counterterm L_{1A} would offer a target for theorists to shoot at in order to gauge their models of short distance NN structure. Clearly this is a high profile and high impact measurement.

4.1.1. Experimental perspectives for the reaction $^2\mathrm{D}(\nu_e, e^-)pp$

The importance and utility of an accurate measurement of the cross section of the reaction $\nu_e + d \rightarrow p + p + e^-$ having now been discussed, the experimental feasibility of one possible technique is presented.

The only signal from this reaction in a water Cherenkov detector is the Cherenkov cone of light from the energetic electron in coincidence with the 600-ns proton pulse on the mercury target. This is similar to the signal from the reaction $^{16}\mathrm{O}(\nu_e, e^-)^{16}\mathrm{F}$ in a light water detector. It would be of great advantage to measure the reaction rates of $^2\mathrm{D}(\nu_e, e^-)ppe^-$ and $^{16}\mathrm{O}(\nu_e, e^-)^{16}\mathrm{F}$ simultaneously in heavy and light water, respectively. Although the theoretical cross sections are significantly different: $\sigma(^2\mathrm{D})/\sigma(^{16}\mathrm{O}) \approx 8$, averaged over the neutrino energy range 10 to 20 MeV [11,31].

There are several experimental approaches that would significantly improve the only existing measured value: $\langle\sigma\rangle = (5.3 \pm 1.8) \times 10^{-42}\ \mathrm{cm}^2$ [73].

The best would very probably result from a smaller version of the Solar Neutrino Observatory (SNO) detector (SNOINO) in which the D_2O is contained in an acrylic vessel embedded in the center of the large (~2000-ton) water Cerenkov detector, as discussed in several conference proceedings [77,78]. Discussions are in progress with Reynolds Polymer Technology, Inc., the company that made the acrylic sphere for the SNO Collaboration. The preliminary design of SNOINO involves a spherical acrylic shell containing 61 tons of D_2O, or 30 fiducial tons. At 50 meters from the SNS target, this would lead to a yield of 9461 events per year. A very conservative estimate of the efficiency is 30%, which would result in a 1% statistical accuracy in 3.5 years.

The need for the large water Cherenkov detector for this application is threefold. First, the 4.64 meters of water between the acrylic vessel and the walls of the large detector will shield it and reduce the background. Second, it will allow simultaneous measurement of the cross section of the reaction $^{16}\mathrm{O}(\nu_e, e^-)^{16}\mathrm{F}$.

Finally, the accurate measurement of any cross sections in the ORLaND laboratory will depend on an accurate measurement of the neutrino flux. The only way to obtain this experimentally is with $\nu - e^-$ elastic scattering.

The total cross section, charge current plus neutral current, neutrino–electron scattering, averaged over the SNS neutrino spectrum, is $\langle\sigma\rangle = 3.96 \times 10^{-43}$ cm^2. The total fiducial mass of H_2O and D_2O will be about 1500 tons and will contain about 5×10^{32} electrons at an average distance of $\sim$ 50 meters. The (νe^-) scattering rate would be $\sim$ 50 events per days, or 18,250 per year. Again, a very conservative estimate of the detection efficiency is 30%, resulting in 5640 events per calendar year. Utilizing neutrino–electron elastic scattering to monitor the neutrino flux is the only way one can hope to make precision measurements of any neutrino-nucleus cross section. This is one of the main justifications of the 2000-ton Cerenkov detector which would run constantly and would calibrate the flux for all measurements at ORLaND.

4.2. Neutrino Oscillations Search

Distinctive spectral shapes and rates of different flavors of neutrinos produced at the SNS (See Fig.s 9 and 10), will produce a unique oportunity to serch of neutrino oscilations at ORLaND. In a presents of large 2 kt water Cherenkov detector, this search will be a by product run in parralel to the other measurements. ORLaND will be sensetive to new unexplored regions of neutrino oscillation parameters in the following three channels: $\bar{\nu}_\mu \to \bar{\nu}_e$, $\nu_\mu \to \nu_e$, and $\nu_e \to \bar{\nu}_e$.

4.2.1. Neutrino oscillation limits for $\bar{\nu}_\mu \to \bar{\nu}_e$

The ORLaND $\bar{\nu}_\mu \to \bar{\nu}_e$ neutrino oscillation search, similar to LSND and KARMEN, is based on a unique feature of neutrino beams from spallation sources, namely the enormous suppression of $\bar{\nu}_e$ production. This feature has the following explanation.

In the SNS, pions are copiously produced from the interaction of 1.3 GeV protons with the mercury target. The rate of pions that are not absorbed in flight is 0.093 π^+ and 0.067 π^- per proton. The absorption of stopped π^+ and associated μ^+ is negligible. As a result of the decay chain,

$$\pi^+ \ (\ \tau = 26 \text{ nsec}) \to \mu^+ + \nu_\mu$$
$$\text{and,}$$
$$\mu^+(\ \tau = 2.2\ \mu \text{ sec}) \to e^+ + \nu_e + \bar{\nu}_\mu,$$

the production rate of $\bar{\nu}_\mu$ is close to that of the initial π^+. For π^-, the situation is different. Most π^- are quickly stopped and captured in the target materials. Detailed simulations show that 99.6% of the negative pions produced in the Hg, are captured before they have a chance to decay. Moreover, a significant number of μ^- between 90% and 94% are captured by heavy elements in the target and in the surrounding reflector. More exact numbers of μ^- capture will be determined after the design of the SNS is completed. This absorption results in a large asymmetry between $\bar{\nu}_e$ to $\bar{\nu}_\mu$ production.

The high intensity of neutrino beams at the SNS, with fine time structure, the large size of the ORLaND water Cherenkov detector, and the underground location, provide a unique opportunity to investigate and significantly extend the region of oscillation parameter space studied by the LSND, and KARMEN collaborations. The overall ORLaND sensitivities will be two orders of magnitude better than those experiments, and one order of magnitude better than the sensitivity of the MiniBooNE experiment, now under costruction at FNAL.

In Fig. 11 the possible limits on oscillation parameters of ORLaND are compared with those of the Mini-BooNE and MINOS proposals. The region favored by the LSND experiment is shown as well. For ORLaND, two limits are shown. One is for the first three years of operation. The second corresponds to the maximum sensitivity of ORLaND.

The very intense SNS neutrino source, together with the massive size of the ORLaND detector provide an unprecedented opportunity for a high-statistics neutrino oscillation search. In one week the ORLaND experiment would be able to accumulate the same statistics as LSND did in three years. If the LSND results are confirmed by experiments (Mini-BooNE), ORLaND will be uniquely positioned to precisely measure the neutrino mixing parameters. This is demonstrated by an example shown in Fig. 12. The contours show how well ORLaND would be able to measure neutrino oscillation parameters inside the LSND region for three randomly selected sets of parameters. The far more restrictive ORLaND contours comparred to those in the LSND region reflect the ability to use a very statistically significant likelihood analysis due to the large detector and greater flux. The results presented are from a full simulations of events in de-

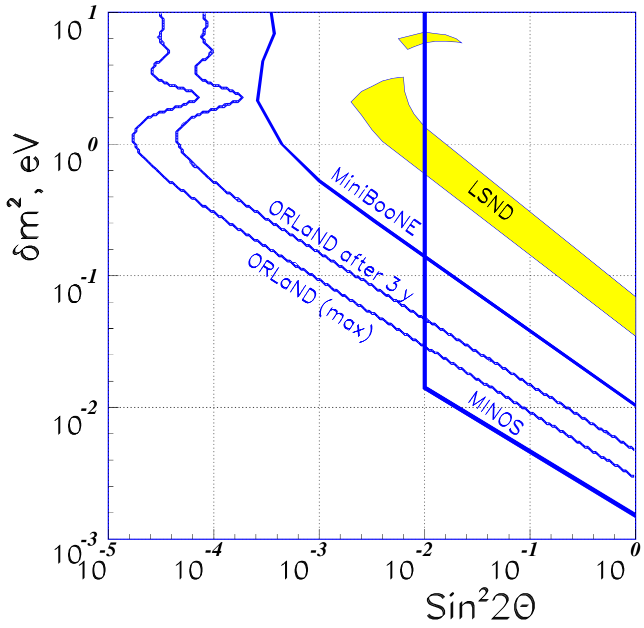

Figure 11. Limits from the ORLaND experiment compared with those of Mini-BooNE, and MINOS proposals.

tector, with analysis of information of energy and events position inside the detector.

4.2.2. Search for $\nu_\mu \to \nu_e$ transitions with monoenergetic neutrinos

The time structure and monoenergetic character of the ν_μ spectrum from the decay, $\pi^+ \to \mu^+ + \nu_\mu$ shown in Fig.s 9 and 10, can be used in the ORLaND facility to search for $\nu_\mu \to \nu_e$ oscillations. These neutrinos will oscillate to ν_e with an observable probability for some values of $sin^2 2\theta$ and δm^2 in the range reported by the LSND collaboration. Let us consider mineral oil based detector. The reaction $^{12}\mathrm{C}(\nu_e, e^-)\,^{12}\mathrm{N}_{g.s.}$ results in a Cerenkov ring, followed by the decay $^{12}\mathrm{N}_{gs} \to ^{12}\mathrm{C} + \mathrm{e}^+ + \nu_\mathrm{e}$. There will, of course, be a background of ν_e from the broad spectrum due to the decay of μ^+; however, it will be suppressed by making use of the time structure of the neutrinos shown in Fig. 9. The events that occur due to $\nu_\mu \to \nu_e$ oscillations would cause a significant distortion of the background spectrum as shown in Fig. 13.

ORLaND will be able to cover almost all of the region of mixing parameters in the LSND region. The detection of neutrino oscillations for the neutrino and antineutrino will make possible a test of CP invariance in the neutrino sector.

The standard model of electroweak interactions allows a CP-violating interaction to take place in the quark sector. The possible existence of massive neutrinos may lead to a complex neutrino mixing mass matrix, in which imaginary phases are the source of a CP-violating interaction in the leptonic sector. This is similar to the well known Kobayashi-Maskawa mechanism.

A possible consequence for such a CP violation is a difference of the transition probabilities of neutrino and antineutrino oscillations (see reference number [127] and references therein) which should be equal to zero if CP invariance holds.

$$D_{\mu e} = P_{\nu_\mu \to \nu_e} - P_{\overline{\nu}_\mu \to \overline{\nu}_e} \qquad (31)$$

The parameter $D_{\mu e}$ can be represented in terms of elements of the unitary mixing matrix U and neutrino oscillation parameters as in [127]:

$$D_{\mu e} = 4 \sum_{k>j} Im(U_{\mu j} U^*_{ej} U^*_{\mu k} U_{ek}) \sin\left(\frac{\Delta m^2_{kj} L}{2p}\right). \qquad (32)$$

Here, indices j and k are used for neutrino mass eigenstates. From the above expression, one can see that experimental results for muon neutrino and muon antineutrino oscillations will lead to a restriction on the possible CP violation.

It should be noted that the only restriction on CP violation in the lepton sector is the limit on the electron electric dipole moment ($d_e = (0.18 \pm 0.12 \pm 0.10) \cdot 10^{-26} e \cdot cm$) [128]. However, it cannot be directly related to the CP-violating parameters in the neutrino mass matrix in a model independent way. This is because a non-zero electron electric dipole moment (if it exists) could be due not to the CP violation in the neutrino sector, but could be caused by a complex mixing mass matrix for the charged leptons themselves. Therefore, in the general case, the limit on the electron dipole moment does not provide a restriction on the CP-violating parameters in the neutrino sector.

To make this measurements, a liduid scintillator detector is required. Accordingly it should be considered as a second generation experiment. If neutrino oscillations will be found by the water cherenkov detector in $\bar{\nu}_\mu \to \bar{\nu}_e$ channel in the region of parameter acsessable for $\nu_\mu \to \nu_e$ mode, this experiment, to test CP in neutrino sector, could become high on the priority list.

4.2.3. Neutrino–antineutrino oscillations

The first neutrino-oscillation phenomenon considered historically (Pontecorvo 1957) [135] involved neutrino antineutrino oscillation $\nu_e \to \bar{\nu}_e$ in analogy with $K^0 - \bar{K}^0$ oscillations. This mode of oscillation violates not only flavor $L(l, \nu_l)$ conservation but also conservation of total lepton number. In addition, any $\nu_l \to \bar{\nu}_l$ oscillation is forbidden by helicity.

There are a number of theoretical investigations of $\nu \leftrightarrow \bar{\nu}$ transitions reported in the literature [129] [126] [130].

Early evidence constraining the probability of transition $\bar{\nu}_e \to \nu_e$ was obtained by Davis and Harmer [131] by placing a tank car of ^{37}Cl rich perchlorethylene in the vicinity of the Savannah River P-reactor and collecting and counting residue gas, searching for ^{37}Ar from the reaction $\bar{\nu}_e + ^{37}Cl \to ^{37}Ar + e^+$. The result was the ratio $\bar{\nu}_e/\nu_e < 0.02$. This implies a bound at least that stringent on the

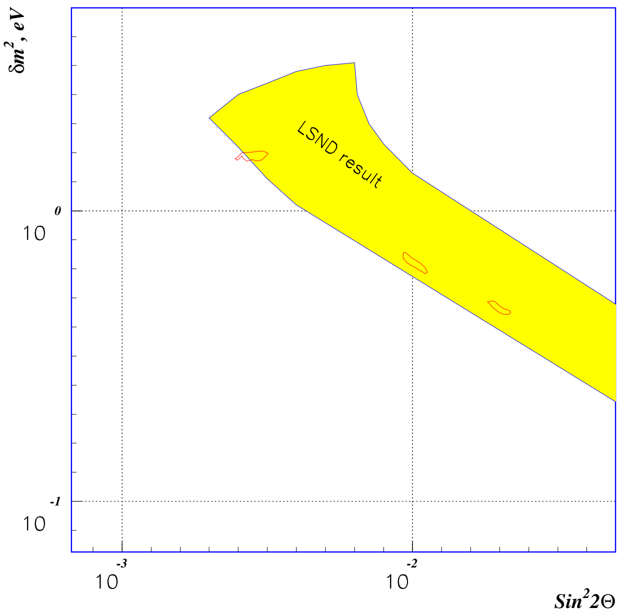

Figure 12. The precision of the measurement of the mixing parameters in the LSND region.

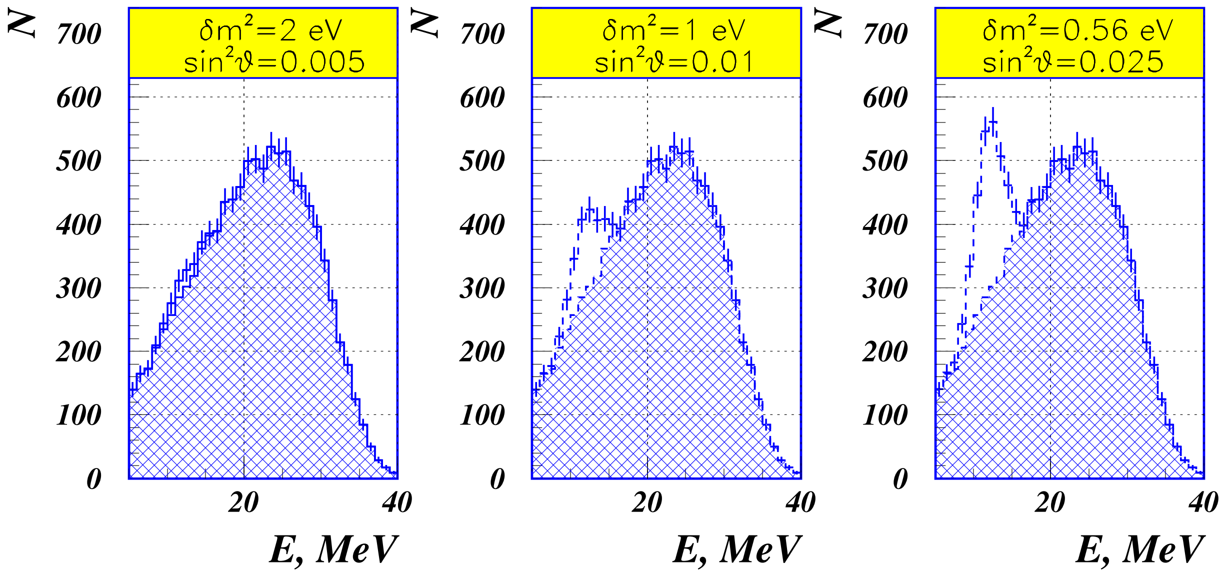

Figure 13. The energy spectrum of electrons from the reaction $^{12}C(\nu_e, e^-)^{12}N_{gs}$. The cross-hatched region contains events due to ν_e from the decay of μ^+. The distributions at the lower energy edge are those predicted for ν_μ to ν_e oscillations for 3 years of data acquisition with ORLaND with a proton beam of 2 MW.

transition $\bar{\nu}_e$ to ν_e for L \ E $\simeq 10$.

In 1978, Bahcall and Primakoff [126] formulated the problem in terms of helicity eigenstates of a Dirac neutrino-antineutrino field. In this formulation the probability of transition, $|\langle\nu_e|e^{-iHt}|\bar{\nu}_e\rangle|^2$, is approximately proportional to $[1-(1-\eta^2)/(1+\eta^2)]$, where the parameter, η, weights the right-handed leptonic current in the weak-interaction Lagrangian.

Modern ν-oscillation experiments could observe $\nu \leftrightarrow \bar{\nu}$ oscillation at or below the level of the bound of Davis and Harmer ($p \sim 0.02$). However, their experiment only placed a bound; the probability could well be zero. Other direct searches also place stringent bounds on the right handed current irrespective of the Dirac/Majorana character of neutrinos. If, on the other hand, neutrinos are purely Majorana in character, then neutrinoless double beta decay experiments place a stringent bound, $\eta < 10^{-5}$ *or* 10^{-6}, depending on the choice of nuclear matrix element used to extract η from the bound on the half-life [132], and [133]. This implies a suppression of Majorana $\nu \leftrightarrow \bar{\nu}$ oscillations between 10^{-10} and 10^{-11}.

Recently, Langacker and Wang [130] have carefully analyzed $\nu \leftrightarrow \bar{\nu}$ transition probabilities for 5 reasonable extensions of the Standard Model. All of their results yield a suppression factor for these transitions between 10^{-6} and 10^{-14}. This is tantamount to searching for flavor oscillations with $\sin^2 2\theta$ on this order. Such theoretical guidance would never encourage anyone to build a detector for the sole purpose of searching for $\nu \leftrightarrow \bar{\nu}$ transition.

Nevertheless, if a detector constructed for another purpose, has the capability of distinguishing $\nu_\alpha \to \bar{\nu}_\alpha$ or $\bar{\nu}_\alpha \to \nu_\alpha$ transitions from flavor oscillations $\bar{\nu}_\alpha \to \bar{\nu}_\beta$ or $\bar{\nu}_\beta \to \bar{\nu}_\alpha$, one should certainly search for such exotic and unexpected physics. Large underground proton-rich scintillation detectors, KAMLAND, for example, can search for $\bar{\nu}_e$'s from the sun that result from $\nu_e \to \bar{\nu}_e$[134].

In the case that there exists some yet-to-be-discovered exotic process that leads to $\nu_e \to \bar{\nu}_e$ transitions that occur within a distance of order of 50 meters, and if a significant fraction of all $\bar{\nu}_e$'s detected were from this process, then ORLaND could observe it. In fact, it could distinguish the resulting $\bar{\nu}_e$ spectrum from that resulting from $\bar{\nu}_\mu \to \bar{\nu}_e$ oscillations. This capability arises from the difference in the spectral shapes of the ν_e spectrum and the $\bar{\nu}_\mu$ spectrum from the decay at rest of μ^+; i.e., $\mu^+ \to e^+ + \nu_e + \bar{\nu}_\mu$. Figure 14 shows the response of the ORLaND detector to both spectra.

The proposed ORLaND project is the only one, proposed or existing, that could do this. In any case, ORLaND could place the most stringent bound on this exotic process.

4.3. Neutrino-Electron Scattering

4.3.1. Flux measurements from ν–e scattering

The neutrino beams incident upon the ORLaND facility are generated from stopped pions and muons in the SNS spallation target and are characterized by energy spectra and an absolute normalization. The energy spectra of these neutrino beams are known to a high accuracy: the line spectrum at 29.8 MeV for the ν_μ from the two-body decay of stopped π^+, and the 0-52.8 MeV Michel spectra for the ν_e and $\bar{\nu}_\mu$ from the three-body decay-at-rest of stopped μ^+. The normalization, the number of neutrinos per proton incident upon the spallation target, comes from Monte Carlo simulations of pion production, transport and decay, followed by muon transport and decay. At present, an absolute normalization[79],[80] for the LSND and KARMEN experiments is provided by measurements made on an instrumented mockup of a beamstop or spallation target; the event-by-event production of pions, followed by signals from pion and muon decay, was used to infer the rate of stopped pion production per incident proton. This technique has resulted in an accuracy of 7%.

The large size of the ORLaND 2000 ton Cherenkov detector, however, will allow the ORLaND facility to accumulate $e^-(\nu_e,\nu_e)e^-$ events at a very high rate, about 6,000 events per calender year. Since the neutrino-electron scattering cross section is known from Standard Model parameters to a high precision, we can use the measured $e^-(\nu_e,\nu_e)e^-$ rate to provide an absolute flux normalization of neutrinos per incident proton with an accuracy of 1-2%. This unprecedented combi-

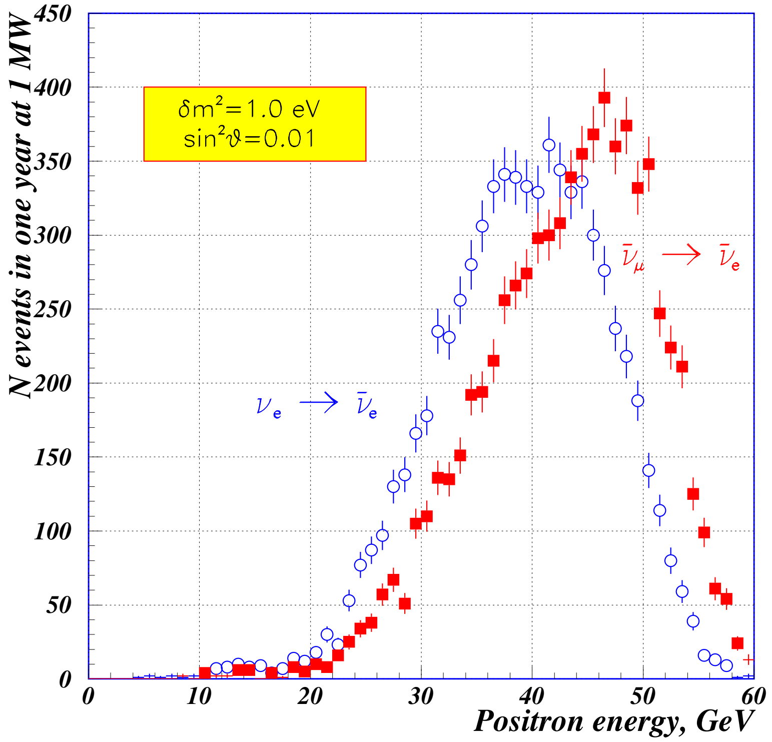

Figure 14. Neutrino - antineutrino vs. flavor oscillations at ORLaND.

nation of an extremely accurate absolute normalization and energy spectra for the neutrino fluxes will allow the ORLaND facility to significantly improve the measurements of neutrino-nucleus cross sections and neutrino properties.

4.3.2. Proposed measurement of $\sin^2\theta_W$ at ORLaND

The high intensity of the SNS neutrino beam, in the combination with its unique time structure will allow an experiment at ORLaND to measure the weak angle $\sin^2\theta_W$ with an accuracy close to 1% at very low momentum transfer.

Precise measurement of the parameter $\sin^2\theta_W$ is very important both for the interpretation of the Standard Model in the context of a complete (renormalizable) $SU(3)_C \times SU(2)_L \times U(1)_Y$ theory and for the search for new physics. The single most accurate determination of the weak mixing angle $\sin^2\theta_W$ at the $\pm 0.1\%$ level has been reported by the SLD collaboration[81]. This single measurement is comparable in precision to the combined results of the measurements of the four LEP experiments [82]. It has been used for definition of some parameters of the Standard Model and for obtaining limits on other ones, such as a of mass Higgs boson.

It should be noted that in the Standard Model the parameter $\sin^2\theta_W$ is the running parameter[83] as a function of the momentum transfer Q^2. Therefore, for the complete test of the Standard Model it is necessarily to study the Q^2 dependence of the parameter $\sin^2\theta_W(Q^2)$. The above mentioned precise value of the $\sin^2\theta_W$ is defined at the point of the mass pole of the Z gauge boson. The analysis of the theoretical predictions for the running $\sin^2\theta_W(Q^2)$ and the comparison with the existing and and future experimental results have been done recently in ref.[84]. The Fig. 15 from the reference [84] illustrates the expected dependence of $\sin^2\theta_W(Q^2)$ on Q due to one-loop quantum corrections, and shows how well it has already been measured for several values of Q^2. It also illustrates the approximate potential of E158 and future e^-e^- and e^+e^- collider measurements at $\sqrt{s} = 1$ TeV.

The interesting fact is a 2σ discrepancy in the atomic parity violation (APV) result[85] as compared with Standard Model expectations. That issue could be made even more interesting by future results from E158 at SLAC. However, this puzzle would not be completely resolved since the SLAC experiment and the APV experiment belong to rather different scales of the momentum transfer Q^2. Therefore, it is very important to find an experimental approach to test the above possible discrepancy at the Q^2 of about the same scale as that of the APV experiment.

It should be noted that the APV experimental result is based on the most precise measurement of the parity violation in the atom of ^{133}Cs and on very complex theoretical calculations. Both the theory and the experiment are at the limits of the best currently available accuracy. Therefore, it is very unlikely that it will be possible to resolve this puzzle using future atomic experiments.

From this point of view, the ORLaND experiment would give the right scale of the momentum transfer

$$Q^2 = 2m_e T \sim 10^{-5} GeV^2, \tag{33}$$

(m_e and T are the electron mass and the recoil electron energy) and the appropriate accuracy. Then, the ORLaND result could prove the running behavior of the parameter $\sin^2\theta_W(Q^2)$ for the Standard Model in the low Q^2 region or could confirm the possible APV experiment discrepancy, and as a consequence, a manifestation of new physics. This would be an important check of the one-loop quantum corrections in the Standard Model at such low values of Q^2.

In the low-energy regime at ORLaND one can write the neutrino and anti-neutrino elastic scattering cross sections as a function of neutrino energy in the laboratory coordinate system, E_ν, and electron recoil energy T, Eq.s(37), and (38). We propose to measure the ratio,

$$R = \frac{\sigma(\nu_\mu e)}{\sigma(\nu_e e) + \sigma(\overline{\nu}_\mu e)}. \tag{34}$$

Omitting terms proportional to the small parameter m_e/E_ν in Eqs. (37)and (38) and integrating over T, we can rewrite this ratio as:

$$R = \frac{3/4 - 3\sin^2\theta_W + 4(\sin^2\theta_W)^2}{1 + 2\sin^2\theta_W + 8(\sin^2\theta_W)^2}. \tag{35}$$

For $sin^2\theta_w = 0.23$, the ratio R is 0.13. When $\sin^2\theta_w$ increases by a given relative amount, the

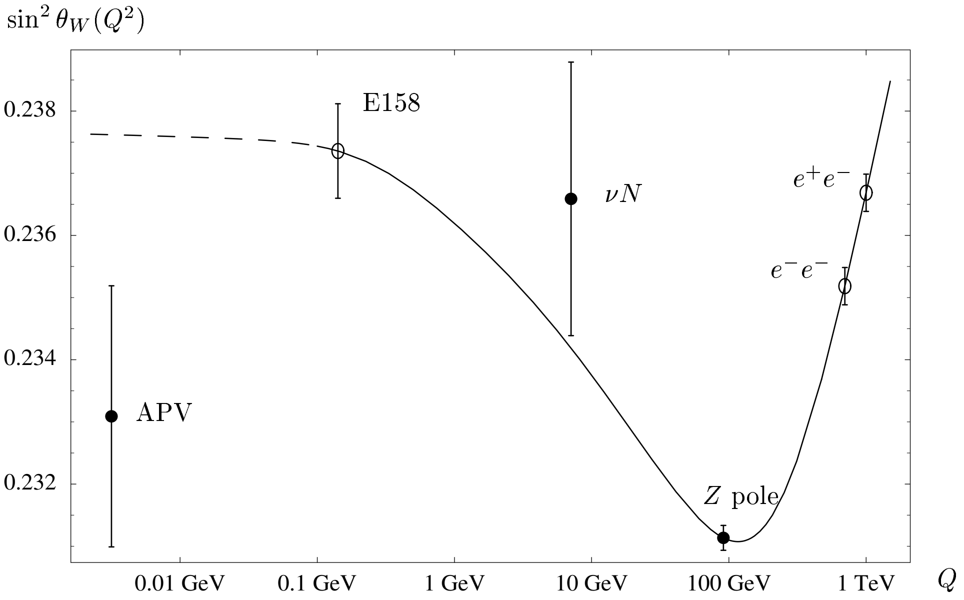

Figure 15. Predicted running of $\sin^2\theta_W(Q^2)$ and evidence from existing experiments (dark circles) along with expectations from potential future Møller scattering (E158) and e^+e^- asymmetry measurements at $\sqrt{s} = 1$ TeV.

ratio R decreases by a larger fraction (2.08 with a 10 MeV electron energy cut, 1.66 with no energy cut).

To separate the contribution of $\sigma(\nu_\mu e)$ from that of $\sigma(\nu_e e) + \sigma(\bar{\nu}_\mu e)$ we propose to use the short time structure of the SNS beam. (A time cut of 700 nsec, will completely eliminate the contribution from ν_μ). Therefore, a precision measurement of the ratio of neutrino electron scattering with neutrinos from pion decay and those from muon decay will be done simultaneously.

Errors have been estimated on the basis of two-kiloton detector located $50m$ from the beam-stop. For four years of data at an intensity of $2MW$, there will be about 50 000 ($\nu_e e$) and 8 600 ($\nu_\mu e$) and 8 300 ($\overline{\nu}_\mu e$) interactions in the detector. These rates will allow the measurement of $\sin^2\theta_W$ with accuracy of about 1%.

4.3.3. Search for the effects of a magnetic moment of the muon neutrino

The existence of a neutrino mass leads to the possibility for the Dirac neutrino to have a magnetic dipole moment or for Majorana neutrinos non-diagonal magnetic transition moments. In that case, neutrino interactions include an electromagnetic part in addition to the standard weak interaction. The electromagnetic part has a characteristic energy behavior in which the differential cross section increases with decreasing energy of the recoiling target. The simplest way to measure the neutrino magnetic moment is to measure the excess of the neutrino differential cross section in the low energy region of the recoil particle. From this point of view, the ORLaND neutrino facility would not be able to measure the electron neutrino magnetic moment as well as reactor neutrino experiments.

However, for muon neutrinos, it provides a unique opportunity to improve the existing restriction on the magnetic moment, $\mu < 7.4 \cdot 10^{-10}\mu_B$, [86].

Assuming that the dominant part of neutrino weak interactions comes from Dirac type neutrinos (consideration of Majorana neutrinos does not change our conclusions significantly) and neglecting contributions from the electron neutrino magnetic moment, one can write the weak and electromagnetic $\sigma(EM)$ neutrino differential cross sections for neutrino $\sigma(\nu)$ and anti-neutrino $\sigma(\overline{\nu})$ on electrons as (see references [87] and [88]):

$$\frac{d\sigma(EM)}{dT} = f^2 \frac{\pi\alpha^2}{m_e^2}(\frac{1}{T} - \frac{1}{E_\nu}), \tag{36}$$

$$\frac{d\sigma(\nu)}{dT} = \frac{2G^2 m_e}{\pi}[g_L^2 + g_R^2(1 - \frac{T}{E_\nu})^2 - g_L g_R \frac{m_e T}{E_\nu^2}], \tag{37}$$

$$\frac{d\sigma(\overline{\nu})}{dT} = \frac{2G^2 m_e}{\pi}[g_R^2 + g_L^2(1 - \frac{T}{E_\nu})^2 - g_L g_R \frac{m_e T}{E_\nu^2}]. \tag{38}$$

Here $g_R = \sin^2\Theta_W$, $g_L = \frac{1}{2} + \sin^2\Theta_W$ for the electron neutrino and antineutrino and $g_R = \sin^2\Theta_W$, $g_L = -\frac{1}{2} + \sin^2\Theta_W$ for the muon neutrino and antineutrino; and f is the muon neutrino (antineutrino) magnetic moment in Bohr magnetons. G is the Fermi constant, m_e is the electron mass, T is electron recoil energy; E_ν is the neutrino (antineutrino) energy in the laboratory coordinate system.

Taking into account that for the decay at rest configurations, the muon neutrino is monochromatic, but the muon antineutrino and electron neutrino energies obey the Michel energy spectrum, one has to average the above cross sections over their energy distributions. Moreover, it must be considered that the muon neutrino flux has a short time pulse compared to other neutrinos. This fact leads to a different sensitivity to the neutrino magnetic moment for different regions of the neutrino time spectrum.

The integral over the short time spectrum gives:

$$R_m = f^2(\frac{6.68 \cdot 10^{19}}{T}), \tag{39}$$

while the long time contribution gives

$$R_m = f^2(\frac{2.04 \cdot 10^{19}}{T}). \tag{40}$$

Now, one can estimate the value of the magnetic moment, which can be extracted from the measurement of the energy dependence of the neutrino electron cross sections. In the general case, these cross sections might be parameterized in terms of a T-dependent function,

$$\frac{d\sigma(T)}{dT} = a + bT + cT^2 + \frac{d}{T}, \tag{41}$$

where parameter a depends on both the weak and electromagnetic neutrino-electron interactions, parameters b and c depend only on the weak interaction, and parameter d depends only on the electromagnetic interaction and is proportional to f^2. Therefore, to obtain the value of the parameter d (and, consequently, the value of the magnetic moment), the experimental value of the cross section needs to be fitted to the above parameterized T-dependent function $d\sigma(T)/dT$, at least for four different values of the energy T. Assuming that one will fit this function for equidistant values of T for the region, where the number of recoil electrons is about the same for each point, and taking into account the simulated recoil electron spectrum, one can conclude that, for an optimal energy resolution of about $\Delta T = 2MeV$, and for a minimum threshold for recoil energy of about $10MeV$, the relative accuracy for the parameter, $\delta d/d$, is about 0.6. Then, one can expect to obtain an experimental restriction on the value of the magnetic moment f of about $0.5 \cdot 10^{-9}$ or $1.0 \cdot 10^{-9}$ for the short- and long-time spectra, correspondingly.

If the absolute value of the neutrino cross section could be measured with high accuracy, one would be able to obtain a limit on the magnetic moment, not only from the energy dependence of the cross section, but also from the absolute excess of the differential cross section integrated over the energy interval of T between 10 MeV and 20 MeV.

In that case, the limit could be even better (see Fig. 16 where integrated intervals of 10.4 MeV and 14.5 MeV were used for short and long time components, correspondingly).

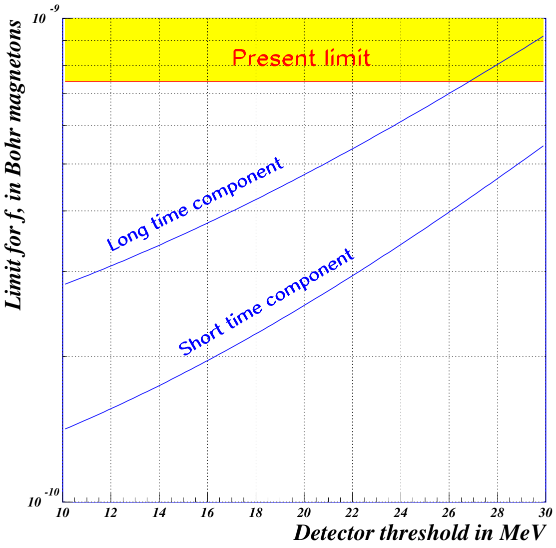

Figure 16. Comparison of possible constraints on the magnetic moment of ν_μ for the absolute measurement of neutrino electron scattering cross sections as a function of detector threshold. The two lines are for the short and for the long time spectrum components. The existing experimental limit is shown by the horizontal line.

Therefore, one can conclude that with ORLaND the existing limit on the muon magnetic dipole moment can be significantly improved.

4.4. H_2O Cerenkov Detectors

4.4.1. Supernova studies using ^{16}O

Water Cerenkov detectors may be used to unambiguously identify neutrino events from supernovae [89]. Supernova ν_x neutrinos, with average energies of 25 MeV, will excite 1^- and 2^- giant resonances in ^{16}O through the neutral current reaction $^{16}O(\nu_x,\nu_x')^{16}O^*$. These resonances are above the particle thresholds and will decay primarily by proton and neutron emission. While much of the cross section for this process will take one to the ^{15}O and ^{15}N ground states some of these decays will go to excited states in these nuclei. If these excited states are below the particle thresholds in ^{15}N ($E^* < 10.2$ MeV) or ^{15}O ($E^* < 7.3$ MeV) they will decay by γ-emission. The first excited states in both nuclei ($E^* = 5.27$ MeV in ^{15}N and $E^* = 5.18$MeV in ^{15}O) are above thresholds for γ-detection at ORLaND. Thus, if these interactions take place, one may study the neutrinos from a supernova using the excitation of ^{16}O and its subsequent decay in a large underground Cherenkov detector.

One would like to know precisely the cross section information that one should see in the event of a supernova explosion. In order to do this, one must understand the response of water Cerenkov detectors and ORLaND offers a good opportunity to do this with a known source.

4.4.2. Measuring differential cross Sections on ^{16}O

The term "differential cross section" is used in the following to denote the scattering angle dependent cross section ($\frac{d\sigma}{d\Omega}$) as well as the cross section differential for the energy of the outgoing lepton ($\frac{d\sigma}{d\epsilon_f}$) or both ($\frac{d^2\sigma}{d\Omega d\epsilon_f}$).

As has been pointed out in a recent paper [90] it is very promising to measure differential neutrino scattering cross sections, for the following reasons:

(1) For sufficiently accurate data it should be possible to extract the weak Coulomb-longitudinal and the weak transverse response from the angular distributions. There are various methods to do this. They are analogous to the Rosenbluth-separation in electron scattering and should have similar benefits. It would be the first step into an unreached area: the measurement of weak nuclear response functions in neutrino scattering.

(2) Haxton has shown that for the $^{16}O(\nu_e,e^-)^{16}F^*$ cross section theory predicts a strong backward peaking of the angular distribution caused by the conserved vector current hypothesis and the calculated weights for excitation of natural and unnatural parity states in ^{16}F [31]. Figure 17 was constructed from the data given in Ref. [31]. The label 'SNT' refers to the supernova temperature and $SNT = 4$, and $SNT = 10$ refer to mean neutrino energies of about 12 MeV and 30 MeV respectively. It is immediately evident that the angular distribution at $SNT = 10$ MeV (left curve and top right curve) is very strongly peaked at back angles. In fact the differential cross section for this temperature at 180 degrees is more than 140 times that $SNT = 4$ MeV. The same ratio at 0 degrees is only 36. This dramatic prediction can be tested at ORLaND as discussed later.

(3) For a given neutrino spectrum the differential cross section $\frac{\mathrm{d}\sigma}{\mathrm{d}\Omega}$ determines the momentum transfer distribution $\frac{\mathrm{d}\sigma}{\mathrm{d}q}$. It is important to know this $|\vec{q}|$-dependence as well for judging the applicability of various nuclear models to the corresponding reactions as for (further) testing of nuclear models (e.g., by comparing with data for electron scattering in that range of momentum transfer).

(4) The strong angular distribution discussed above in (2) could be very useful in testing various $\nu_\tau \to \nu_\mathrm{e}$ and $\nu_\mu \to \nu_\mathrm{e}$ oscillation hypothese in supernovae collapse scenarios. Supernova neutrino data from large Cherenkov detectors, SuperK, for example, could be analyzed with respect to the electron angular distribution to search for evidence for or to place bounds on these scenarios. This might well be the only experimental way to directly search for evidence for the $\nu_\tau \to \nu_\mathrm{e}$ from either the vacuum or from MSW conversions.

(5) The experimental feasibility at ORLaND was evaluated for the 2000 ton water Cherenkov detector. The current design allows approximately 1475 tons of ^{16}O in the fiducial volume.

Using the cross section $\sigma(E_\nu)$ gicen by Haxton [31], the rate $R = \langle\sigma(E)\phi(E)\rangle N$ was calculated for the case with $N = 4.9 \times 10^{31}$ atoms of ^{16}O. At 50 meters from the SNS target station, $\phi(\nu_\mathrm{exd} = 3 \times 10^6 \nu_\mathrm{e}/\mathrm{cm}^2/\mathrm{sec}$. Folding this with the cross section and multiplying by N yields about 41,000 events per year.Correcting this result for a detector efficiency of about 30% yields 12,300 events per year. A statistically accurate measurement is certantly feasible over a period of a few years.

Although no angular distribution data exist for the reaction $^{16}O(\nu_e, e^-)^{16}F$, the LSND collaboration did measure the angular distribution of electrons from the reaction $i^{16}O(\nu_e, e^-)^{12}N_{gs}$. These data did agree in general with the RPA calculations; however, the experimental errors are too large to provide an adequate test of theory. A measurement at ORLaND could provide statistically accurate data to provide such tests in ^{16}O as well as ^{12}C.

4.4.3. Measuring strangeness with ^{16}O

The strangeness content of the nucleus or the nucleon arises from the "sea" of virtual strange quark-antiquark pairs [36]. The effect of such pairs on the low-energy properties of the nucleon is a central question in nuclear physics. A comparison of weak nucleon form factors with the values expected in the nuclear domain approximation, (where the sea is ignored), can provide a direct measure of nuclear matrix elements of strange quark operators and thus probe the effects of the sea on static nuclear properties.

There are several possible approaches for strangeness measurements. At ORLaND, the most promising would be the elastic axial form factor, $G_A^Z(Q^2)$, at low momentum transfer. In the Standard Model, the axial current operator at tree level is pure isovector, and is thus related by a simple isospin rotation to the (known) charge changing axial current. The difference between $G_A^Z(Q^2)$ and $G_A^W(Q^2)$ (i.e. the corresponding charge changing matrix element, obtained at low Q^2 directly from β-decay or from charge changing neutrino cross sections) measures the strange axial form factor, $G_A^s(Q^2)$. Neutrino-nucleus elastic cross sections at low Q^2 at ORLaND would provide a clean and significant measure of $G_A^s(0)$.

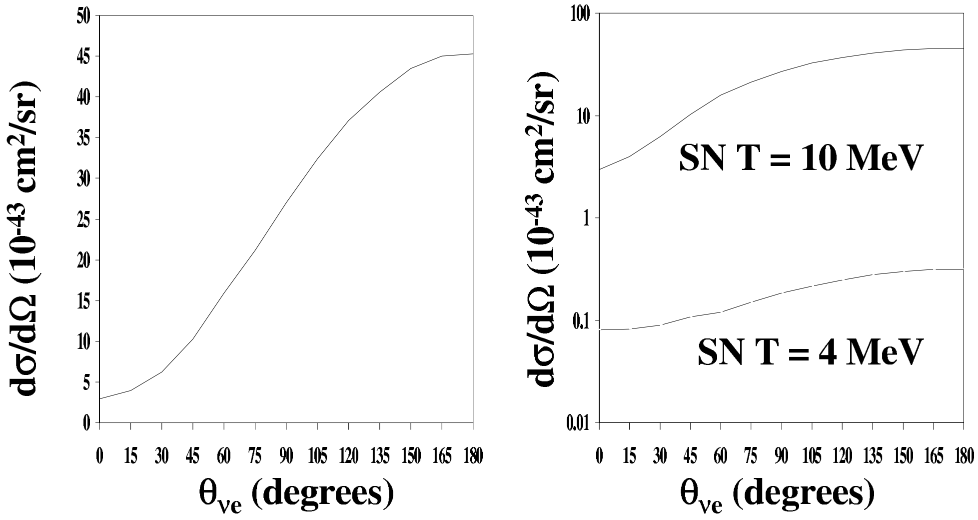

Figure 17. Neutrino differential cross sections at two different supernova temperatures as discussed in the text [31].

Among the first experiments could be measurements of neutrino-oxygen cross sections using a 2000 ton water Cerenkov detector. By adding Gd_2Cl_4 to the water, one can attempt to measure the cross section of the reaction ν + ^{16}O $\rightarrow$ ν' + n + γ + ^{15}O by triggering on nuclear gamma-rays, and later on the capture gamma-rays. With the addition of Gd_2Cl_4 it is also possible to observe the gamma rays from the reaction ^{16}O + $\nu \rightarrow \nu'$ + p + γ + ^{15}N, not followed by the capture gamma rays. The ratio R=$\sigma(\nu,\nu' p\gamma)/\sigma(\nu,\nu' n\gamma)$ of proton to neutron quasielastic cross sections is proportional to $G_A^s(0)$ and thus uniquely sensitive to the desired axial strangeness content[93]. In this ratio, beam normalization, final state interactions, and Q^2 dependence of the axial form factor all cancel to leading order.

Again, using the proposed 2000 ton water Cherenkov detector, and using cross sections calculated in reference [93] the expected rates are as follows: $^{16}O(\nu_x, nu_x, n\gamma)^{15}$O - 4200 y^{-1} $^{16}O(\nu_x, nu_x, p\gamma)^{15}$N - 21500 y^{-1}

These total rates will be reduced by the efficiency of the detector which is estimated to be at least 30%.

The ratio of these rates will be needed to search for the effects of strangeness; therefore, research and development on chemical techniques for maintaining significant quantities of a cadmium compound, Cd_2Cl_4 for example, in an acquious solution, without significant degradation of the optical absorption length will be needed.

4.5. Neutral and Charged Current Measurements on Carbon

4.5.1. Neutrino cross sections on ^{12,13}C:

The proposed 2000 ton Cherenkov detector will be designed to function both as a water Cherenkov detector or, with a dilute scintillator in mineral oil, as a scintillating Cherenkov detector. additionally, It can also be operated with pure mineral oil as a Cherenkov detector. The present concept is to begin with experiments using water to measure the reaction ^{16}O(ν_e,e$^-$)^{16}F, and at a later date to remove the water and fill it with mineral oil and a dilute scintillator.

The ORLaND facility could be a unique laboratory for the measurement of neutrino cross sections for both neutral current and charged current interactions with various nuclei. The distinct time structure of the neutrinos from the SNS spallation target will allow us to seperate monoenergetic ν_μ from π^+ decay at rest and $\bar{\nu}_\mu + \nu_e$ from μ^+ decay at rest with a simple time-cut. Neutrino fluxes accurate to 2-3% with well known ν–energy spectra, together with good detector energy resolution, will provide accurate integral and differential cross sections for energies interesting for both astrophysics and nuclear physics.

At present, the only extensive set of neutrino-nucleus cross section measurments are on carbon. A significant increase in the accuracy of these measurements will be achieved with the ORLaND facility, thereby enabling critical comparisons with the various calculational approaches. Most methods begin with the assumption that the transition operators are one-body in nature, so that the nuclear matrix elements can be expanded in terms of single-particle matrix elements in some convenient basis. Then for electroweak semi-leptonic interactions there are just seven basic classes of multipole operators, and only a subset of these can occur for a given transition involving initial and final nuclear states of specific angular momentum and parity. The total transition rate is proportional to the weighted sum of the transition rates between the single-particle states, where the weight factors (one-body density matrix elements) contain the detailed connections to the nuclear many-body problem. Of relevance here is the reaction $^{12}\mathrm{C}(\nu_e, e^-)^{12}\mathrm{N}_{gs}$, where the q^2-dependence of the nuclear form factors can be constrained by using existing electron scattering, muon capture and beta-decay measurements, permitting a reasonably complete determination of the one-body density matrix elements and hence calculations of the neutrino cross section.

Transition rates between ^{12}C and the (unbound) excited states in nitrogen are harder to estimate, in that fewer data are available to constrain the one-body matrix elements and transition form-factors. These transitions involve a variety of spin-isospin transfers; having accurate neutrino cross sections for a larger set of final states (involving a variety of multipoles) will enable additional tests of the nuclear models and approximations inherent in the calculations. When the possible "quenching" of Gamow-Teller matrix elements is considered, additional variations by as much as a factor of three in calculations for the reaction $^{13}\mathrm{C}(\nu_e, e^-)X$ have been reported [94]. Thus, future experimental observations of some specific transitions, with sufficient precision, would allow sensitive tests of the theoretical methodology. In particular, the very important question of Gamow-Teller quenching in neutrino-nuclear reactions could be subject to direct experimental test.

The inclusive charged-current reaction on ^{13}C serves as an example of how a measurement of a neutrino reaction can be made on a nuclear isotope even though isotopically-separated targets of sufficient tonnage are not feasible. In certain cases, it may be possible to discriminate between neutrino reactions on the different isotopes by tagging decay transitions in the final state, or by utilizing the different energy spectra of the outgoing charged particles. In the charged-current reactions on carbon, $^{12}\mathrm{C}(\nu_e, e^-)^{12}X$ and $^{13}\mathrm{C}(\nu_e, e^-)X$, the very different Q-values allow the outgoing e^- to be distinguished.

4.5.2. Cross sections of ^{12}C:

Organic scintillator contains two carbon isotopes: 98.9% ^{12}C and 1.1% ^{13}C. The ^{12}C nucleus is part of the $A = 12$ isospin triplet $^{12}\mathrm{B}_{gs}$–$^{12}\mathrm{C}^*$ (15.1 MeV)–$^{12}\mathrm{N}_{gs}$ with $J^\pi T = 1^+1$, see Fig. 18

By measuring neutrino induced transitions from the ^{12}C–ground state ($J^\pi T = 0^+0$) to the isospin triplet, ^{12}C serves as a spin–isospin filter, allowing us to investigate in detail the isovector and axialvector part of the weak hadronic current. These reactions are theoretically well understood [95],[96]. Transitions to excited states ($^{12}\mathrm{N}^*$) are more difficult to calculate, but in this instance calculations are available from several authors [97], [96].

SNS-neutrinos would allow us to measure four reactions:

1. Charged current $^{12}\mathrm{C}(\nu_e, e^-)^{12}\mathrm{N}_{gs}$: In this reaction a prompt electron with kinetic energy $E_e = E_\nu - 17.4$ MeV ≤ 35.5 MeV will be

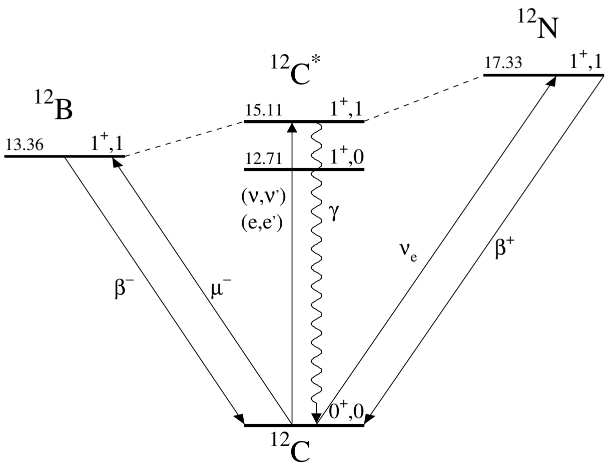

Figure 18. A=12 isospin triplet with charged current reaction to $^{12}N_{gs}$, neutral current reaction to $^{12}C^{*}$ to the 15.1 MeV level and μ^- capture to ^{12}B.

observed. ^{12}N$_{gs}$ subsequently undergoes β–decay ($\tau = 15.9$ ms), emitting a positron with kinetic energies up to 16.3 MeV. The spatial and temporal correlation provides a unique signature to effectively separate this neutrino reaction from background events.

2. Charged current ^{12}C$(\nu_e, e^-)^{12}$N*: The energy spectrum for electrons from transitions to excited states of nitrogen is similar to the spectrum of reaction 1. Excited nitrogen however does not undergo β–decay but emits a proton going to ^{11}C, as seen in Fig. 19

3. Neutral current ^{12}C$(\nu_e + \bar{\nu}_\mu, \nu_e + \bar{\nu}_\mu)^{12}$C(15.1 MeV): The neutral current excitation of the 15.1 MeV level of ^{12}C can be identified by a monoenergetic gamma emitted in 88% of the transitions back to the ground-state of ^{12}C. Because neutral current reactions occur for all neutrino flavors with the same strength, we will measure the sum of the cross sections for ν_e and $\bar{\nu}_\mu$ from muon decay at rest. For background events the same arguments apply as for reaction 2.

4. Neutral current ^{12}C$(\nu_\mu, \nu_\mu)^{12}$C(15.1 MeV): Muon neutrinos from π^+ decay at rest are monoenergetic with an energy of 29.8 MeV. These events can be separated from the first three reactions by a simple time-cut. Cosmic background for these events can be suppressed even better, because of the smaller time window, compared to neutrinos from muon decay at rest.

These cross sections (see table 4 and 5) have been measured recently by several other experiments at Lampf [98], [99] and Rutherford–Appleton–Laboratory [100], in good agreement with theoretical predictions. The statistical errors given by KARMEN and LSND are already below their systematic errors, which are dominated by uncertainties in the neutrino flux [79],[104]. For ORLaND, however, neutrino–electron scattering can be used to normalize the neutrino flux to 2–3%, improving the accuracy of existing cross sections by a factor of 3-4.

4.5.3. Cross section of ^{13}C

The inclusive charged-current reaction on ^{13}C serves as an example of how a measurement of a neutrino reaction can be made on a nuclear isotope even though isotopically-separated targets of sufficient tonnage are not feasible. In certain cases, it may be possible to discriminate between neutrino reactions on the different isotopes by tagging decay transitions in the final state, or by utilizing the different energy spectra of the outgoing charged particles.

The natural abundance of ^{13}C is 1.1%. The Q-value of the inclusive charged current reaction $^{13}C(\nu_e, e^-)^{13}X$ is 2.2 MeV, compared to 17.4 MeV for the same reaction on ^{12}C. Thus, electrons with energies higher than 35.5 MeV will be due to the neutrino reactions on ^{13}C. The cross section for this reaction is about one order of magnitude larger than that of ^{12}C, thus providing a measurable number of ^{13}C events. The electron energy $E_e = E_\nu - Q$ can reach up to 50 MeV, with $Q = 2.2$ MeV. Above 35 MeV the *single prong* spectrum is dominated by ^{13}C. The KARMEN experiment measured this cross section for the first time [100]:

$$\langle\sigma(^{13}C(\nu_e, e^-)^{13}N)\rangle = [50 \pm 37_{\rm stat} \pm 10_{\rm syst}] \cdot 10^{-42}{\rm cm}^2 \qquad (42)$$

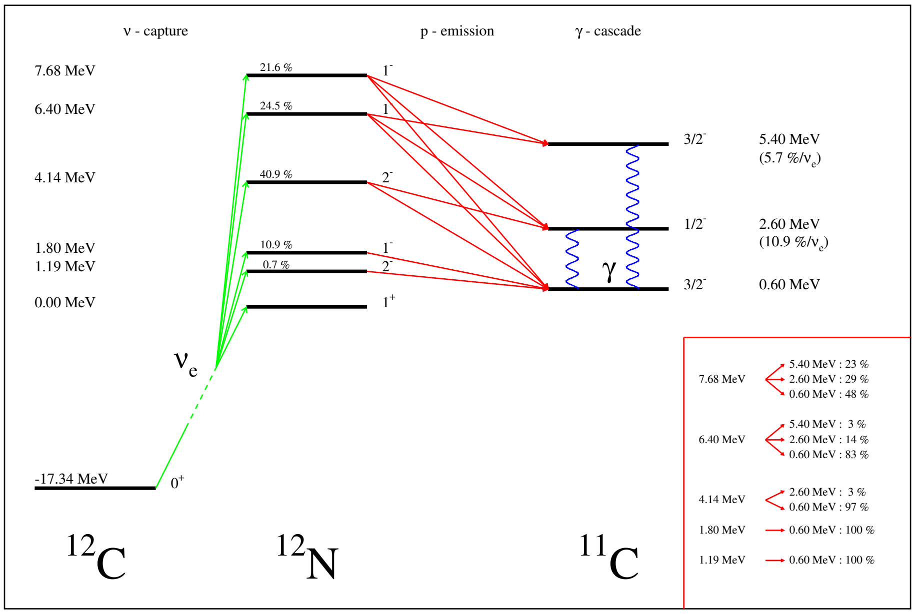

Figure 19. Calculated level scheme and branching ratios of the excited ^{12}N nucleus [101].

Table 4
Theoretical and experimental *charged current* cross sections, averaged over the corresponding DAR neutrino spectrum. Different theoretical models are EPM (elementary particle model), DWM (Donnelly–Walecka model), CRPA (continuum random phase approximation). The first error given for experimental values is the statistical error, the second one is the systematic error.

model	$\langle\sigma\rangle^{CC}$ in 10^{-42} cm^2 $^{12}C(\nu_e,e^-)\,^{12}N_{gs}$	$^{12}C(\nu_e,e^-)\,^{12}N^*$	μ–e–universality $R=\langle\sigma\rangle^{NC}/\langle\sigma\rangle^{CC}$
EPM [95]	9.2	—	1.08
DWM [97]	9.4	3.7	1.27
CRPA [96]	9.3	5.4	1.13
E225 [98]	$9.3 \pm 0.4 \pm 0.8$	5.4 ± 1.9	—
LSND [99]	$9.1 \pm 0.4 \pm 0.9$	$5.7 \pm 0.6 \pm 0.6$	—
KARMEN [100]	$9.3 \pm 0.4 \pm 0.8$	$5.1 \pm 0.6 \pm 0.5$	$1.17 \pm 0.11 \pm 0.012$

Table 5
Theoretical and experimental *neutral current* cross sections, averaged over the corresponding DAR neutrino spectrum. Different theoretical models are EPM (elementary particle model), DWM (Donnelly–Walecka model), CRPA (continuum random phase approximation). The first error given for experimental values is the statistical error, the second one is the systematic error.

model	$\langle\sigma\rangle^{NC}$ in 10^{-42} cm^2 of the reaction $^{12}C(\nu,\nu')\,^{12}C^*$			
	$\langle\sigma\rangle^{NC}(\nu_e)$	$\langle\sigma\rangle^{NC}(\bar{\nu}_\mu)$	$\langle\sigma\rangle^{NC}(\nu_e+\bar{\nu}_\mu)$	$\langle\sigma\rangle^{NC}(\nu_\mu)$
EPM [102]	4.6	5.7	10.3	—
EPM [95]	4.5	5.4	9.9	2.74
EPM [103]	4.9	5.8	10.6	2.70
DWM [97]	4.7	7.2	11.9	2.64
CRPA [96]	4.6	5.9	10.5	2.80
KARM. [100]	—	—	$10.9 \pm 0.7 \pm 0.8$	$3.1 \pm 0.8 \pm 0.5$

Table 6
Estimated count rates for inelastic neutrino scattering on ^{12}C in the ORLaND 2Kt detector. These numbers are based on cross sections measured by KARMEN. The second number is the estimated detection efficiency of the ORLaND detector for these reactions, with all cuts applied. The last column gives the number of detected events after cuts for one year of running time.

reaction	estimated efficiency	detected events for 1 yr. of running
$^{12}C(\nu_e,e^-)^{12}N_{gs}$ and $^{12}N_g s \rightarrow^{12} C+\nu_e+e^-$	40%	20,500
$^{12}C(\nu_e,e^-)^{12}N*$	40%	11,300
$^{12}C(\nu_e+\bar{\nu}_\mu,\nu_e+\bar{\nu}_\mu)^{12}C*$	45%	27,000
$^{12}C(\nu_\mu,\nu_\mu)^{12}C*$	54%	9,300
$^{13}C(\nu_e,e^-)^{13}N$	35%	1,100

Although the statistical error is rather large, the cross section is the same order of magnitude as the theoretical predictions [94]. The higher neutrino flux and larger detector we should determine the inclusive charged current cross section for ^{13}C with a statistical error of 3%, or better.

4.5.4. Limit on ω_L

The electron spectrum from reaction $^{12}\mathrm{C}(\nu_e, e^-)^{12}\mathrm{N}_{gs}$ can be used to derive the original ν_e spectrum, taking into account $E_\nu = E_e + Q(17.8\ \mathrm{MeV})$, the detector response function, and the $(E_\nu - Q)^2$ dependence of the differential cross section. As pointed out by Fetscher [105] and more recently by Grueb et al. [106], the shape of the ν_e spectrum from μ^+ decay at rest is sensitive to scalar and tensor admixtures to pure V–A interaction. Analogous to the Michel parameter ρ, which determines the shape of the electron spectrum in muon decay, non-V–A components of the ν_e spectrum are described by the ω_L parameter:

$$\frac{dN_\nu}{dx} = \frac{G_F^2 m_\mu^5}{16\pi^3} Q_L^\nu \left[G_0(x) + G_1(x) + \omega_L G_2(x)\right] \quad (43)$$

where m_μ is the muon mass, $x = 2E_\nu/m_\mu$ is the reduced neutrino energy, and Q_L^ν is the probability for emission of a left-handed ν_e. G_0 describes pure V–A interaction, G_1 takes into account radiative corrections, and $\omega_L G_2$ includes effects of scalar and tensor components.

In the Standard Model, ω_L is exactly zero. The effect of a non-vanishing ω_L on the shape of the ν_e spectrum would be most prominent at the endpoint. As seen in Fig. 20, Karmen measured $\omega_L = (2.7^{+3.8}_{-3.3}(stat) \pm 3.1(syst)) \times 10^{-2}$ and found an upper limit of $\omega_L \leq 0.113$ (90%CL). With its much higher statistics ORLaND could improve the statistical error by one order of magnitude. Since this measurement is only sensitive to the shape of the energy spectrum and not to the accuracy of the neutrino flux, the sensitivity of ORLaND would be limited mainly by systematic errors of the energy calibration around 35 MeV. A positive result would point to non-standard couplings in weak interaction.

4.5.5. Test of μ–e–universality

The Standard Model assumes that the coupling constants of the weak interaction are the same for e, μ and τ. ORLaND can test this universality for muons and electrons by comparing cross sections for different neutrino reactions. Two ratios could be compared with theoretical predictions:

$$R_1 = \frac{\sigma_{NC}(\nu_e + \bar{\nu}_\mu)}{\sigma_{NC}(\nu_\mu)}$$

and

$$R_2 = \frac{\sigma_{NC}(\nu_e + \bar{\nu}_\mu)}{\sigma_{CC}(^{12}C(\nu_e, e^-)^{12}N_{gs})} \quad (44)$$

In these ratios the systematic uncertainty of the neutrino flux cancels out. Calculations are available from different authors (see table 4 and 5). ORLaND will be able to improve previous results from the KARMEN experiment [100] by one order of magnitude, reaching a limit governed by systematic errors.

4.6. Charged Current Measurements with a Segmented Fe Detector

4.6.1. Background

The first estimate of the neutrino-iron cross section was made by Bugaev [107] using the independent particle model. More recently, the inclusive cross section of $^{56}\mathrm{Fe}(\nu_e, e^-)^{56}Co$, averaged over the stopped muon decay neutrino spectrum, was calculated by Kolbe, Langanke, and Martinez-Pinedo [108], and by Kolbe and Langanke [109]. In ref. [109], the neutral current cross sections for the production of neutrinos and their spectra are presented for both Fe and Pb.

The charged-current neutrino-nucleus cross section between nuclear states with specific angular momenta and isospin was derived by Walecka [110], and by Donnelly and Peccei [111]. This cross section involves a Gamow-Teller (GT) contribution and forbidden transitions. Random phase approximations (RPA) are not as reliable as shell model calculations for transitions mediated by the GT operator; however, they do describe forbidden transitions adequately [108].

The shell model calculation of the GT contributions to the cross section $^{56}\mathrm{Fe}(\nu_e, e^-)^{56}Co$ of refs. 5

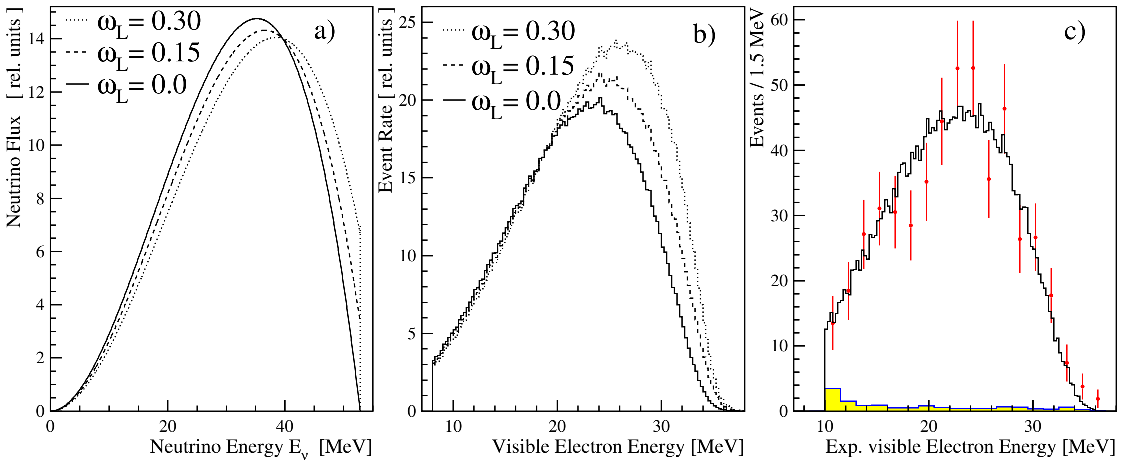

Figure 20. Influence of different values of ω_L on the neutrino spectrum from muon decay at rest (a), the visible electron spectrum for the reaction $^{12}C(\nu_e, e^-)^{12}N_{gs}$ simulated for the KARMEN detector (b), and the measured spectrum (c).

and 6 were performed within the complete pf-shell using the large-space Strasbourg-Madrid codes developed by Caurier [112], [113]. The forbidden transitions were calculated with the RPA.

The resulting cross section, weighted by the neutrino spectrum from decay of a stopped muon, is $2.38 \cdot 10^{-40} cm^2$. The only measurement of this cross section was reported by the KARMEN collaboration $[2.56 \pm 1.08(stat) \pm 0.43(sys)] \cdot 10^{-40} cm^2$ [114]. A much more accurate measurement is needed.

According to a computational feasibility study reported here, it could be measured with a statistical accuracy of a few percent with a high-granularity detector described below called SOUDANINO.

4.6.2. Proposed detector

The geometry and principle of operation of the SOUDANINO detector are similar in principle those of the Soudan-II detector, from which it gets its name [115]. It is composed of iron tubes with thin walls, each containing a position-sensitive gas tube; see Fig. 21. The signal would be read out separately from each individual tube. Particle energy is reconstructed by the range of the particle track or by the total number of fired cells. Directional information can be extracted from the reconstruction of the track. In principle, this detector can be constructed in such way that iron tubes will be replaceable. After making measurements with one set of "target" tubes, they might be replaced by the tubes made from a new material (new target). As a result, neutrino interactions with different nuclei can be studied with the same detector.

Detectors with gas tubes as the sensitive elements have a number of advantages compared, for example, to those with scintillator rods. In general, they are less expensive, and do not require a complex light-readout system. In addition, the low mass of this part of the detector eliminates the necessity to subtract interactions in the target from the interactions in the detector itself. The energy resolution for electrons in the energy range of a few tens of MeV is better by measurement of the track length than by measurement of total energy deposition.

The design of such a detector should be a reasonable compromise between cost and performance. The thinner the tube walls, the better the energy and angular resolution. On the other hand, the thinner tube walls give the detector less average density and, as a result, increase the size and the

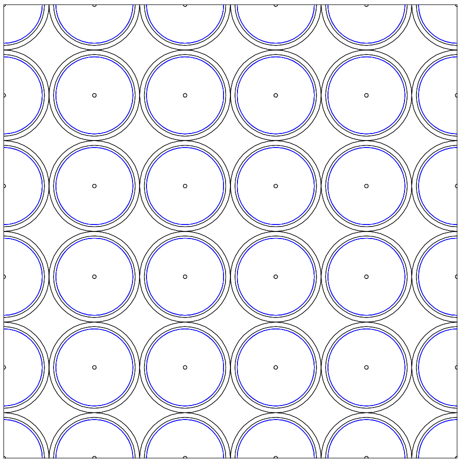

Figure 21. Schematic view of proposed SOUDANINO detector.

number of channels. We obtained an initial optimization of the detector using a GEANT Monte Carlo code. As a result of this study, we conclude that the optimum iron wall thickness is 0.5 mm. The dimensions are OD = 10 mm and ID = 9 mm.

In the rate calculations, the detector was assumed to be at a distance of 50 m from the 2-megawatt target of the Spallation Neutron Source (SNS). For the theoretical cross section of $2.64 \cdot 10^{-40} cm^2$, the neutrino flux at the detector of $3 \cdot 10^6 \nu_e cm^{-2} sec^{-1}$, and the number of iron atoms in one ton ($9.9 \cdot 10^{27} ton^{-1}$), the expected reaction rate is 250 events $y^{-1} ton^{-1}$. We estimate a detection efficiency of 30%. For a desired reconstructed event rate of 1000 y^{-1}, the active detector mass should be 13.3 tons, corresponding to a fiducial volume of 2.5 x 2.5 x 2.5 m^3. This fiducial part of the detector should be surrounded by at least 50 cm of active detector. As a result, the total detector size would be 3.5 x 3.5 x 3.5 m^3 and would consist of a 314 x 314 array of parallel tubes.

During the Monte Carlo study of the SOUDANINO performance we compared two types of active elements for the detector, scintillator rods, and gaseous drift tubes. The results of the simulation of SOUDANINO, for 30-MeV electrons for both gas tubes and scintillator rods, are shown in

Fig. 22. For this simulation, an ideal light readout (no photo-electron statistical fluctuations) was assumed. The energy resolution by measurement of the total energy is 21.4%; the energy resolution measured by track range is 23.4%. For the real detector, the first value will be worse because of the fluctuations in the light collection system. On the lower part of the figure, the simulation of the detector with gas tubes is shown. The average number of fired cells is less and resolution is slightly worse for gas tube detectors compared with scintillator, because of the lower efficiency to low-energy photons.

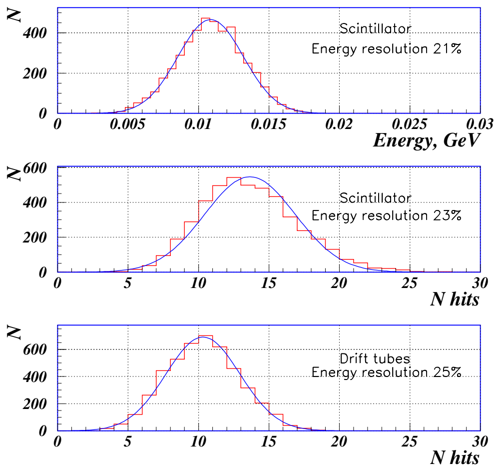

Figure 22. Detector energy resolution, with scintillator and gas drift tube sensitive volume. Energy reconstructed by total energy deposition (upper figure), by the number of fired cells for scintillator (middle figure), and by number of gas drift tubes (lower figure). The electron energy is 30 MeV.

For the energies of interest, the probability to start an electromagnetic shower is small; therefore, the measurement of the energy using the number of fired cells for electrons has excellent linearity as can be seen in Fig. 23.

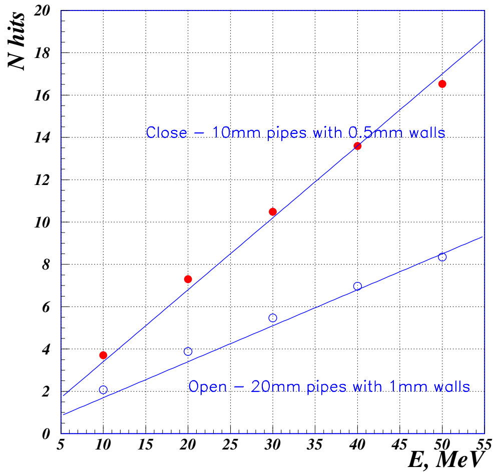

Figure 23. Linearity of the SOUDANINO detector for two different tube thickness for gas drift tubes.

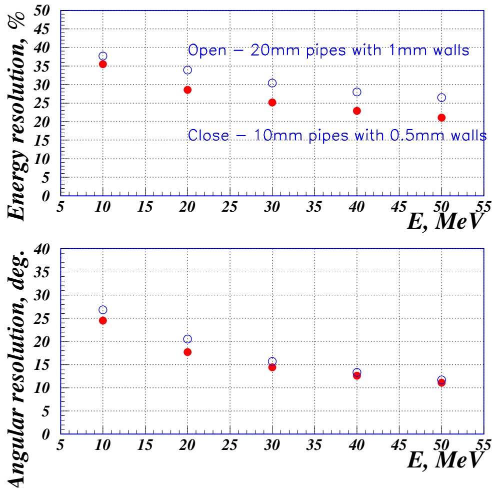

Figure 24. Energy and angular resolution for the the SOUDANINO detector for two different tube thicknesses.

For the iron detector with tubes 1 cm in diameter and walls 0.5 mm thick, the average density will be 1.35 $g\ cm^{-3}$. The 13.5-ton cubic detector will have a fiducial dimension of 2.5 meters on a side. With a fiducial cut of 0.5 meters around the entire detector, the total dimension should be 3.5 x 3.5 x 3.5 m^3. The number of tubes to be read out will be about 10^5. The measurement of the energy by range does not require amplitude information from the tubes, and as a result, a relatively simple, inexpensive electronic system can be used. The results of simulations for this type of detector are presented in Fig. 24 where the energy and angular resolutions are presented. For electrons with an energy of 30 MeV, the predicted energy resolution will is 25% and the angular resolution is about 15^o.

The major source of beam-correlated background will be interactions of high -energy neutrons produced in the SNS target and penetrating into the ORLaND facility. Their interaction might knock out a high-energy proton which could imitate the track of an electron. However, to fire the same number of cells as an electron, the proton should have a much higher energy, see Fig. 25. For example, a 140-MeV proton can produce the same number of hits as a 35-MeV electron. Already this energy-cut significantly reduces the contribution from this source of background. In addition, it is possible to separate electrons from protons with the same number of hits by the shape of the track. The proton tracks are more linear, and the electron tracks are irregular in shape because of the emission of photons. In Fig. 26, examples of the coordinates of firing cells, for 40-MeV electrons and 125-MeV protons are shown. By the introduction of the "track linearity parameter," which is the χ^2 of how well one can fit the track with a straight line, one can separate electrons from protons for a signal with the same number of hits. See Fig 27, and Fig 28. Of course, more sophisticated algorithms can produce better separation.

An accurate cross section of the reaction ^{56}Fe$(\nu_e, e^-)^{56}$Co can be measured with such detector placed at 50 meters from the target station of the SNS (under construction at ORNL). Detailed Monte Carlo computations show that simple gas tube detectors with position sensitivity give an energy resolution comperable to scintillation detec-

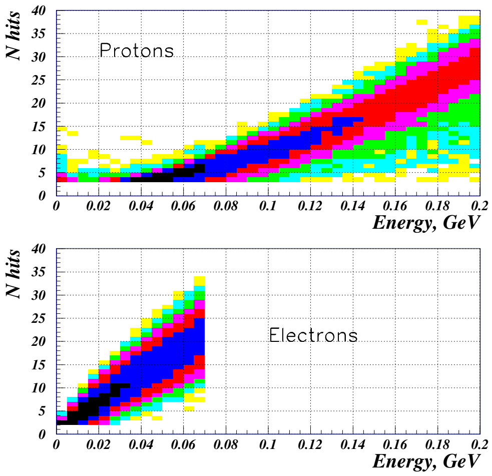

Figure 25. Detector response for protons and electrons.

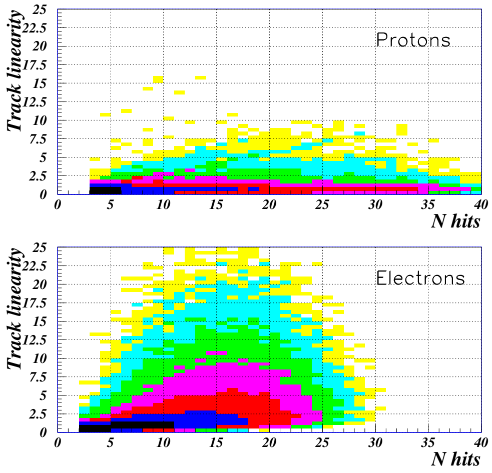

Figure 27. Track Linearity parameter for the protons and electrons in the detector.

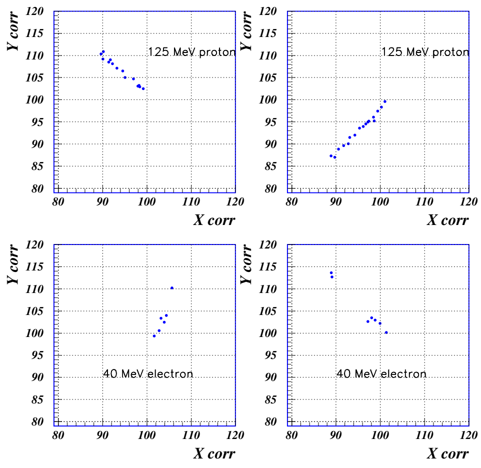

Figure 26. Sample track for 125-MeV proton and 40-MeV electron in the SOUDANINO detector.

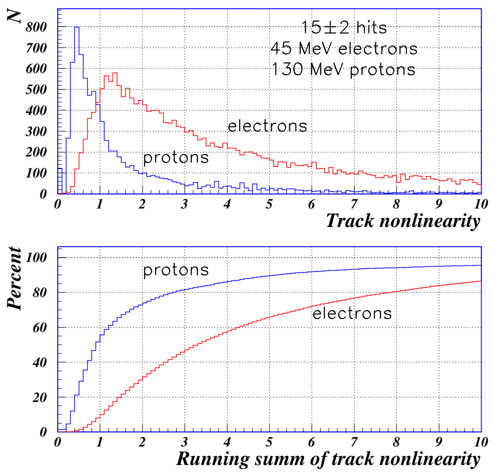

Figure 28. Rejection of the protons from the electrons by Track Linearity parameter.

tors. This technique can be applied to any targets that can be fabricated into tubes of 1 cm OD, with thin walls and with lengths of 3.5 m. These measurements would yield ν_e-nucleus cross section of great importance to neutrino astrophysics.

4.7. Radiochemical measurements

The investigation of apparently reduced neutrino emission by the Sun has led to a number of spectacular explanations. The most compelling and attractive is that neutrinos change their flavor as they pass through the Sun (matter oscillations) or during the flight from the Sun to the Earth (vacuum oscillations). Such a conversion of ν_e into ν_μ or ν_τ is totally unexpected under conventional Standard Model physics. The convincing demonstration of such a flavor transformation would open a window into the new world of physics.

The ideal demonstration of this flavor transformation would be to have ν_μ from the Sun interact via inverse beta decay and produce μ^-. However, this requires neutrinos whose energy is greater than the 105 MeV rest mass of the muon. Unfortunately, the upper end of the solar neutrino spectrum is 15 MeV. We are therefore left with only one detection interaction for ν_μ, neutral current reactions, such as elastic scattering from electrons. Neutral current reactions occur at the same rate for all flavor neutrinos and, in the case of neutrino-electron elastic scattering, are difficult to distinguish from the larger cross section charged current scattering of ν_e from electrons. The only approach available is to determine the ν_e flux with a pure charged current reaction and then subtract this flux from that determined by the elastic scattering rate.

As an example of this approach, consider the Superkamiokande measurement of the ^{8}B neutrino flux from the Sun. If they assume that all of the events are due to ν_e, then their detection rate corresponds to a ^{8}B flux of $2.4 \times 10^6 \nu_e$/cm2 sec. This result is about 46% of the Bahcall-Pinneasault prediction of $5.15 \times 10^6 \nu_e$/cm2 sec. An alternate explanation of the Superkamiokande observation is that the ^{8}B ν flux is really consists of $1.8 \times 10^6 \nu_e$/cm2 sec and $3.4 \times 10^6 \nu_\mu$/cm2 sec which result from neutrino flavor transitions, giving exactly the B-P total ^{8}B production rate. Since the neutral current scattering cross section for these ν_μ is a factor 6 smaller, they appear to give the same rate as charged current scattering by a ν_e flux of 0.6×10^6 /cm2 sec and thus the SK observed rate.

These two types of fits to the data can be distinguished by measuring the electron neutrino flux with a detector that is sensitive only to electron neutrinos, such as ^{37}Cl, ^{127}I, or ^{2}H, and then subtracting this result from the Superkamiokande measurement. A statistically significant difference must be due to neutral current scatterings of $\nu_m u$.

This subtraction process requires not only good statistical measurements of the individual experiments, but also precise knowledge of the relevant neutrino cross sections for each of the detectors. Given the size of the neutral current scattering contribution, this requires that the relevant cross sections be known to 2% or better.

4.7.1. The intense SNS ν_e source

The intense primary proton beam of the SNS and the very sharp time structure of this beam provide the ideal neutrino source for the direct calibration of these solar neutrino detector targets.

The SNS will have a 1.5 mA beam of 1.3 GeV protons. At this energy there is a 10% probability that a proton produces a π^+. Each of these π^+ will stop in the mercury beam target and decay into a μ^+ and a ν_μ with a lifetime of 25 ns. The μ^+, in turn, will decay into a ν_μ and a ν_e with a lifetime of 2.2μsec. Since the primary proton beam consists of 600 ns wide bursts that are separated by 16 msec, there is a very distinct temporal separation between the pion and muon decay products.

4.7.2. Calibration of the ^{37}Cl solar neutrino detector at the SNS

We propose the construction of a high neutrino flux room beneath the main SNS target building with a front wall that is about 13 meters from the primary beam target. The electron neutrino flux at this location from the decay of stopped positive muons in the beam target is $4.3 \times 10^7 \nu_e$/cm2 sec. The expected cross section for electron neutrinos from stopped muon decay on ^{37}Cl is 1.2×10^{-40} cm2. A 50 ton C_2Cl_4 target contains about 1.8×10^{29} ^{37}Cl atoms. Multiplying these factors together gives a ^{37}Ar production rate of 80 events per day or 20,000 per SNS year (250 days).

A two year run at the above rate should provide us with a better than 1% statistical measure of the total cross section. Converting the above neutrino interaction rate into a cross section, requires precise knowledge of the neutrino production rate in the SNS beam target. This will be done in a separate neutrino-electron scattering detector. Again, it will be necessary to accumulate a similar number of events or have a event rate of about 100 per day. The fiducial volume required to carry out this measurement depends on the distance from beam target to detector.

The chlorine detector used for solar neutrinos will be a hybrid electronic-radiochemical detector, that is, a radiochemical detector whose extraction is triggered by an array of photomultiplier tubes in the detector medium that detect the Cerenkov radiation. Each interaction that results in a Cerenkov pulse above a given threshold initiates an extraction of the ^{37}Ar atom just produced.

The time of occurrence of this Cerenkov signal relative to the arrival time of the proton pulse at the beam target determines the event category. Most electron neutrino events, due to muon decays, should occur in the several microsecond window immediately following the end of the proton pulse. This is the time window of interest. Setting this time window at 10 microseconds per pulse gives a total "on time" of 51 seconds per day.

The events that occur the "muon decay" time window will also be classified by the energy of the secondary electron as determined by the Cerenkov pulse height. The charcoal trap in which a given ^{37}Ar atom is stored will depend on the event energy. We will set ten energy windows, with about 4000 total ^{37}A in each of these traps. This should permit a 2% measurement of the partial cross section in each of these energy intervals.

There is an additional 15% contribution from muons that decay during the 600 ns beam pulse. This time period also contains the monoenergetic, 30 MeV ν_μ from pion decay. Interactions between these neutrinos and ^{37}Cl resulting in a secondary electron and an ^{37}Ar are not allowed, so there should not be any excess of 30 MeV secondary electrons.

4.7.3. Background reactions

There is the potential of fast neutron induced ^{37}Ar production. This would occur by a two step process, a (n,p) reaction in the detector producing a fast proton followed by ^{37}Cl(p,n)^{37}Ar. No Cerenkov pulse would be generated in this reaction. However, the neutron secondary will moderate in the detector and then will be captured by a ^{37}Cl atom in the detector. The event timing is thus determined by neutron moderation time and so will occur in a 10 microsecond to 1 millisecond "neutron" window after the proton pulse, quite distinguishable from the muon decay window.

An extraction can be carried out after each of the triggers in the neutron window to insure that these ^{37}Ar atoms are removed from the detector and do not confuse a later extraction. These ^{37}Ar atoms will be stored in a separate charcoal trap and will be used to measure the neutron induced background. Preliminary shielding estimates suggest that the fast neutron induced ^{37}Ar production rate will be at least an order of magnitude smaller than the neutrino induced rate.

There will also be background production of ^{37}Ar by cosmic rays. These occur uniformly in time and are not beam time correlated. The likelihood of having such a cosmic ray production during the 10 μsec. muon decay window is 6×10^{-4}. By utilizing the 15 milliseconds between the end of the neutron time window and the next proton beam pulse as a cosmic ray window, we can get a clear measure of this background rate and use it for background correction. This background rate will also be measured during the beam off times. The detector room will have sufficient overhead shielding to absorb the nucleonic component of the cosmic rays.

Based on previous measurements, we estimate that the total cosmic ray induced ^{37}Ar production will be comparable to the neutrino induced ^{37}Ar production. Of course, only 6×10^{-4} of that will fall into the muon time window. Furthermore, the most likely cosmic ray induced ^{37}Ar production mechanism is the same as that associated with fast neutrons, namely a (p,n) production process followed by a delayed thermal neutron capture. In many or most of these cases there will also be a prompt, extremely big cosmic ray pulse associated with the traversal of the primary muon or an accompanying shower. This two pulse pattern should be quite distinctive. Tests can be made both during beam-off times and also during the 15 millisecond cosmic ray time window.

Just as with the fast neutron initiated triggers, each cosmic ray trigger will initiate a detector extraction. The product atom will be stored in a dedicated charcoal trap.

4.7.4. False triggers

The above description of the detector characteristics and rate estimates suggests that backgrounds are not a significant problem and should not interfere with the proposed measurement. There is, however, another concern, that of false triggers. These can be initiated by slow neutrons that enter the detector, thermalize in the detector and then capture on ^{35}Cl will resulting in the emission of one or more gamma rays with a total energy of about 8 MeV. These gammas will then produce Cerenkov radiating fast electrons either by pair production or Compton scattering. An initial estimate of the effective signal generated by this process is that it is the equivalent of the Cerenkov radiation of a 4 MeV electron. These slow neutrons can be appreciably attenuated by an appropriate shield surrounding the detector.

Since we cannot distinguish a neutron capture associated with a fast neutron initiated ^{37}Ar production followed by a delayed thermal neutron capture from those of a slow neutron entering the detector and captured by a ^{35}Cl *without* an ^{37}Ar production, we will have to carry out an extraction for each such pulse detected during an appropriate time window. This might result in a rather high rate of extractions, with each extraction results in a 2 minute detector deadtime. The deadtime effect can be reduced by dividing the detector volume into a number of separate modules. An extraction will only be carried out in the module in which the triggering event occurred. The other modules of the detector will be on during this extraction period.

Present estimates indicate that dividing the detector into one ton modules should be sufficient to keep the deadtime below 10%. Tests of the false trigger rates will be carried out before a significant number of modules is constructed. The fairly tight energy distribution of these thermal neutron capture events should permit one to easily investigate these triggers and investigate shield that will reduce them.

Similar false triggers can also be initiated by external gamma rays that enter the detector. We anticipate that the rate of these will be considerably less than those due to neutron capture and so should not change the effective deadtime.

4.7.5. ^{127}I detector

The general behavior of the ^{127}I detector, NaI dissolved in water, will be quite similar to the C_2Cl_4 detector described above. Using our LAMPF determined cross section of 2.4×10^{-40} cm^2 for muon decay electron neutrinos producing ^{127}Xe, we expect about 30,000 events per year in a 50 ton detector.

Although the thermal neutron capture cross section on ^{127}I, 6.2 bns, is considerably smaller than the 44 bn thermal capture cross section in ^{35}Cl, it will still be the dominant neutron capture reaction in the NaI detector and the resultant excited nucleus, ^{127}I will have a similar gamma emission pattern to that of ^{36}Cl.

There are, however, some significant background reaction differences. The higher Coulomb barrier of iodine, Z=53, compared to that of chlorine, Z=17, requires higher energy protons to initiate the (p,n) producing process and so appreciably reduces the probably of this reaction per generated proton. This reduction is partially counterbalanced by the presence of large numbers of protons in the water which increases the number of targets available for (n,p) scattering.

Our earlier measurements indicate that the rate of cosmic ray induced production of ^{127}Xe in a NaI detector is a factor 20 lower than in the C_2Cl_4 detector. Similar reductions are expected for reactions due to fast neutrons.

4.7.6. ν_e flux from supernova

In the gravitational collapse of massive stars, supernova formation, enormous numbers of all neutrino species, $\nu_e, \bar{\nu_e}, \nu_\mu, \bar{\nu_\mu}, \nu_\tau$, and $\bar{\nu_\tau}$ are produced. The high density of neutrons in the collapsed core provides a significant opacity for high energy ν_e and thus results in an average energy for ν_e that is significantly lower than that of the other neutrino species. However, if ν_τ transform via MSW (matter) oscillations into ν_e outside the neutron sphere, then the resultant ν_e will find the remaining stellar shell transparent and so will exit the collapsed star the an energy characteristic of the initial ν_τ. The energy differences between these two possibilities are about a factor 3. The cross sections for these two energies are very different. These two effects will permit a clear distinction between $\nu_e \rightarrow \nu_\tau$ flavor transformations in the collapsed core and no transformations in this core.

Thus, a measure of the ν_e energy spectrum and flux from a supernova and the comparison of these parameters with those of other neutrino species as measured by electron scattering detectors such as Superkamiokande, will provide both a demonstration of the matter flavor transformation phenomenon in supernova and a measure of the ν_τ mass. Since the energy spectrum of supernova neutrinos is similar to that of neutrinos emitted by the decay of stopped muons, the SNS cross section measurement is also of great importance to this supernova investigation of this $\nu_\tau \rightarrow \nu_e$ flavor transformation.

4.8. (ν,n) Reactions on Pb and Fe for Supernova Neutrino Detection

The collapse of a massive star and the subsequent explosion as a supernova is an incredibly dramatic cosmic event; it is eclipsed only by the big bang. It produces a few times 10^{53} ergs of energy in neutrinos in ten seconds or so, transfers about 1% of that energy into the mechanical energy that leads to the explosion of the star, and ultimately emits about 0.01% of the energy associated with the neutrinos as the light output of the supernova. Even this small fraction renders it as bright as an entire galaxy. The energy in the neutrinos is 1000 times the total energy that our Sun will emit over its entire life, and for a few seconds the energy in the neutrinos rivals that of the observable light in the universe ([116]).

It is essential to detect the neutrinos from one or more supernovae. Observing the light output of a supernova tells little about the internal mechanics of the star, and nothing about the processes of the collapse or the subsequent formation of a neutron star or black hole. The neutrinos, by contrast, will yield information on all of these aspects of the supernova. They may also be able to tell us about the masses of the neutrinos of different flavors from the differences in their times of flight, and about oscillations through the effects this would have on the energy spectra of the different neutrino flavors. If the collapse goes to a black hole, the neutrinos will confirm that a black hole has been formed, and they might well allow diagnosis of that process.

The Observatory for Multiflavor NeutrInos from Supernovae, OMNIS, is being proposed to detect supernova neutrinos. It will operate by detecting the neutrons that are emitted when they interact with "converters", lead and iron, to produce neutrons. The number of events associated with each possibility depends on the relationship between the energies of the neutrinos and the thresholds for neutron production of the various converter nuclei. The mean energy of the ν_μ's, $\bar{\nu}_\mu$'s, ν_τ's, and $\bar{\nu}_\tau$'s from supernovae is expected to be about 25 MeV, that for $\bar{\nu}_e$'s about 16 MeV, and that for ν_e's about 11 MeV ([117]). The neutron emission threshold via neutral current interactions in iron is 11.30 MeV, whereas that for the charged-current process leading to neutron emission is high enough that virtually no events are produced therefrom. Thus the yield from iron will occur totally from the ν_μ's, $\bar{\nu}_\mu$'s, ν_τ's, and $\bar{\nu}_\tau$'s. The neutral current threshold for lead is only 7.37 MeV, and for (ν_e,e$^-$n) is 9.77 MeV. Thus lead will be sensitive to both charged- and neutral-current interactions, except that the neutrinos that would initiate the charged-current interactions are low in energy. For this reason, even lead is sensitive primarily to the neutral-current interactions initiated by the ν_μ's, $\bar{\nu}_\mu$'s, ν_τ's, and $\bar{\nu}_\tau$'s, barring possible oscillations or effects that would redistribute the energies of the various flavor neutrinos.

However, accurate unscrambling of all the possible effects that can affect the yields from the lead and iron modules requires a good knowledge of the dependence of the yields on the energies of the neutrinos. At present this depends on nuclear theory, estimated by the authors of one recent paper ([118]) to be reliable to only about a factor of two. Thus it is imperative that the "theoretical calibrations" be tested experimentally in a measurement, if that is at all possible. In addition, the energies of the neutrons produced from the decays of the nuclear states populated by the neutrino induced interactions is important to their detection efficiency. Use of probes other than neutrinos in a calibration runs the danger of populating different states from those the neutrinos would populate, or in populating them with strengths that are quite different from those that the neutrinos would produce. Either problem would be expected to skew the predicted detection efficiency. Thus we propose to use the neutrino flux from ORLaND to test the theoretically predicted OMNIS yields.

4.8.1. Neutrino astrophysics from OMNIS

The process of collapse of a massive star involves several subtle effects involving neutrinos, such as neutrino trapping during the collapse, escape of the neutrinos from the proto-neutron star, and possible scattering effects that would produce more energy sharing than might otherwise be expected. The neutrino trapping results from the low entropy in the regions just outside the core of the collapsing star; if the entropy were high the preexisting nuclei would be destroyed, and the coherence effects associated with neutrino scattering from composite nuclei would vanish. This would greatly reduce the opacity of the trapping environment, resulting in prompt emission of the neutrinos produced as the star collapses. The 10^{53} ergs of supernova neutrino energy is thought to be produced in roughly 10 ms ([116]), but were observed on a time scale of seconds from SN1987a, as predicted by the standard model of stellar collapse. Of course, the neutrinos observed for SN1987a were $\bar{\nu}_e$'s, but the trapping time scale is not expected to be profoundly different for the other neutrino flavors.

The neutrinos are trapped within their neutrinospheres until they can random walk their way out of the core of the collapsing star. While this part of the description of stellar collapse is not thought to be in doubt, it could depend on details of the neutron star formation that might be detectable in the observed neutrinos. Thus this aspect of the neutrino distribution would also be important.

In addition, some recent papers have suggested that poorly-understood scattering effects might affect the neutrino energy distributions, possibly at an important level. For example, the process of neutrino bremsstrahlung, would affect both the neutrino energies and their number, while the "inelastic scattering process," would affect their energies ([119]). Furthermore, the neutrino distribution may be Fermi-Dirac, or it may be pinched at both the low- and high-energy ends by scattering processes ([120]). Finally, if convection can occur to an appreciable extent in the nascent neutron star, this would redistribute the highest temperature regions to nearer the neutrinospheres, increasing the energies of the neutrinos emitted.

OMNIS would also provide the capability for observing stellar collapse to a black hole, should that occur fairly promptly. In this event, the neutrinos emitted from the core of the star would become trapped by the infalling matter, to be swallowed shortly thereafter by the black hole as it grew past the neutrinospheres. The ν_e's and $\bar{\nu}_e$'s interact via both the charged- and neutral-current interactions, so this might lead one to expect that they would be trapped somewhat farther from the center of the star than would the ν_μ's, $\bar{\nu}_\mu$'s, ν_τ's, and $\bar{\nu}_\tau$'s, which interact only by neutral-current interactions at supernova neutrino energies. Recent studies ([121], [122]) suggest that this time difference is of order one ms. OMNIS's intrinsic event detection time is much better than 100 μs, so the actual detection time would be statistics limited ([122]). With the statistics expected for OMNIS from a galactic supernova, the timing of the black hole cutoff would be accurate to a few ms, but a close supernova might provide the statistics necessary to measure the sizes of the neutrinospheres of the different neutrino flavors.

4.8.2. Particle physics from OMNIS

The neutrino signals from a galactic supernova might allow the determination of neutrino masses from the times-of-flight of the different flavor neutrinos. The time difference between a light neutrino and a more massive one is given by

$$\Delta t = 2.0(m_x/E_x)^2 L, \tag{45}$$

where the time difference, Δt, is in s; the distance to the supernova, L, is in units of 10 kpc; m_x is the mass of the massive neutrino in eV/c^2; and E is its energy in MeV. The distributions, however, would be smeared out, so would be difficult to differentiate below a level of about 30 eV/c^2. The leading edge of each distribution would provide the best time definition ([123]), provided the detector were capable of such timing (which OMNIS is). Furthermore, OMNIS would have to run in coincidence with Super-Kamiokande or some water Cerenkov successor. However, if collapse went to a black hole, a much better mass limit might be achieved; better than 6 eV/c^2 for the most massive neutrino, for a fairly prompt (but not too prompt) collapse.

An additional feature of supernova neutrino detection with OMNIS will be a large sensitivity to neutrino oscillations of the type ν_μ or $\nu_\tau \rightarrow \nu_e$. This results from the fact that the ν_μ's or ν_τ's coming from a supernova are expected to have considerably higher energies than are the ν_e's. Thus this type of oscillation would produce considerably higher energy ν_e's than would otherwise emerge from a supernova, producing a large number of ν_e's that could produce neutrons from ^{208}Pb(ν_e,e$^-$n)^{207}Bi. Indeed, the neutron yield in the lead modules would increase by a factor of 4 if complete oscillations occurred. However, the most dramatic signal would be in the number of events in which not one, but two neutrons were emitted from each lead nucleus that interacted with a neutrino. This process has a higher threshold, 14.98 MeV, for proceeding by the charged-current interaction than do those in which a single neutron is emitted, but that threshold is still low enough to be very probable if the ν_e's have the sorts of energies characteristic of the ν_μ's and ν_τ's emitted from a supernova. Thus the ratio of two-neutron to one-neutron events would increase by about a factor of 40 if complete oscillations of this type occurred.

4.8.3. Calibrating neutrino yields in iron and lead with ORLaND

The neutrino "beams" from ORLaND would provide an excellent setting for calibrating the yields from OMNIS or, for that matter, any lead or iron detector. Ultimately all such yields will depend on calculations, as it will not be possible to duplicate the distributions of neutrinos from a supernova with any terrestrial source (even assuming that we knew what they were!). However, the monoenergetic ν_μ beam at 30 MeV is at an almost perfect energy for determining the veracity of the calculations for neutral-current neutron production by neutrinos, as that energy is very close to the 25 MeV mean energy expected for the ν_μ's, $\bar{\nu}_\mu$'s, ν_τ's, and $\bar{\nu}_\tau$'s from supernovae. It should be straightforward to utilize the time structure of the neutrinos from the SNS to choose intervals during which the ν_μ's dominate. Furthermore, although the $\bar{\nu}_\mu$ and ν_e yields are comparable during most of the neutrino exposure period, the cross section for charged-current interactions dominates by a large factor over that for neutral-current interactions. Thus the neutrino beams should also allow a test of the calculated yields from charged-current processes initiated by ν_e's. Note that, to take advantage of the time structure separation of neutrino flavors from the SNS, it will be necessary to detect neutrino-induced events on a time scale of the order of a hundred ns. Our event signature combines a prompt signal from the neutrons' first few scatters from the protons in the scintillator, together with a delayed signal from the capture of the neutron on the Gd in the scintillator. Our Monte-Carlo simulations ([124]) suggest that the time required for OMNIS to detect the prompt signal is around 200 ns, as that is the time required for them to move from their production site in the lead or iron and lose about 95% of their energy by scattering from protons in the scintillator.

We therefore propose to set up a mini-version of OMNIS at the ORLaND site to perform these tests of the calculated rates for OMNIS. The materials to be used in the ORLaND experiment could be the same as those used in OMNIS. The materials for the ORLaND experimnent would first be shipped to Oak Ridge, then shipped to New Mexico after the ORLaND experiment was completed. Or, if the time scales for that scenario did not work out, a reduced scale OMNIS module would be constructed at ORLaND. The actual size of the ORLaND installation could depend on the rates realized, the time over which the experiment would be performed, and the configuration used in the measurements. Our estimates of the event rates are given in table 7.

With these yields, a running time of one month on the lead module and several months on the

Table 7
Parameters for the mini–OMNIS at ORLaND

ν_μ flux	1x10^{15} s^{-1}
ν_e flux	1x10^{15} s^{-1}
Detector area normal to the neutrino beam:	3.6x3.4 m^2
Distance of detector from the neutrino source:	50 m
Thickness of the detector:	3.4 m
Mass of the Pb detector:	350 T
Mass of the Fe detector:	242 T
Cross sections (Ref. [118]; Ref. [125]; at 30 MeV)	
Neutral current for Fe	2.6x10^{-41} cm^2
Neutral current for Pb	6.9x10^{-40} cm^2
Charged current (ν_e,e^- n) for Pb (1-neutron)	3.2x10^{-39} cm^2
Charged current (ν_e,e^- n) for Pb (2-neutron)	7.7x10^{-39} cm^2
Neutron detection efficiency per neutron	40%
The resulting yields are given below:	
Neutral current for Fe (from ν_μ's)	70 day^{-1}
Neutral current for Pb (from ν_e's)	350 day^{-1}
Charged current ($\nu_)$) for Pb (1-neutron)	150 day^{-1}
Charged current (ν_e) for Pb (2-neutron)	150 day^{-1}

iron module should provide an excellent calibration for OMNIS. Note that, although charged-current events will occur on the iron module, those are not relevant to our considerations. However, they would be readily identifiable by the time structure of the SNS pulses.

Another feature of OMNIS that is important to its detection efficiency is the energy spectrum of the neutrons emitted. If the neutrons are too low in energy, the signals they produce as they lose their energy to the protons will be difficult to detect above the backgrounds. Thus it is also important to measure these energies; we would also hope to do this with our measurement at ORLaND. Our data would provide an adequate measurement of the energy of the neutrons from the energy deposited in the scintillators in the first 200 ns of the signal.

Backgrounds are likely to require serious consideration, especially those that result in neutrons. We expect not to have neutron backgrounds from the SNS; the shielding of ORLaND should take care of that. However, cosmic ray interactions with the lead and iron will produce neutrons, so active shielding would be required to reduce that problem to acceptable limits. Of course, the pulsed nature of the ν_μ beam will help greatly in identifying and removing background contributions. In addition, it might be necessary to modularize the detector somewhat in order to maintain acceptable event rates for the data acquisition systems.

Of course, the calibrations need not precede the construction of OMNIS; the calibrations only need to be done in order to understand fully the events from the supernova neutrinos.

4.9. Lead Perchlorate as a Neutrino Detection Medium

Because of the high cross section, lead is an attractive neutrino detection medium and has been proposed for use in studies of supernovae [138,139] and neutrino oscillations[140]. This interest has stimulated new calculations of the neutrino cross sections[138,118,141]. The detectors proposed for these studies are typically of a segmented construction employing proportional counters interleaved with liquid or plastic scintillators. These techniques do not generally lend themselves to realizing massive, high resolution, cost effective detectors.

Lead perchlorate ($Pb(ClO_4)_2$) dissolves readily in water yielding a high density, transparent liquid. This raises the possibility of building massive detectors using the well demonstrated water Čerenkov technique. The detector would be capable of measuring not only charged particles and gamma rays but also neutrons which are produced in the ν-Pb interactons. These neutrons are detected via the gamma rays emmitted as a result of neutron capture on the chlorine contained in $Pb(ClO_4)_2$. The ability to simultaneously measure the energy, spatial and temporal information of charged particles, gamma rays and neutrons make this a potentially powerful detector technique.

The neutrino interactions of interest in Pb may occur by either the charged current (CC) or the neutral current (NC) reactions given below

$$\begin{array}{lcll} \nu_e +^{208} Pb & \rightarrow & ^{208}Bi^* + e^- & (CC) \\ & & \downarrow & \\ & & ^{208-Y}Bi + X\gamma + Yn & \\ & & & \\ \nu_x +^{208} Pb & \rightarrow & ^{208}Pb^* + \nu_x^{'} & (NC) \\ & & \downarrow & \\ & & ^{208-Y}Pb + X\gamma + Yn & \end{array}$$

The number of neutrons produced, 0,1 or 2, depends on the neutrino energy and the particular reaction. At 30 MeV, the energy regime of interest to supernova and accelerator beam stop neutrino studies, the CC cross section is approximately 600 times that of carbon, while the NC cross section is approximately 100 times that of carbon. The $\bar{\nu}_e$ cross section on Pb is quite small, however solutions of $Pb(ClO_4)_2$ contain large quatities of hydrogen and the reaction:

$$\bar{\nu}_e + P \quad \rightarrow \quad n + e^+$$

has a significant rate. The NC and CC events are distinguished from each other by the amount of prompt $\gamma + e^-$ energy. NC events only have significant prompt energy when no neutrons are produced. Thus events that have significant prompt energy *and* are accompanied by one or more neutrons are candidates for ν_e or $\bar{\nu}_e$ interactions. The ν_e and $\bar{\nu}_e$ events would be separated off-line. Since only the ν_e can produce two neutron events, these events provide information on the ν_e energy spectrum. The energy spectrum of the one neutron events is a mixture of ν_e and $\bar{\nu}_e$ and one would extract the information on the $\bar{\nu}_e$ by comparison of the one and two neutron prompt energy spectra. The presence of hydrogen in the $Pb(ClO_4)_2$ solution results in the neutrons quickly thermalizing and capturing on ^{35}Cl, which has a high neutron capture cross section of 44.0 b, in approximately 10 μsec. The neutron capture results in multiple gamma rays totaling 8.6 MeV which are detected by way of the Compton scattered electrons.

An 80% solution can be made by dissolving approximately 500 g of $Pb(ClO_4)_2$ in 100 g of water [142]. The resulting transparent liquid has a density of 2.7 gm/cc and a refractive index of 1.5. An energetic electron will produce about 185 Čerenkov photons per centimeter in the wavelength region to which photomultipliers are generally sensitive. The stopping power of the 80% solution is approximately 0.2 cm/MeV, resulting in a photon yield of around 37 photons/MeV. To realize a large Čerenkov detector with the photomultipliers distributed around the periphery requires that the liquid has excellent transparency in the wavelegths of interest. We have made measurements of the transmission and attenuation of light in an 70% solution of $Pb(ClO_4)_2$. Attenuation lengths of greater than 4 m have been obtained. It is encouraging to note that in this unpurified sample there are no significant absorption lines. To measure the attenuation length we constructed a 1 m tall cell through which monochromatic, collimated light from a light emmitting diode was passed. The transmitted light was recorded by measuring the base current from a photomultiplier tube as the height of the liquid was varied in the cell.

We are currently working to understand the processes that influence the light transmission in $Pb(ClO_4)_2$. The present attentuation length value would be appropriate for an experiment at a stopped pion neutrino source such as the proposed OrLAND neutrino facility at the Oak Ridge Laboratory Spallation Neutron Source (SNS)[143]. A 10-t detector (about 3 m^3) could measure the ν-Pb cross section and event signatures in a few months with the anticipated neutrino flux at ORLaND. With this demonstration of the detector technology plus a measurement of the ν-Pb cross sections, one would be in a position to consider a massive $Pb(ClO_4)_2$ based oscillation experiment at a stopped pion facility or a supernova detector.

4.10. Experiments with decay in-flight neutrinos

Both proton storage rings have injector beam dumps that will continuously bleed several percent of the beam at all times while running. This will be minimized; nevertheless estimates of between 3% and 5% are realistic according to the SNS management. The present SNS plan view shows the end of the dump located about 225 meters from the proposed site of the ORLaND detector. After several years of operation and in the case that $\overline{\nu}_\mu \rightarrow \overline{\nu}_e$ oscillations were observed, it would be reasonable to request funding to install a bending magnet of ~3 Tesla with a radius of ~1 meter to direct the one GeV protons to a new target and into a pion horn and a 30 meter decay tunnel with a concrete shield at the end to absorb muons and prevent them from decaying in flight.

Since the fiducial volume of ORLaND is a factor or 18 larger than that of LSND, the event rate for DIF π^+ decay neutrinos could be between 43 and 72 times that in LSND. In addition, the pulse of neutrinos from π^+ decay (ν_μ) will occur within the pulse width of 1.03 msec.

4.10.1. $\nu_\mu p \rightarrow \nu_\mu p$ scattering

The semileptonic νp elastic scattering is a simple reaction and provides a powerful tool to measure the strange quark content, Δs of the proton and its relative contribution to the proton spin. Cross sections for these reactions are well known, within small theoretical uncertainty, and radiative corrections are small, characteristic of neutral-current neutrino scattering. Dependence on the the nucleon form factors are all known from electron scattering measurements, except for the strange form factor.

The form of the neutral current νp elastic scattering cross section can be reduced to the following [136] [137]:

$$\frac{d\sigma}{dQ^2} = \frac{G_F^2}{2\pi}[(-0.63+\frac{G_1^s}{2})^2(1+\frac{Q^2}{4E_\nu^2}) + 0.001156(1-\frac{Q^2}{4E_\nu^2})] \qquad (46)$$

In Eqn. 46, the only unknown is G_1^s, which is the strange quark contribution to the spin of the proton. A measurement of the above cross section will determine this strange quark contribution to the proton spin.

We can also search for ν_μC $\rightarrow p\nu_\mu$X and ν_μC $\rightarrow$ $n\nu_\mu$X quasielastic reactions. Contribution from ν_μp $\rightarrow \nu_\mu$p scattering can be eliminated by applying energy threshold of 60 MeV. The ratio of the proton-to-neutron knock-out reactions for these reactions is a sensitive way to determine the strange axial form factor of the nucleon[46]. We can distinguish between neutrons and protons by the neutron capture on H and the resulting 2.2 MeV γ. We can write this as:

$$R = \frac{\sigma(\nu,\nu' p)}{\sigma(\nu,\nu' n)} = 1 - 16/5G_s \qquad (47)$$

Note that in the ratio method most systematic errors are cancelled. Furthermore, the knock-out neutrons and protons are higher in energy than the free recoil protons because of the Fermi momentum of the nucleons inside the nucleus. For ^{12}C the Fermi momentum is about 220 MeV/c.

While these measurements would be extremely valuable, they will present a significant challenge. The measurement of the absolute cross section would require accurate knowledge of the neutrino flux and spectrum shape, which will be difficult to achieve.

The ratio of the cross section for knocking out protons to that for knocking out neutrons is far more promising; however, by no means straight forward. The identification of the neutron channel will depend on the same techniques as those used for the $\bar{\nu}_\mu \rightarrow \bar{\nu}_e$ neutrino oscillation. The identification of the energetic protons will be more difficult because of the lack of Particle ID. Nevertheless, the restriction to events more than meter from the detector walls will reduce the background significantly. This would only be feasible in a large detector like ORLaND.

Finally, it might turn out that a smaller segmented detector with tracking capabilities, used for cross section measurements would be more appropriate for these measurements. The importance of the physics involved here justifies an R&D efford during the first phase of the experiment.

4.11. Second target station

In addition to the fist SNS target station presently under construction, the National Science Foundation is funding a study to produce a Concept Design Report (CDR), for a second target station. The concept is to optimize this station for slow neutron beams. The accumulator ring will supply both target stations; it will supply 50 Hz to the first target, and 10 Hz to the second. Until the completion of the second target station, the accumulator ring will supply 60 Hz to the first target as discussed elsewhere in this report. This implies that the second station will have 5 times less beam power than the first.

The ORLaND facility will be located about 50 meters from the first target station, and approximately 110 meters from the second. Placing ORLaND close to the second target would make neutrino-nucleus measurements impractical. This station at a further distance will be very valuable for $\bar{\nu}_\mu \rightarrow \bar{\nu}_e$ oscillation measurements in that it will produce a completely different curve on the $sin^2 2\theta$, δm^2 plane consistent with the oscillation signal than that from the first target, and the intersection of these distinct curves could significantly constrain the parameters. This is demonstrated by an example shown in Fig. 29.

For neutrino appearance oscillation experiments, the neutrino flux for an isotopic source, for small δm^2, does not depends on the distance, while at the same time, beam related background falls quadratically. The probability of appearance N(app.)

$$\begin{aligned} N(app) &= \sin^2 2\theta \ \sin^2(1.27\Delta m^2 L/E)/L^2 \\ &= \sin^2 2\theta \ (1.27\Delta m^2/E)^2 \qquad (48) \end{aligned}$$

While the beam related background falls as $1/r^2$. This argument of reduction of beam associated background is very important because there will always be some $\bar{\nu}_e$ flux produced from decay of μ^-. Value of this contamination, usually is a result of very complicated calculations and depends of the exact design of the target station. The second target station would help in an experimental determination of this irreducible background and would be truly unique.

This could result in a more sensitive measurement of $\bar{\nu}_\mu \rightarrow \bar{\nu}_e$ appearance experiment at low δm^2 region. This could be the ultimate such experiment for a stop pion facility, namely, one detector and two neutrino sources. However, the low total beam power and the long distance will result in low neutrino intensities, severely restricting its usefulness to neutrino-nucleus cross section measurements.

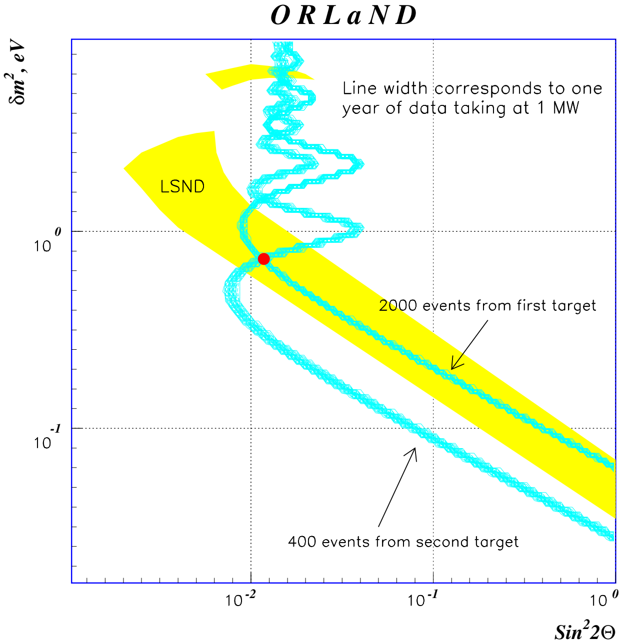

Figure 29. The precision of the measurement of the mixing parameters in the LSND region. Narrow bands correspond to regions of allowed parameters, using the number of events from the first and second target stations for one year of data collection with a spallation source power of 1 MW per target.

5. ORLaND Facility Cost and Schedule

We must begin the discussion of the cost and schedule of the ORLaND project with a few words of disclaimer and explanation. Our concept of ORLaND is of a user facility, housing experiments developed by independent collaborations to be selected by a broad-based program advisory committee. Nevertheless, the Department of Energy will require an estimate of total project cost for ORLaND. We have made such an estimate, including the cost of an initial suite of experiments, and the results are included here. It must be realized that the initial experiments that we have costed are merely straw-men, based largely on input from participants at the May 2000 Oak Ridge Workshop. While we believe that they serve the purpose of providing a reasonably accurate total facility cost estimate, the actual choice of initial experiments to be put on the floor will be the result of open proposal solicitation and a proposal evaluation process.

In spite of these considerations, we feel that the cost estimate developed for the Department of Energy will be of use to the scientific community as they consider this project. Therefore, with some reservations, we include here a discussion of this preliminary design concept and corresponding cost estimate for the ORLaND detector hall and a prototypical initial suite of experiments.

This design is based on basic parameters defined by Monto Carlo studies of event rates, shielding, and background suppression. These parameters were incorporated into a facility concept during a year-long study carried out with the engineering firm, Stone and Webster. In addition to developing the preliminary design concept, Stone and Webster developed a cost estimate and carried out a feasibility study. The conclusion of the feasibility study is that ORLaND can be built without any significant impact on the SNS.

In our present concept, the basic components of the ORLaND facility from the user's point of view are a large underground detector hall, a control room ($\sim 20\text{m}^2$) to house data acquisition and control equipment for all ORLaND experiments, and a set of storage tanks on the surface with a volume large enough to store all fluid used in the large ORLaND detector.

The ORLaND detector hall is a cylindrical underground laboratory 78 feet in diameter and $\sim$ 110 feet deep, including the foundation. The hall contains a large cylindrical tank 48 feet in diameter and 48 feet high. This large tank can be filled with approxiamtely 2k-ton (1500 ton fiducial mass) of any one of several appropriate liquids (see discussion of experiments in Section 4), and will probably serve as the primary flux monitor for all experiments. The current plan for the detector hall consists of three operating floors with only $\sim$ 40% of the area of each floor occupied by the large detector tank. Thus, a significant amount of space exists on each level to house detectors of mass on the order of 10^2 tons, in addition to the large detector tank.

There are a number of reasons that the detector hall must be placed underground. First and most important, the detectors must be shielded by at least ten meters of steel equivalent ($\sim$ 8 kg/cm^2) from neutrons produced in the SNS spallation target. This was one of the lessons learned by the LSND collaboration at LANL. It would be prohibitively expensive to provide the required shielding for an above-ground facility if iron or concrete were used, and require too much space if earth were used.

It is also necessary to eliminate the residual hadronic component of cosmic rays from all experiments housed in the laboratory. For this reason, in addition to the earth shielding provided by the underground location, an overburden of thickness 3 kg/cm^2 will be provided.

A probable location for the ORLaND detector hall on the SNS site was determined as a part of the Stone and Webster feasibility study, in close consultation with the SNS project engineering staff. The location is determined not only to optimize the neutrino-science potential, but also by constraints related to the SNS target-building construction schedule, the requirement of non-interference with any aspect of the SNS, and by limitations on possible profiles for provision of funds for ORLaND by the DOE Nuclear Physics Program Office. Figure 4 on page 24 is a plan view of the SNS facility with two target buildings shown. Only the first of these targets, Target Building 1 (labeled "Target Building" on Figure 4), is part of the initial construction. Target Building 1 is designed to handle the full power of the SNS proton beam and operate at 60 Hz. The second or Long Wave-length Target Station (LWTS) will handle $\sim$ 1 MW of beam power, and is intended to operate at 10 Hz (labeled "Future Target Building" in Figure 4).

The construction of Target Building 1 (TB-1) will begin in the first quarter of fiscal year 2001 (FY01) and continue for three years. The installation of neutron scattering instruments on the southwest side (lower left in Figure 4) of TB-1 will begin in the second quarter of FY04 and continue until the second quarter of FY05. Installation of neutron scattering instruments on the northeast side of TB-1 will begin in FY06. The current (much softer) plan for the LWTS calls for its construction to occur between the beginning of FY04 and the third quarter of FY06. From the point of view of cost minimization and minimal interference, the ideal time for construction of the ORLaND target hall is during construction of an SNS target building. The ideal location for ORLaND is on the southwest (SW) side of TB-1 as near as possible to the neutron production target position. Because the earliest anticipated funding date for ORLaND occurs too late, and because of interference with SNS instruments on the SW side of TB-1, it will not be possible to locate there. The next best site is a corresponding site on the NE side of TB-1, between TB-1 and the LWTS, but as close as possible to TB-1. This is the position selected in our feasibility study. The exact location (i.e., the minimum distance between the outer wall of the ORLaND hall and TB-1) has not been defined precisely as yet, but it is clear that we will be able to achieve center-to-center distance between the SNS target and the large detector tank of < 55m.

The Stone and Webster study provided a careful evaluation of costs and cost profiles for the ORLaND project. A number of scenarios were investigated that encompass a range of $\sim$ 10% in total project cost with the greatest cost effectiveness achieved if construction is carried out simultaneously with construction of one of the SNS target buildings. In the cost profiles presented here, we have assumed construction of ORLaND will coincide with construction of the LWTS (FY04-05 based on the tentative SNS schedule for the LWTS). The estimated total project cost is \$62M, including CDR, engineering escalation, and contingency. Of this total, \$34M is required to construct the underground detector laboratory, while the remaining \$28M is the estimated cost of the three straw-man experiments. The separation is not completely clean, since the cost of procuring the large (2000-ton) detector tank and installing it in the detector hall ($\sim$ \$5M) is included in the construction costs. However, all other costs associated with large tank experiments (fill liquids, photomultipliers, signal processing electronics, etc.) are included in the experiment costs. A breakdown of the construction and experiment costs into a few broad categories is shown in Table 5. It is useful to break down construction costs further to understand the possible impact of the necessity to integrate with SNS construction. We have identified those parts of the construction whose timing with respect to SNS construction is considered critical. Of the \$34M construction cost (\$25M direct cost and \$9M in escalation and contingency), a total of \$7.7M (\$6.2M direct plus \$1.5M escalation and contingency) is time critical. The estimated time required for civil construction of the detector hall is about eleven months, which fits comfortably within the constraints of the present SNS schedule.

We have not yet carried out a careful analysis of the operating budget that will be required for ORLaND. Current ball-park estimates range from \$2M to \$3M per year. Funding for commissioning and "pre-operation" is included in the \$62M total project cost.

Table 8
ORLaND Cost Breakdown

	Construction	Experiments & Commissioning	Total
CDT & planning	1.9	0.0	1.9
Engineering & design	3.0	2.6	5.6
Civil construction	8.6	0.0	8.6
Detectors, exp. equip., etc.	4.4	11.0	15.4
ES&H	0.4	0.0	0.4
Management	4.2	0.9	5.1
Contract burdens	2.1	0.0	2.1
Commissioning, preops	0.0	5.0	5.0
Total direct cost	24.6	19.5	44.1
Contingency	6.8	5.9	12.6
Escalation	2.5	2.6	5.1
Grand Total	33.8	28.0	61.7

6. Worhshop Participants

Yurdanur Akovali	Oak Ridge National Laboratory
Frank T. Avignone	University of South Carolina
Cyrus Baktash	Oak Ridge National Laboratory
Bryan Barmore	Oak Ridge National Laboratory
Jon Batchelder	Oak Ridge Associated Universities
Jim Beene	Oak Ridge National Laboratory
Carrol Bingham	University of Tennessee
Jeff Blackmon	Oak Ridge National Laboratory
Richard Boyd	Ohio State University
Robert Burman	Los Alamos National Laboratory
Lali Chatterjee	Cumberland University
Vincent Cianciolo	Oak Ridge National Laboratory
David Dean	Oak Ridge National Laboratory
George W. Dodson	SNS/ORNL
Guido Drexlin	Karlsruhe Institut fur Kernphysik
Mostafa A. Elaasar	Southern University at New Orleans
Steven R. Elliott	University of Washington
Jonathan H. Engel	University of North Carolina
Ali R. Fazely	Southern University
Tony A. Gabriel	SNS/ORNL
Alfredo Galindo-Uribarri	Oak Ridge National Laboratory
Valdimir Gudkov	University of South Carolina
W. Raphael Hix	University of Tennessee
Barry R. Holstein	University of Massachusetts
Richard L. Imlay	Louisiana State University
Edwin E. Kolbe	University of Basel
Kenneth Lande	University of Pennsylvania
Karlheinz Langanke	Aarhus University
Felix Liang	Oak Ridge National Laboratory
Luke W. Mo	Virginia Tech
Paul E. Mueller	Oak Ridge National Laboratory
Andreas G. Piepke	University of Alabama
Franz Plasil	Oak Ridge National Laboratory
Steven J. Pollock	University of Colorado
David C. Radford	Oak Ridge National Laboratory
Carl Rosenfeld	University of South Carolina
Dubravka Rupnik	Southern University
Krzysztof Rykaczewski	Oak Ridge National Laboratory
Dan Shapira	Oak Ridge National Laboratory
Michael S. Smith	Oak Ridge National Laboratory
Paul Stankus	Oak Ridge National Laboratory
Dan Stracener	Oak Ridge National Laboratory
Michael R. Strayer	Oak Ridge National Laboratory
Yang Sun	University of Tennessee
Kenneth S. Toth	Oak Ridge National Laboratory
Robert L. Varner	Oak Ridge National Laboratory

Petr Vogel	CalTech
Glenn R. Young	Oak Ridge National Laboratory
Chang-Hong Yu	Oak Ridge National Laboratory

7. Acknowledgement

The concept of the ORLaND facility and much of the science described in this "white paper" was developed over the past few years by contributions from a group of scientists from many universities and laboratories. The authors of the present document are indebted to all who have contributed for their early work. We include below a list that we hope contains the names of those who participated in the early development work.

Carleton University: C. Hargrove
Drexel University: C. Lane
Duke University and TUNL: E. Bilpuch, L. DeBraeckeleer, W. Tornow
Embry Riddle Aeronautical University: D. Smith
Institute for Theoretical and Experimental Physics: M. Danilov, V. Nosik, O. Zeldovich
Jefferson Laboratory: P. Degtiarenko
Kent State University: B. Anderson, J. Watson, W.-M. Zhang
Los Alamos National Laboratory: R. L. Burman
Louisiana State University: R. Imlay, W. Metcalf, B. Svoboda
Louisiana Tech University: Z. Greenwood
North Carolina State University: C. Gould
Oak Ridge Associated Universities: K. Carter
Oak Ridge National Laboratory: T. Awes, J. Blackmon, F. Bertrand, C. Baktash, J. Ball, D. Bardayan, J. Beene, V. Cianciolo, C. Britton, D. Dean, Y. Efremenko, A. Galindo-Uribarri, A. Mezzacappa, F. Plasil, M. Strayer, A.Wintenberg, G. Young
Ohio State University: R. Boyd, A. Murphy
SNS/ORNL: T. A. Gabriel, G. Dodson
Southern University, Baton Rouge: A. Fazely, D. Rupnik, R. Tashakkori
Southern University, New Orleans: R. Gunasingha, M. Elaasar
Tel Aviv University: S. Nussinov
University of Alabama: J. Busenitz, A. Piepke, I. Stancu, J. Wolf
UCLA: D. Cline
University of California, Riverside: G. VanDalen
University of Mississippi: J. Reidy
University of Pennsylvania: K. Lande, P. Wildenhain
University of South Carolina: F. Avignone, V. Gudkov, K. Kubodera, S. Mishra, C. Rosenfeld
University of Tennessee, Knoxville: S. Berridge, W. Bugg, L. Chatterjee, H. Cohn, T. Handler, E. Hart, Y. Kamyshkov
Valparaiso University: T. Stanislaus, D. Koetke, R. Manweiler
Virginia Tech L. Mo, T. Nunamaker

REFERENCES

1. See, *e.g.*, W. C. Haxton and B. R. Holstein, Am. J. Phys. **68**, 15 (2000).
2. M. N. Butler and J. W. Chen, *Nucl. Phys.* **A675**, 575 (2000).
3. M. N. Butler, J. W. Chen, and X. Kong, `nucl-th/0008032`.
4. M.N. Butler and J. W. Chen, in preparation.
5. S. D. Ellis and J. N. Bahcall, *Nucl. Phys.* **A114**, 636 (1968); J. N. Bahcall and R. M. May, *Ap. J* **55**, 501 (1969).
6. R. Schiavilla *et al.*, *Phys. Rev.* **C58** 1263 (1998).
7. J. N. Bahcall, K. Kubodera, and S. Nozawa, *Phys. Rev.* **D38**, 1030 (1987).
8. N. Tatara, Y. Kohyama and K. Kubodera, *Phys. Rev.* **C42**, 1694 (1990).
9. M. Doi and K. Kubodera, *Phys. Rev.* **C45**, 1988 (1992).
10. S. Ying, W. C. Haxton and E. M. Henley, *Phys. Rev.* **C45**, 1982 (1992); *Phys. Rev.* **D40**, 3211 (1989).
11. K. Kubodera and S. Nozawa, *Int. J. Mod. Phys.* **E3**, 101 (1994); Y. Kohyama and K. Kubodera, USC(NT)-report-92-1, unpublished.
12. S. Nakamura, T. Sato, V. Gudkov, and K. Kubodera, `nucl-th/0009012`.
13. S. Weinberg, *Phys. Lett.* **B251**, 288 (1990); *Nucl. Phys.* **B363**, 3 (1991); *Phys. Lett.* **B295**, 114 (1992).
14. D. B. Kaplan, M. J. Savage and M. B. Wise, *Phys.Lett.* **B424**, 390 (1998); *Nucl. Phys.* **B534**, 329(1998).
15. D. B. Kaplan, M. J. Savage and M. B. Wise, *Phys. Rev.* **C59**, 617 (1999).
16. T.-S. Park, K. Kubodera, D.-P. Min, M. Rho, *Nucl. Phys.* **A646**, 83 (1999).
17. J. W. Chen, G. Rupak and M. J. Savage *Nucl. Phys.* **A653**, 386 (1999); *Phys. Lett.* **B464**, 1 (1999).
18. J. W. Chen and M. J. Savage , *Phys. Rev.* **C60**, 065205 (1999).
19. G. Rupak, `nucl-th/9911018`.
20. X. Kong and F. Ravndal, `nucl-th/0004038`; *Nucl. Phys.* **A665**, 137 (2000); *Nucl. Phys.* **A656**, 421 (1999);*Phys. Lett.* **B470**, 1 (1999).
21. T. -S. Park, K. Kubodera, D. -P. Min and M. Rho, *Ap. J.* **507**, 443 (1998). Xd
22. M. Liebendörfer, A. Mezzacappa, F.-K. Thielemann, O. E. B. Messer, W. R. Hix, and S. W. Bruenn, Phys. Rev. Letts., submitted, 2000.
23. A. Mezzacappa and S. W. Bruenn, Ap.J. **405**, 637 (1993).
24. A. Mezzacappa and S. W. Bruenn, Ap.J., **410**, 740 (1993).
25. S. E. Woosley, D. H. Hartmann, R. D. Hoffman, and W. C. Haxton, Ap.J. **356**, 272 (1990).
26. W. Haxton, Topics in neutrino astrophysics. In *Proceedings of the 1998 TASI Summer School*, 1999.
27. B. S. Meyer, Ann. Rev. of Astronomy and Astrophysics, **32**, 153 (1994).
28. Y.-Z. Qian, W. C. Haxton, K.-H. Langanke, and P. Vogel, Phys. Rev., **C55**, 1532 (1997).
29. W. C. Haxton, K.-H. Langanke, Y.-Z. Qian, and P. Vogel, Phys. Rev. Letts. **78**, 2694 (1997).
30. B. S. Meyer, G. C. McLaughlin, and G. M. Fuller, Phys. Rev. **C58**, 3696 (1998).
31. W. Haxton,Phys. Rev. **D36**, 2283 (1987).
32. K.-H. Langanke, P. Vogel, and E. Kolbe, Phys. Rev. Letts. **76**, 2629 (1996).
33. R. N. Boyd, Omnis, the observatory for multiflavor neutrinos from supernovae. In S. Kubono and T. Kajino, editors, *Origin of Matter and Evolution of Galaxies*, Singapore, 2000. World Scientific.
34. Y. Fukuda *et al.*, Phys. Lett. **B433**, 9 (1998).
35. A. Athanassopoulos, *et al.*, Phys. Rev. Lett. **77**, 3082 (1996).
36. M. J. Musolf *et al.*, Phys Reports **239**, 1 (1994).
37. T.P. Cheng, Phys. Rev. **D13**, 2161 (1976); J. Gasser, H. Leutwyler, and M. E. Sainio, Phys. Lett. **B168**, 105 (1986).
38. J. Ashman et al., Nucl. Phys. **B328**, 1 (1989); P. L. Anthony et al., Phys. Rev. Lett. **71**, 959 (1973); B. Adeva et al., Phys. Lett. **B302**, 533 (1994); D. Adams et al., Phys. Lett. **B329**, 399 (1994); K. Abe et al., Phys. Rev. Lett. **74**, 346 (1995).

39. J. F. Donoghue and C. Nappi, Phys. Lett. **B168**, 105 (1986).
40. See, *e.g.*, R. L. Jaffe, Phys. Lett. **B229**, 275 (1989); M. J. Musolf and M. Burkardt, Z. Phys. **C61**, 433 (1994); H. Forkel et al., Phys. Rev. **C50**, 3108 (1994); W. Koepf, S.J. Pollock, and E. M. Henley, Phys. Lett. **B288**, 11 (1992); W. Koepf and E. M. Henley, Phys. Rev. **C49**, 2219 (1994); T. Cohen, H. Forkel, and M. Nielsen, Phys. Lett. **B316**, 1 (1993); N. W. Park, J. Schechter, and H. Wiegel, Phys. Rev. **D43**, 869 (1991); H. Wiegel et al., Phys. Lett. **B353**, 20 (1995); M. J. Musolf, H.-W. Hammer, and D. Drechsel, Phys. Rev. **D55**, 2741 (1997); H. Forkel, F. S. Navarra, and M. Nielsen, Phys. Rev. **C61**, 055206 (2000).
41. K. A. Aniol *et al.*, Phys. Rev. Lett. **82**, 1096 (1999).
42. D. T. Spayde *et al.*, Phys. Rev. Lett. **84**, 1106 (2000).
43. D. T. Spayde *et al.*, (SAMPLE), nucl-ex/9909010
44. S.-L. Zhu *et al.*, hep-ph/0002252.
45. L. A. Ahrens, Phys. Rev. Lett. **35**, 785 (1987).
46. G. T. Garvey et al, Phys. Lett. **B289**, 249 (1992).
47. E. Kolbe, *et. al.*, APJ Lett. **401**, L89 (1992).
48. T. W. Donnelly *et al.*, Nucl Phys. **A503**, 589 (1989).
49. R. L. Jaffe, Phys. Lett. **B229**, 275 (1989).
50. J. J. Cowan, F.-K. Thielemann, J. W. Truran, Phys. Rep. **208**, 267 (1991).
51. There are many review articles on this subject. See for example T. W. Donnelly, Prog. Part. Nucl. Phys. **13**, 183 (1985).
52. T. W. Donnelly and W. C. Haxton, At. Dat. Nucl. Dat. Tab. **23**, 103 (1979).
53. B. S. Pudliner, V. R. Pandharipande, J. Carlson, S. C. Pieper, and R. B. Wiringa, Phys. Rev. **C56**, 1720 (1997).
54. R. B. Wiringa, J. Carlson, S. C. Pieper, and V. R. Pandaripande, Phys. Rev. C, (in press, 2000).
55. M. Hjorth-Jensen, T. T. S. Kuo, and E. Osnes, Phys. Rep. **261**, 125 (1995).
56. S. Cohen and D. Kurath, Nucl. Phys. **73**, 1 (1965).
57. B. A. Brown and B. H. Wildenthal, Ann. Rev. Nucl. Part. Sci. **38**, 29 (1988).
58. A. Poves and A. P. Zuker, Phys. Rep. **70**, 235 (1981).
59. S. E. Koonin, D. J. Dean, and K. Langanke, Phys. Repts. **278**, 1 (1997).
60. C. Volpe, N. Auerbach, G. Colo, T. Suzuki, and N. Van Giai, Phys. Rev. **C62**, 15501 (2000).
61. E. Kolbe, K. Langanke, P. Vogel, Nucl. Phys.**A652**, 91 (1999).
62. A. C. Hayes, Phys. Repts. **315**, 257 (1999).
63. K. Langanke, D. J. Dean, P. B. Radha, Y. Alhassid, and S. E. Koonin, Phys. Rev. **C52**, 718 (1995).
64. G. Martinez-Pinedo, K. Langanke, and D. J. Dean, ApJS **126**, 493 (2000).
65. G. M. Fuller, W. A. Fowler and M.J. Newman, ApJS **42**, 447 (1980); **48**, 279 (1982); ApJ **252**, 715 (1982); **293**, 1 (1985).
66. D. Dean, *et. al.* Phys. Rev. **C58**, 536 (1998).
67. R. L. Burman, M. E. Potter and E. S. Smith, Nucl. Instr. and Meth. A 291 (1990) 621; R. L. Burman, A. C. Dodd and P. Plischke, Nucl. Instr. and Meth. in Phys. Res. A 368 (1996) 416.
68. R. C. Allen, *et al.*, Nucl. Instr. and Methods **A284** (1989) 347.
69. R. E. Prael and H. Lichtenstein, The LAHET Code System, Los Alamos National Laboratory report LA-UR-89-30, (Sept. 1989). The Bertini model was first widely available through the Oak Ridge National Laboratory code HETC, see T. A. Gabriel *et al.*, Oak Ridge National Laboratory report ORNL-TM-3319 (1970); the HETC code is now embodied in LAHET.
70. Hugo W. Bertini, Phys. Rev. 188 (1969) 1711.
71. G. A. Aardsma *et al.*, *Phys. Lett.* **B194**, 321 (1987).
72. G. T. Ewan *et al.*, **SNO proposal SNO-87-12** (1987).
73. S. E. Willis *et al.*, Phys. Rev. Lett. **D4**, 522 (1980).

74. See, *e.g.* D. B. Kaplan, M. J. Savage, and M. B. Wise, Phys. Lett. **B424**, 390 (1998); Nucl. Phys. **B534**, 329 (1998).
75. M. Butler and J. Chen, nucl-th/9905059.
76. X. Kong and F. Ranvdal, nucl-th/0004038.
77. F. T. Avignone and Yu. V. Efremenko, Nucl. Phys. (Proc. Suppl.) **87**, 304 (2000). xs
78. F. T. Avignone and Yu. V. Efremenko, Proc. of the 2000 Carolina Conference on Neutrino Physics, ed., K. Kubodera (World Scientific, 2000), in press.
79. R. L. Burman *et al.*, NIM **A291**, 621 (1990).
80. R. L. Burman *et al.*, NIM **A368**, 416 (1996).
81. M. L. Swartz, (1999), in Proc. of the 19th International Symposium on Lepton and Photon Interactions at High-Energies, Stanford, California, August 1999.
82. D. Charlton, (1999), in Proc. of the 19th International Symposium on Lepton and Photon Interactions at High-Energies, Stanford, California, August 1999; A.Gurtu, (2000), in Proc. of the 30th Rochester Conference, Osaka, Japan, 2000.
83. A. Czarnecki and W. J. Marciano, Int. J. Mod. Phys. **A13**, 2235 (1998).
84. A. Czarnecki and W. J. Marciano, *BNL-HET-00/2, hep-ph/0003049* (2000).
85. S.C. Bennett and C. E. Wieman, *Phys.Rev.Let.* **82**, 2484 (1999).
86. The European Physical Journal **C3**, 1 (1998).
87. A. V. Kyuldjiev, Nucl. Phys. **B243**, 387 (1984).
88. L. B. Okun, "Leptons and Quarks," North Holland (1982).
89. K. Langanke, P. Vogel, and E. Kolbe, Phys. Rev. Lett. **76**, 2629 (1996).
90. E. Kolbe, Phys. Rev. **C54**, 1741 (1996).
91. R. C. Allen, H. H. Chen, P. J. Doe, R. Hausamann, and W. P. Lee, Phys. Rev. Lett. **64**, 1871 (1990).
92. LAMFP Research Proposal LA-UR-89-3764 (1989), Spokesman: W.C. Louis.
93. E. Kolbe, *et. al.* EPJ **A3**, 389 (1998).
94. M. Fukugita *et al.*, Phys. Rev. **C41**, 1359 (1990).
95. M. Fukugita *et al.*, Phys. Lett. **B212**, 139 (1988).
96. E. Kolbe *et al.*, Phys. Rev. C **49**, 1122 (1994).
97. T. W. Donnelly, *programm NUEE for calculations of cross sections used for ISIS neutrinos by KARMEN*, private communication (1991).
98. D. A. Krakauer *et al.*, Phys. Rev. **D45**, 2250 (1992).
99. C. Athanassopoulos *et al.*, Phys. Rev. **C55**, 2078 (1997).
100. R. Maschuw *et al.*, ProgṖart. Nucl. Phys. **40**, 183 (1998), Ed. A. Faessler (Elsevier Oxford)
101. H. Tietzel, diploma thesis, University of Erlangen, Germany (1993).
102. J. Bernabéu and P. Pascual, Nucl. Phys. **A324**, 365 (1979).
103. M. Pourkaviani and S.L. Minz, J. Phys. G: Nucl. Part. Phys. **16**, 569 (1990).
104. R. L. Burman *et al.*, *Neutrino Flux Calculations for the ISIS Spallation Neutron Facility*, Forschungszentrum Karlsruhe (1995) FZKA 5595.
105. W. Fetscher, Phys. Rev. Lett. **69**, 2758 (1992); **71**, 2511(E) (1993).
106. C. Grueb, D. Wyler, and W. Fetscher, Phys. Lett. **B 324**, 480 (1994).
107. E. V. Bugaev *et al.*, *Nucl. Instrum. Methods* **A324**, 350 (1979)
108. E. Kolbe, K. Langanke and G. Martinez-Pinedo, Preprint: arXiv:nucl-th/9905001 3 Aug, 1999.
109. E. Kolbe and K. Langanke, Preprint: arXiv:nucl-th/0003060 27 March 2000.
110. J. D. Walecka, in Muon Physics, eds. V. W. Hughes and C. S. Wu (Academic Press, New York, 1975) p.113.
111. T. W. Donelly and R. D. Peccei, Phys. Rev.**A50**, 1 (1979).
112. E. Caurier, computer code ANTOINE, CRN, Strasbourg, 1989.
113. E. Caurier, G. Mart'nez-Pinedo, F. Nowacki, A. Poves, J. Retamosa and A. P. Zukes *Phys. Rev.* C **C59**,

2033 (1999)
114.K. Eitel, Private Communication, G. Ruf, diploma the sis, University of Bonn.
115.W. W. M. Allison, *Nucl. Instrum. Methods* **A376**, 36 (1996).
116.A. Burrows, Ann. Rev. Nuc. Part. Sci. **40**, 181 (1990).
117.Y.-Z. Qian, G. M. Fuller, G. L. Mathews, R. W. Mayle, J. R. Wilson, and S. E. Woosley, Phys. Rev. Lett. **71**, 1965 (1993).
118.G. M. Fuller, W. C. Haxton, and G. McLaughlin, Phys. Rev. **D59**, 085005 (1999).
119.S. Hannestad, and G. Raffelt, Ap.J. **507**, 339 (1998).
120.T. Totani, K. Sato, H. E. Dalhed, and J. R. Wilson, Ap.J. **496**, 216 (1998).
121.T. W. Baumgarte, H.-Th. Janka, W. Keil, S. Shapiro, and S. Teukolsky, Ap.J.bf 468, 823 (1996).
122.J. Beacom, R. N. Boyd, and A. Mezzacappa, private communication (1999).
123.J. Beacom, private communication, (2000).
124.J. J. Zach, D. Marriott, A. st. J. Murphy, and R. N. Boyd, private communication (1999).
125.E. Kolbe, K. Langanke, G. Martinez-Pinedo, Phys. Rev. **C60**, 052801 (1999); E. Kolbe, and K. Langanke, preprint (2000).
126.J .Bahcall and H. Primakoff, Phys. Rev. **D18**, 3463 (1978).
127.S. M. Bilenky, C. Giunti, and W. Grimus, Phys. Rev. **D58**, 033001 (1998).
128.E. D. Commins, S. B. Ross, D. DeMille, B. C. Regan, Phys. Rev. A **50**, 2960 (1994).
129.R. Davis, Phys. Rev. **97** 766 (1955).
130.P. Langacker and J. Wang Phys. Rev. **D58**, 093004 (1998).
131.R. Davis and D. Harmer, Bull. Am. Phys. Soc. **4**, 217 (1959).
132.C. E. Aalseth *et al.*, Nucl. Phys. (Proc.Supl.) **B70**, 236 (1998).
133.L. Baudis *et al.*, Phys. Lett. **B407**, 219 (1997).
134.P. Alivisatos et al, (KAMLAND Proposal) Stanford-HEP-98-03.
135.B. Pontecorvo, JETP **33**, 549 (1957).
136.L. A. Ahrens *et al.* Phys. Rev.**D35**, 785(1987).
137.David B. Kaplan and Aneesh Manohar, Nucl. Phys. **B310**, 527(1988).
138.C. K. Hargrove, *et al.*, Astroparticle Physics **5**, 183 (1996).
139.D. B. Cline *et al.*, Phys. Rev. **D50**, 720 (1994); P. F. Smith, Astroparticle Physics **8**, 27 (1997).
140.C. K. Hargrove and R. T. Siegel, "A Proposal to Measure the ν-Pb Charged and Neutral Current Cross Sections for Neutrinos from Stopped Pion Decay", 15 January 1998, (unpublished).
141.E. Kolbe, K. Langanke, arXiv:nucl-th/0003060, 27 March 2000.
142.CRC handbook of Chemistry and Physics, 66^{th} edition, CRC Press, Inc.
143.B. D. Anderson, F. Avignone et al., A Large Neutrino Detector Facility at the Spallation Neutron Source in Oak Ridge Natonal Laboratory. Proposal to the US Department on Energy (in preparation).